

Feedback control solves pseudoconvex optimal tracking problems in nonlinear dynamical systems

Tingli Hu and Sami Haddadin^{*}

Chair of Robotics and Systems Intelligence,
MIRMI - Munich Institute of Robotics and Machine Intelligence,
Technical University of Munich,
Georg-Brauchle-Ring 60/62, 80992 München, Germany.

^{*}To whom correspondence should be addressed; E-mail: haddadin@tum.de.

Abstract

Achieving optimality in controlling physical systems is a profound challenge across diverse scientific and engineering fields, spanning neuromechanics, biochemistry, autonomous systems, economics, and beyond. Traditional solutions, relying on time-consuming offline iterative algorithms, often yield limited insights into fundamental natural processes. In this work, we introduce a novel, causally deterministic approach, presenting the closed-form *optimal tracking controller* (OTC) that inherently solves pseudoconvex optimization problems in various fields. Through rigorous analysis and comprehensive numerical examples, we demonstrate OTC's capability of achieving both high accuracy and rapid response, even when facing high-dimensional and high-dynamical real-world problems. Notably, our OTC outperforms state-of-the-art methods by, e.g., solving a 1304-dimensional neuromechanics problem 1311 times faster or with 113 times higher accuracy. Most importantly, OTC embodies a causally deterministic system interpretation of optimality principles, providing a new and fundamental perspective of optimization in natural and artificial processes. We anticipate our work to be an important step towards establishing a general causally deterministic optimization theory for a broader spectrum of system and problem classes, promising advances in understanding optimality principles in complex systems.

Keywords: feedback control, time-variant systems, nonlinear optimization, optimal tracking control

Introduction

Optimality principles exist widely in natural and artificial processes, including neuromechanics [1, 2], biochemistry [3–5], autonomous systems [6–8], economics [9], electricity grid [10–12], telecommunication [13], logistics [14], human-resource allocation [15], and others [16, 17]. These processes exhibit causally determinism, adhering to the classical perspectives. Fully understanding these processes has been significantly benefiting our society in various aspects, e.g., healthcare, transportation, environmental management, finance, or manufacturing. Despite their inherent complexity and diversity, these processes can be generalized as nonlinear time-variant dynamical systems from a system theory point of view. Numerous theories have been established to analyze their properties, including stability [18, 19], controllability [20, 21], and observability [22, 23]. Moreover, the optimality principles governing these systems are often formulated as convex or convexifiable optimization problems, whose (local) optima are founded by iterative algorithms, such as active-set methods [24, 25], interior-point methods [24–27], and sequential quadratic programming [25], grounded on the Karush-Kuhn-Tucker conditions [24, 25, 27]. However, these iterative algorithms demand ultrahigh computational power, resource, and/or time, particularly when dealing with high-dimensional systems, posing significant challenges for practical scalability.

Given the significant, yet, separate advancements made in these related fields and the growing demand for fast and reliable ways of achieving optimality, it is the time for development of a unified mathematical theory encapsulating causally deterministic processes leading to optimality, which we call *causally deterministic optimization theory*. Although this theory provides a closed-form solution, serving as a potent method in controlling artificial systems in accordance with their optimality principles, its significance extends beyond practical utility; the theory constitutes a system interpretation of the optimality principles in nature, offering valuable insights into the underlying governing processes. Over the past four decades, researchers have been endeavoring to bridge the gap between the causal determinism of physical processes and the iterative nature of numerical optimization [28–33]. Despite notable achievements, existing solutions are often catering only to specific cases and/or lacking full causal-determinism interpretability. Moreover, while the efficiency in solving low-dimensional problems have been demonstrated in these works, the validity and performance of these solutions for high-dimensional systems remain uncertain. Without a scalable, causal-deterministically interpretable, closed-form solution capable of tackling high-dimensional real-world problems, our understanding in optimality principles may remain superficial, limited to explaining and interpreting offline-optimization trajectory results for specific problem instances, without gaining comprehensive fundamental insights and knowledge into the structure and meaning of these trajectories. Furthermore, the potential for the closed-loop control of such systems remains an unsolved challenge, despite the rapid advancement in optimization and machine learning.

Contribution

In this work, we propose a *causally deterministic optimization theory* for any-dimensional nonlinear dynamical systems, see Figure 1. These systems encompass diverse domains, including large-scale biological systems such as neuromechanics [1, 2] and metabolic networks [3, 4], economic networks such as asset market [9], electricity grid [11, 12], as well as autonomous systems such as a fleet of vehicles [6, 7]. Specifically, we constitute a closed-form *optimal tracking controller* (OTC) for nonlinear time-variant control-affine systems such that its state trajectory follows, in an exponential rate of convergence, the optimum of the associated pseudoconvex optimization problem. Through rigorous analysis in convergence behavior and computational complexity, we confirm that the proposed tracking controller guarantees a deterministic behavior in both accuracy and response time.

In addition to the theoretical framework mentioned above, we demonstrate, with comprehensive numerical examples, the applicability and efficiency of the proposed OTC in solving challenging, and even high-dimensional, real-world problems in diverse fields. Specifically, OTC exhibits a shorter and fixed response time, indicating its real-time capability and allowing it to be implemented on a real-time computer. This demonstrates its superior performance over the state-of-the-art method, which—if converging at all—is often accompanied with longer, variable and unpredictable response time, especially for large-scale problems. Concretely, with the considered examples, we can show that OTC is capable of solving a 1304-dimensional problem 1311 times faster (on the same level of accuracy) or 113 times more accurate (if the effect of response delay is considered). Practically, we have replaced virtually offline convex (pseudoconvex) optimization algorithms with an any-dimensional real-time tracking controller. We believe, this step constitutes an important advancement to tackling convex (pseudoconvex) optimization problems for even high-dimensional and high-dynamical nonlinear systems; a feat previously deemed unattainable.

Results

Almost all physical processes are in essence nonlinear systems. In this work, we study the broad class of nonlinear time-variant control-affine systems

$$\dot{\mathbf{x}} = \mathbf{f}_A(\mathbf{x}) + \mathbf{B}(\mathbf{x})\mathbf{u}, \quad (1a)$$

$$\mathbf{y} = \mathbf{h}(t, \mathbf{x}), \quad (1b)$$

where $\mathbf{x} = [x_1 \ x_2 \ \cdots \ x_{d_x}]^\top$, $\mathbf{u} = [u_1 \ u_2 \ \cdots \ u_{d_x}]^\top$, and $\mathbf{y} = [y_1 \ y_2 \ \cdots \ y_{d_y}]^\top$ are the state, the input, and the output, respectively, of this d_x -dimensional system, and t denotes time. For instance, \mathbf{x} can denote the activation level of muscles in a human limb [34], electric current of a motor in an aerial vehicle [6], or the capital invested on an asset market [9]. Correspondingly, \mathbf{u} can denote neural excitation, voltage, and capital reallocation, respectively; and \mathbf{y} the resulting joint torques acting on the human limb, the linear and angular acceleration of the aerial vehicle, or return on capital, respectively. Given the reference trajectory \mathbf{y}_{ref} which \mathbf{y} should follow, the

optimality principle associated with (1) can be representatively written as either the pseudoconvex optimization problem

$$\begin{aligned} \min_{\boldsymbol{\chi}} \sigma(t, \boldsymbol{\chi}) \quad \text{subject to } \mathbf{0} = \mathbf{h}(t, \boldsymbol{\chi}) - \mathbf{y}_{\text{ref}}(t), \\ \mathbf{0} \geq \mathbf{g}(t, \boldsymbol{\chi}) := \mathbf{G}(t)\boldsymbol{\chi} + \mathbf{c}(t) \end{aligned} \quad (2)$$

for every time instant $t \geq 0$ or the optimal tracking control problem

$$\begin{aligned} \min_{\boldsymbol{\phi}} \int_0^{t_f} \sigma(t, \boldsymbol{\phi}(t)) dt \quad \text{subject to } \mathbf{0} = \mathbf{h}(t, \boldsymbol{\phi}(t)) - \mathbf{y}_{\text{ref}}(t) \quad \forall t \in (0, t_f], \\ \mathbf{0} \geq \mathbf{g}(t, \boldsymbol{\phi}(t)) \quad \forall t \in (0, t_f], \\ \mathbf{x}(0) = \boldsymbol{\phi}(0) \end{aligned} \quad (3)$$

for the time period $[0, t_f]$. Let $\boldsymbol{\chi}^{\otimes}(t) \in \mathbb{R}^{d_x}$ denote a local optimum of (2) at t and $\boldsymbol{\phi}^{\otimes} : [0, t_f] \rightarrow \mathbb{R}^{d_x}$ a local optimum of (3) for the time period $[0, t_f]$, then the state $\mathbf{x}(t)$ of (1) is called optimal if $\mathbf{x}(t) = \boldsymbol{\chi}^{\otimes}(t)$ or $\mathbf{x}(t) = \boldsymbol{\phi}^{\otimes}(t)$. It means that a minimal cost ($\sigma(t, \mathbf{x})$ or time integral of $\sigma(t, \mathbf{x})$) is preferred as long as \mathbf{y} matches \mathbf{y}_{ref} (i.e., $\mathbf{0} = \mathbf{h}(t, \mathbf{x}) - \mathbf{y}_{\text{ref}}$) and the state remains within boundaries (i.e., $\mathbf{0} \geq \mathbf{g}(t, \mathbf{x})$). Concrete examples are: lower activation level of muscles is preferred while an intended movement can be accomplished within physiological feasibility [34]; a minimal energy consumption is desired for an aerial vehicle, as long as an assigned task can be finished while every motor operates within its payload capacity [6]; and the risk shall be as low as possible while the total return meets the investor's expectation according to his investment capability [9].

The closed-form *optimal tracking controller* (OTC)

$$\mathbf{u} = \boldsymbol{\mu}(t, \mathbf{x}, \mathbf{y}_{\text{ref}}; K_x), \quad K_x > 0 \quad (4)$$

that solves problems (2) and (3) for system (1) is our *first main result*. In fact, system (1) being controlled by (4) exhibits an exponentially convergent tracking behavior:

- $\mathbf{y}(t)$ follows the reference $\mathbf{y}_{\text{ref}}(t)$ with exponential convergence and time constant K_x^{-1} ,
- $\mathbf{x}(t)$ follows $\boldsymbol{\chi}^{\otimes}(t)$ and $\boldsymbol{\phi}^{\otimes}(t)$ with exponential convergence and a time constant $\propto K_x^{-1}$,
- the tracking error $\mathbf{x}(t) - \boldsymbol{\chi}^{\otimes}(t)$ or $\mathbf{x}(t) - \boldsymbol{\phi}^{\otimes}(t)$ converges to the interior of a d_x -dimensional ball which is centered at zero and has a radius $\propto K_x^{-1}$.

In other words: the higher K_x is, the more responsive and accurate OTC will be. The reader may refer to Section *Methods* for details of the system and problem class (1)–(3) and the concrete mathematical formulation behind OTC (4). Moreover, we also show by mathematical deductions that (2) and (3) are equivalent to each other, i.e., $\boldsymbol{\chi}^{\otimes}(t) = \boldsymbol{\phi}^{\otimes}(t) \quad \forall t \in (0, t_f]$, in discrete-time and numerical contexts – this is our *second main result*.

Indeed, under the control of (4), the state $\mathbf{x}(t)$ of (1) is able to follow $\boldsymbol{\chi}^{\otimes}(t)$ and $\boldsymbol{\phi}^{\otimes}(t)$ closely for all $t > 0$, as Figure 2 shows for a two-dimensional, yet, comprehensive

system, cf. (33). These trajectories of $\mathbf{x}(t)$, starting from distinct initial points $\mathbf{x}(0)$, demonstrate an exponential convergence to the corresponding $\chi^{\otimes}(t)$ and $\phi^{\otimes}(t)$ with an initial transient phase of < 0.1 . Despite the occasional abrupt jumps in trajectories $\chi^{\otimes}(t)$ and $\phi^{\otimes}(t)$, the OTC consistently guarantees a rapid first-order convergence behavior of \mathbf{x} towards a local minimizer. This fast and robust convergence behavior underscores the effectiveness of OTC in swiftly achieving desired optimal outcomes in time-variant contexts.

This closely tracking behavior is confirmed further by an exhaustive numerical verification with scalable exemplary real-world systems of d_x ranging from 28 to 9600 (see Table 1 for overview and Section *Methods* for details). Figure 3 shows the values of two accuracy metrics:

- E_x : mean absolute difference between $\mathbf{x}(t)$ and $\chi^{\otimes}(t)$, capturing the absolute accuracy.
- E_σ : the ratio between the time integral of $\sigma(t, \mathbf{x}(t))$ and that of $\sigma(t, \chi^{\otimes}(t))$, capturing the relative accuracy.

The closer E_x is to 0 and E_σ is to 1, the more accurate the OTC’s trajectory $\mathbf{x}(t)$ is. Evidently, low $E_x \leq 0.002$ (all) and E_σ within 1.00 and 1.02 (majority) underscore the effectiveness of OTC in accurately producing and tracking the optimal solution.

Although K_x determines the responsiveness of system dynamics, the practical response time is lower bounded by the CPU time evaluating $\boldsymbol{\mu}$. By analyzing the computational time complexity, we determine that the CPU time $\mathcal{T}(\text{OTC})$ of OTC is proportional to d_x^3 for large d_x and is a time-*invariant* quantity, despite the time-variant property of the considered system and problem class (1)–(3), i.e.,

$$\mathcal{T}(\text{OTC}) = \mathcal{O}(d_x^3). \quad (5)$$

For comparison, the CPU time $\mathcal{T}(\text{SQP})$ of the most efficient state-of-the-art algorithm sequential quadratic programming (SQP) [24, 25, 35] for (2) is

$$\mathcal{T}(\text{SQP})(t) = \mathcal{O}(\sqrt{d_x} \log(d_x \ell(t))) \times \mathcal{O}(d_x^3), \quad (6)$$

which grows faster than $\mathcal{O}(d_x^{3.5})$ and is with the time-variant quantity $\ell(t)$ inheriting from the time-variant property of the considered problem class. The reader may refer to Section *Methods* for the derivation of $\mathcal{T}(\text{OTC})$ and $\mathcal{T}(\text{SQP})(t)$. The comparison between $\mathcal{T}(\text{OTC})$ and $\mathcal{T}(\text{SQP})(t)$ makes it evident that OTC exhibits lower time complexity than SQP. Particularly, in contrast to $\mathcal{T}(\text{SQP})(t)$, which fluctuate over time, $\mathcal{T}(\text{OTC})$ is steady and constant. This time-invariant performance in solving the time-variant system and problem class is fundamental to time-critical and even real-time inference, as will be discussed in Section *Discussion*. This real-time capability of OTC, superior to state-of-the-art methods, is our *third main result*.

In our exhaustive numerical verification examples (see Table 1 for overview and Section *Methods* for details), we measured the time duration $\tau_{\text{C,OTC}}(t)$ and $\tau_{\text{C,SQP}}(t)$ (in seconds per sample) needed by OTC and SQP, respectively, to complete computation for the sample at time instant t . Figure 4 depicts box plots illustrating the variability of $\tau_{\text{C,OTC}}(t)$ and $\tau_{\text{C,SQP}}(t)$ within each numerical scenario. Notably, the data points of $\tau_{\text{C,OTC}}$ cluster tightly at a very low median value with zero dispersion, indicating

consistently fast performance. In contrast, $\tau_{C,SQP}$ display high median values and high dispersion, reflecting the diverse computational demands imposed by different problem instances. Figure 5 shows the growth of average computation time duration $\bar{\tau}_{C,OTC}$ and $\bar{\tau}_{C,SQP}$ with system's dimension d_x . The linear growth of $\sqrt[3]{\bar{\tau}_{C,OTC}}$ with d_x and the superlinear increase of $\sqrt[3]{\bar{\tau}_{C,SQP}}$ agree with the derived time complexity $\mathcal{T}(OTC)$ and $\mathcal{T}(SQP)$. Notably, all data points of $\bar{\tau}_{C,OTC}$ are closely aligned with the corresponding best-fit trendlines, see Figure 5, and only two distinct trendlines are observed for OTC, see Figure 5(d). This phenomenon arises from the diagonality-dependent computational procedure in the practical implementation of OTC (see Supplementary Information [SI], Section 4). In contrast, the computation time of SQP exhibits greater variability in terms of closeness to the best-fit trendlines, see Figure 5, and the existence of six distinct trendlines, see Figure 5(d). This observation suggests the dependency of computational performance on the specific problem instances.

Overall, the superior performance of OTC over SQP originates in the higher accuracy and the steady, consistent, and lower computation time. Remarkably, OTC solves a 1304-dimensional problem (Example R2, Scenario $d_x = 1304$, $\mathbf{Q} = \text{diag.}$) 1311 times faster (on the same level of accuracy, see Figure 5(b)) or 113 times more accurate (if the effect of response delay is considered, see SI, Section 5). This superior performance makes OTC a more suitable choice for real-time computing applications, particularly in closed-loop control systems.

The main results of this work are as follows.

- Result 1: Closed-form OTC for nonlinear time-variant control-affine systems. This controller ensures an exponentially convergent tracking behavior towards optimum with time constant and tracking error inversely proportional to one control design parameter. This high tracking accuracy is verified exhaustively by exemplary real-world systems of $d_x = 28\dots9600$.
- Result 2: A trajectory which is optimal for an entire time period is also optimal at each time instant within that period, and vice versa. This theoretically deduced equivalency between nonlinear optimization and optimal tracking control is confirmed numerically by a comprehensive mathematical example.
- Result 3: The time complexity of OTC is a time-invariant degree-3 polynomial $\mathcal{O}(d_x^3)$ of system's dimension d_x , despite the time-variant property of the considered system and problem class. For comparison, the complexity of state-of-the-art methods for this system and problem class is time-variant and growing faster than a degree-3.5 polynomial of d_x . Numerical verification examples with real-world systems of $d_x = 28\dots9600$ confirm this difference in time complexity.

Together, these three main results highlight that OTC inherently solves *pseudoconvex optimal* tracking problems in *real-time* for nonlinear time-variant control-affine systems of *any dimension*. This unparalleled feature makes OTC advantageous across a wide range of fields, enabling solutions to practical challenges previously considered unfeasible. These applications, including its potential in time-critical optimal inference, will be elaborated on in Section *Discussion*.

Discussion

In this work, we developed OTC as part of causally deterministic optimization theory. The considered system and problem class cover all *convex* optimization and a *special case of pseudoconvex* optimization for time-variant *control-affine* and *continuously differentiable* systems. This system and problem class is common in the real world. Examples include neuromechanics (muscle-force distribution [1], motor-unit recruitment [2]), metabolic networks (flux balance analysis [3], multidimensional optimality [4]), beamforming in localization and communication systems [13], autonomous systems (omnidirectional vehicle [6], multirobot network [7]), electricity grid (optimal power flow [10–12]), and economics (Markowitz portfolio optimization [9]). Due to its causally deterministic nature, OTC is not just a new method, it is, most importantly, a system interpretation of optimality principles in physical systems (e.g., neuromechanics, metabolic networks). It provides a new and fundamental perspective of optimization in natural and artificial processes. This indicates the potential of OTC serving as a model in grey-box identification, enabling the discovery of unknown optimality principles in physical systems.

Inheriting from the causal determinism, the high accuracy and fixed response time make OTC a real-time capable method, allowing it to be implemented on a real-time computer. Although the state-of-the-art algorithms may achieve (sub)optimality of low-dimensional linear or trivial systems in real-time, as demonstrated in [36, 37], the OTC’s real-time capability in achieving optimality even extends to high dimensionality, high nonlinearity, and complex dynamics. This is essential for any time-critical applications and has been unrealizable till today.

The most common approach to time-critical application with optimality considerations is model-predictive control (MPC), which determines optimal actions by solving a finite-horizon constrained optimal control problem, such as (3), at *each* sampling instant [38]. By using OTC in place of the iterative optimization solver in MPC, a real-time optimal inference at higher sampling frequencies and over longer prediction horizons would become possible. This brings the system’s behavior closer to its true optimum and has thus the potential to significantly boost economic efficiency and environmental sustainability in industries [39] such as process engineering, climate control systems, and manufacturing. OTC-enhanced MPC holds particular promise for spacecraft operations [8, 40], as it would enable the *real-time on-board solution* for computing optimal actions in response to unpredictable environmental changes, without jeopardizing the mission due to either delayed or suboptimal actions. For instance, executing a least-fuel-consumption maneuver to avoid an incoming unforeseen object such as an asteroid would ensure the spacecraft’s immediate safety while conserving enough fuel to complete the mission.

Moreover, a different interpretation of the considered system and problem class reveals the potential of OTC as a generalization of a wide spectrum of control methods to *state-constrained controllers* (see Section *Methods*). By successfully generalizing the linear-quadratic regulator [41] to a state-constrained variant (SI, Section 6) and given its inherent optimality, we believe that OTC is a promising candidate for *state-constrained nonlinear-convex controller* – functioning simultaneously as both an

optimal trajectory planner and a tracking controller for nonlinear time-variant constrained systems and convex cost functions. This is a topic worth exploring in future work.

While OTC addresses the considered system and problem class well, it is important to acknowledge that the nature extends beyond continuity, control-affinity, and (pseudo)convexity. In hybrid systems, discontinuities occur from mechanical contacts, impacts, and Coulomb frictions during interactions [42]. Control-affinity does not hold in systems where the number of inputs are less than that of states, including almost all network systems [20], although we believe that OTC can be extended for completely controllable non-affine systems (future work). Combinatorial optimization which are widely applied in logistics [14], human-resource allocation [15], and synthetic biology [5] have discrete feasible sets, making themselves nonconvex and inconvexifiable. Exploring these facets of system dynamics and optimality principles are essential to achieve a more general causally deterministic optimization theory. In fact, complementary to this work, [32] has provided a way to integrate nonlinear inequality constraints, while [43, 44] have dealt with controlling nonaffine systems. We believe that these works and our work have together paved an initial path towards that ultimate objective.

Methods

This section presents the workflow of deduction from system and problem class (1)–(3), via significant intermediate milestones, to finally arrive at the concrete form of OTC (4), its convergence behavior and computational complexity, without, however, showing the details of every step. For a detailed version of all mathematical steps, statements, and proofs, please refer to Supplementary Information (SI).

System and problem class

The system (1) we consider in this work possesses the following properties:

1. The functions $\mathbf{f}_A : \mathbb{R}^{d_x} \rightarrow \mathbb{R}^{d_x}$ and $\mathbf{B} : \mathbb{R}^{d_x} \rightarrow \mathbb{R}^{d_x \times d_x}$ are such that (1a) satisfies existence and uniqueness theorem, i.e., there exists one and only one trajectory $\mathbf{x} : \mathbb{R}_{>0} \rightarrow \mathbb{R}^{d_x}$ for any $\mathbf{u} : \mathbb{R}_{\geq 0} \rightarrow \mathbb{R}^{d_x}$ and any $\mathbf{x}(0) \in \mathbb{R}^{d_x}$.
2. The input matrix $\mathbf{B}(\mathbf{x}) \in \mathbb{R}^{d_x \times d_x}$ is invertible $\forall \mathbf{x} \in \mathbb{R}^{d_x}$.
3. The output function $\mathbf{h} : \mathbb{R}_{>0} \times \mathbb{R}^{d_x} \rightarrow \mathcal{Y}$ with $\mathcal{Y} \subset \mathbb{R}^{d_y}$ is continuous in t and twice continuously differentiable (differentiability class C^2) and surjective in \mathbf{x} , for all $t \geq$ and all $\mathbf{x} \in \mathbb{R}^{d_x}$.

Due to the surjection \mathbf{h} , for any reference output \mathbf{y}_{ref} , there exist infinitely many possible solutions for the control \mathbf{u} such that $\lim_{t \rightarrow +\infty} \|\mathbf{y}(t) - \mathbf{y}_{\text{ref}}(t)\|_2 = 0$. This motivates us to find the optimal solution among all these possible ones. We specify the optimality by (2) or (3), where $\sigma : \mathbb{R}_{\geq 0} \times \mathbb{R}^{d_x} \rightarrow \mathbb{R}$ is the time-variant cost function, the output function \mathbf{h} accounts for the time-variant equality constraint, reflecting the desired output tracking behavior, and $\mathbf{g} : \mathbb{R}_{\geq 0} \times \mathbb{R}^{d_x} \rightarrow \mathbb{R}^{d_c}$ the time-variant linear inequality constraint. Hereby, we introduce the following further properties:

4. For any time instant $t \geq 0$, the cost function $\sigma(t, \boldsymbol{\chi})$ is twice continuously differentiable and strongly convex in $\boldsymbol{\chi}$.

5. There exists always ($\forall t \geq 0$) at least one local minimizer for (2);
 6. if multiple local minimizers exist, they are isolated points in \mathbb{R}^{d_x} .
- Furthermore, we suppose
7. There exists a differentiable $\chi^\circ : \mathbb{R}_{\geq 0} \rightarrow \mathbb{R}^{d_x}$ such that for any $t \geq 0$, $\chi^\circ(t)$ is a local minimizer of (2).
 8. Any local minimizer $\phi^\circ : [0, t_f] \rightarrow \mathbb{R}^{d_x}$ of (3) is differentiable.

Interior-point iteration

For solving optimization problems with both equality and inequality constraints such as (2), we adopt the idea of introducing a *barrier function* β from interior-point algorithms [25, 26, 35]: the barrier function penalizes points that are outside of the feasible region (SI, Definition 2). One example of β is

$$\beta(s) = \frac{p_2}{p_1} \ln(1 + \exp(p_1 s)), \quad p_1 \gg 1, \quad p_2 \gg 1 \quad (7)$$

(see Supplementary Figure S2). For the purpose of penalization, we combine σ and \mathbf{g} into an *augmented cost function* ρ with the aid of β ; this results in

$$\rho(t, \chi) := \sigma(t, \chi) + \frac{1}{2} \beta(\mathbf{g}(t, \chi))^\top \beta(\mathbf{g}(t, \chi)). \quad (8)$$

Consequently, we convert (2) into the time-variant optimization problem

$$\min_{\chi} \rho(t, \chi) \quad \text{subject to} \quad \mathbf{0} = \mathbf{h}(t, \chi) - \mathbf{y}_{\text{ref}}(t). \quad (9)$$

Since p_1 and p_2 can be chosen arbitrarily large (SI, Lemma 1 and Section 4), the local minimizers of (9) are the same to those of (2).

For the equality-constrained problem (9), we formulate the Lagrangian function

$$L(t, \chi, \zeta) = \rho(t, \chi) + \zeta^\top (-\mathbf{h}(t, \chi) + \mathbf{y}_{\text{ref}}(t))$$

with Lagrange multipliers $\zeta \in \mathbb{R}^{d_y}$. By eliminating ζ without introducing further assumptions (SI, Lemma 3), we obtain the *interior-point iteration*

$$\chi^{[k+1]}(t) = \chi^{[k]}(t) + \eta(t, \chi^{[k]}(t), \mathbf{y}_{\text{ref}}(t)), \quad (10)$$

$$\eta(t, \boldsymbol{x}, \mathbf{y}_{\text{ref}}) := \mathbf{H}(t, \boldsymbol{x})_{\mathbf{R}(t, \boldsymbol{x})}^\# (\mathbf{y}_{\text{ref}} - \mathbf{h}(t, \boldsymbol{x})) - (\mathbf{I} - \mathbf{H}(t, \boldsymbol{x})_{\mathbf{R}(t, \boldsymbol{x})}^\# \mathbf{H}(t, \boldsymbol{x})) \mathbf{R}(t, \boldsymbol{x})^{-1} \mathbf{r}(t, \boldsymbol{x}), \quad (11)$$

where $\boldsymbol{x} \in \mathbb{R}^{d_x}$ denote a general argument of functions, $\mathbf{H}(t, \boldsymbol{x}) := \partial \mathbf{h}(t, \boldsymbol{x}) / \partial \boldsymbol{x}$ is the Jacobian of the equality constraint, $\mathbf{r}(t, \boldsymbol{x}) := [\partial \rho(t, \boldsymbol{x}) / \partial \boldsymbol{x}]^\top$ and $\mathbf{R}(t, \boldsymbol{x}) := \partial \mathbf{r}(t, \boldsymbol{x}) / \partial \boldsymbol{x}$ are the gradient and Hessian of $\rho(t, \boldsymbol{x})$, and $\mathbf{A}_W^\#$ is the \mathbf{W} -weighted right pseudoinverse of a matrix \mathbf{A} , i.e.,

$$\mathbf{A}_W^\# = \mathbf{W}^{-1} \mathbf{A}^\top (\mathbf{A} \mathbf{W}^{-1} \mathbf{A}^\top)^{-1}.$$

The interior-point iteration (10) is in principle a quasi-Newton iteration and the resulting $\boldsymbol{\chi}^{[k]}(t)$ converges quotient-linearly to $\boldsymbol{\chi}^{\otimes}(t)$ as $k \in \mathbb{N}$ increases (SI, Theorem 1).

Output tracking controller with full-state feedback

We construct firstly the control

$$\boldsymbol{u} = \boldsymbol{B}(\boldsymbol{x})^{-1} \left(-\boldsymbol{f}_A(\boldsymbol{x}) + \boldsymbol{f}'_A(t, \boldsymbol{x}) + \boldsymbol{u}' \right) \quad (12)$$

to shape (1) to

$$\dot{\boldsymbol{x}} = \boldsymbol{f}'_A(t, \boldsymbol{x}) + \boldsymbol{u}', \quad (13a)$$

$$\boldsymbol{y} = \boldsymbol{h}(t, \boldsymbol{x}). \quad (13b)$$

Subsequently, we apply feedback linearization on (13) to establish an output tracking controller. This results in the controller

$$\boldsymbol{u}' = \overbrace{\boldsymbol{H}(t, \boldsymbol{x}) \#_{\boldsymbol{Q}'} K_y (\boldsymbol{y}_{\text{ref}} - \boldsymbol{h}(t, \boldsymbol{x}))}^{\text{output tracking}} \overbrace{-\boldsymbol{H}(t, \boldsymbol{x}) \#_{\boldsymbol{Q}'} \boldsymbol{H}(t, \boldsymbol{x}) \boldsymbol{f}'_A(t, \boldsymbol{x})}^{\text{full-state feedback}}, \quad (14)$$

\boldsymbol{Q}' is SPD, $K_y > 0$

and the closed-loop system

$$\dot{\boldsymbol{y}} = -K_y (\boldsymbol{y} - \boldsymbol{y}_{\text{ref}}), \quad (15)$$

$$\dot{\boldsymbol{x}} = \boldsymbol{H}(t, \boldsymbol{x}) \#_{\boldsymbol{Q}'} K_y (\boldsymbol{y}_{\text{ref}} - \boldsymbol{h}(t, \boldsymbol{x})) + \left(\boldsymbol{I} - \boldsymbol{H}(t, \boldsymbol{x}) \#_{\boldsymbol{Q}'} \boldsymbol{H}(t, \boldsymbol{x}) \right) \boldsymbol{f}'_A(t, \boldsymbol{x}). \quad (16)$$

Evidently, $\boldsymbol{y}(t)$ converges exponentially to $\boldsymbol{y}_{\text{ref}}$ as $t > 0$ increases (SI, Lemma 6), while with

$$\boldsymbol{Q}' = \boldsymbol{R}(t, \boldsymbol{x}), \quad (17a)$$

$$\boldsymbol{f}'_A(t, \boldsymbol{x}) = -K_x \boldsymbol{R}(t, \boldsymbol{x})^{-1} \boldsymbol{r}(t, \boldsymbol{x}), \quad K_x = K_y > 0 \quad (17b)$$

Equation (16) becomes

$$\dot{\boldsymbol{x}} = K_x \boldsymbol{\eta}(t, \boldsymbol{x}, \boldsymbol{y}_{\text{ref}}). \quad (18)$$

The equilibrium points \boldsymbol{x}^* of (18) are same as those of (10) and the latter are local minimizers; this concludes $\boldsymbol{x}^* = \boldsymbol{\chi}^{\otimes}$.

Exponential convergence

For analyzing the convergence behavior of \boldsymbol{x} towards an equilibrium $\boldsymbol{\chi}^{\otimes}$, we firstly consider the case where (1) and (2) are time-*invariant*. We choose a Lyapunov candidate function

$$V(\boldsymbol{x}) = \frac{1}{2} (\boldsymbol{x} - \boldsymbol{\chi}^{\otimes})^\top K_x^{-1} (\boldsymbol{x} - \boldsymbol{\chi}^{\otimes}) \quad (19)$$

for (18). Its time derivative is

$$\frac{d}{dt}V(\mathbf{x}) = \frac{\partial V(\mathbf{x})}{\partial \mathbf{x}} \dot{\mathbf{x}} = (\mathbf{x} - \boldsymbol{\chi}^{\otimes})^\top \boldsymbol{\eta}(t, \mathbf{x}, \mathbf{y}_{\text{ref}}). \quad (20)$$

From the quotient-linear convergence of (10), it can be shown that

$$(\mathbf{x} - \boldsymbol{\chi}^{\otimes})^\top \boldsymbol{\eta}(t, \mathbf{x}, \mathbf{y}_{\text{ref}}) \leq -\alpha \|\mathbf{x} - \boldsymbol{\chi}^{\otimes}\|_2^2 - \frac{1}{2} \|\boldsymbol{\eta}(t, \mathbf{x}, \mathbf{y}_{\text{ref}})\|_2^2, \quad (21)$$

with some constant $\alpha \in (0, 0.5)$ accounting for the rate of convergence (SI, Lemma 11). Consequently, $dV(\mathbf{x})/dt \leq 0$ and Lyapunov stability are concluded. Further, by applying LaSalle's invariance principle [45] and Grönwall's inequality [46], we conclude that $\mathbf{x}(t)$ converges exponentially to $\boldsymbol{\chi}^{\otimes}$ as $t > 0$ increases (SI, Lemma 10).

Due to the exponential convergence for the time-invariant case, we infer that similar convergence behavior holds even when (1) and (2) are time-variant, provided that $\boldsymbol{\chi}^{\otimes}(t)$ is band-limited in the frequency domain. This means, by considering (18) as a *slowly varying system* [47], i.e., $\exists D_\chi \geq 0 : \|\dot{\boldsymbol{\chi}}^{\otimes}(t)\|_2 \leq D_\chi \forall t \geq 0$, we conclude

$$\begin{aligned} \|\mathbf{x}(t) - \boldsymbol{\chi}^{\otimes}(t)\|_2 &\leq \|\mathbf{x}(0) - \boldsymbol{\chi}^{\otimes}(0)\|_2 \exp(-\kappa t) + \int_0^t \exp(-\kappa(t-\tau)) \|\dot{\boldsymbol{\chi}}^{\otimes}(\tau)\|_2 d\tau \\ &\leq \|\mathbf{x}(0) - \boldsymbol{\chi}^{\otimes}(0)\|_2 \exp(-\kappa t) + \kappa^{-1} D_\chi, \end{aligned} \quad (22)$$

where $\kappa := \alpha K_x$ (SI, Lemma 12). This inequality conveys that

1. the tracking error $\mathbf{x}(t) - \boldsymbol{\chi}^{\otimes}(t)$ converges, as $t \geq 0$ elapses, exponentially with a time constant $\kappa \propto K_x^{-1}$ to the interior of a d_x -dimensional ball which is centered at zero and has a radius $\kappa^{-1} D_\chi \propto K_x^{-1}$;
2. if (1) and (2) are time-invariant ($\Rightarrow D_\chi = 0$), the radius becomes 0.

Optimal tracking controller

Let a numerical approach be considered in finding $\boldsymbol{\phi}^{\otimes}$ of (3). For this, we parameterize the trajectory $\boldsymbol{\phi} : [0, t_f] \rightarrow \mathbb{R}^{d_x}$ as the stacked vector

$$\boldsymbol{\varphi} := [\boldsymbol{\phi}(1\delta t)^\top \quad \boldsymbol{\phi}(2\delta t)^\top \quad \dots \quad \boldsymbol{\phi}(N\delta t)^\top]^\top$$

of the coordinates $\boldsymbol{\phi}(n\delta t)$ at the n -th discrete time instant. Herein, $N\delta t = t_f$, and we omit $\boldsymbol{\phi}(0)$ purposely since $\boldsymbol{\phi}(0) = \mathbf{x}(0)$ is given explicitly as a boundary condition in (3). Consequently, the continuous-time problem (3) can be approximately written in discrete-time as

$$\begin{aligned} \min_{\boldsymbol{\varphi}} \zeta(\boldsymbol{\varphi}) \quad \text{subject to } \mathbf{0} &= \boldsymbol{\mathcal{H}}(\boldsymbol{\varphi}) - \boldsymbol{y}_{\text{ref}}, \\ \mathbf{0} &\geq \boldsymbol{\mathcal{G}}(\boldsymbol{\varphi}), \end{aligned} \quad (23)$$

where

$$\begin{aligned} \varsigma(\boldsymbol{\varphi}) &:= \sum_{n=1}^N \sigma(n\delta t, \boldsymbol{\phi}(n\delta t)), \\ \boldsymbol{h}(\boldsymbol{\varphi}) &:= \begin{bmatrix} \boldsymbol{h}(1\delta t, \boldsymbol{\phi}(1\delta t)) \\ \boldsymbol{h}(2\delta t, \boldsymbol{\phi}(2\delta t)) \\ \vdots \\ \boldsymbol{h}(N\delta t, \boldsymbol{\phi}(N\delta t)) \end{bmatrix}, \quad \boldsymbol{y}_{\text{ref}} := \begin{bmatrix} \boldsymbol{y}_{\text{ref}}(1\delta t) \\ \boldsymbol{y}_{\text{ref}}(2\delta t) \\ \vdots \\ \boldsymbol{y}_{\text{ref}}(N\delta t) \end{bmatrix}, \\ \boldsymbol{g}(\boldsymbol{\varphi}) &:= \begin{bmatrix} \boldsymbol{g}(1\delta t, \boldsymbol{\phi}(1\delta t)) \\ \boldsymbol{g}(2\delta t, \boldsymbol{\phi}(2\delta t)) \\ \vdots \\ \boldsymbol{g}(N\delta t, \boldsymbol{\phi}(N\delta t)) \end{bmatrix}. \end{aligned}$$

Since δt can be chosen arbitrarily close to zero, (3) and (23) are isomorphic to each other.

For the constrained optimization problem (23), we adopt the interior-point iteration (see Subsection *Interior-point iteration*, cf. (10)–(11)) to find a local optimum $\boldsymbol{\varphi}^{\circledast}$ iteratively. This means

$$\begin{aligned} \boldsymbol{\varphi}^{[k+1]} &= \boldsymbol{\varphi}^{[k]} + \mathcal{H}(\boldsymbol{\varphi}^{[k]})^{\#}_{\mathcal{R}(\boldsymbol{\varphi}^{[k]})} (\boldsymbol{y}_{\text{ref}} - \boldsymbol{h}(\boldsymbol{\varphi}^{[k]})) \\ &\quad - \left(\boldsymbol{I} - \mathcal{H}(\boldsymbol{\varphi}^{[k]})^{\#}_{\mathcal{R}(\boldsymbol{\varphi}^{[k]})} \mathcal{H}(\boldsymbol{\varphi}^{[k]}) \right) \mathcal{R}(\boldsymbol{\varphi}^{[k]})^{-1} \boldsymbol{r}(\boldsymbol{\varphi}^{[k]}) \end{aligned} \quad (24a)$$

$$\mathcal{H}(\boldsymbol{\varphi}) := \frac{\partial \boldsymbol{h}(\boldsymbol{\varphi})}{\partial \boldsymbol{\varphi}}, \quad (24b)$$

$$\boldsymbol{r}(\boldsymbol{\varphi}) := \left[\frac{\partial \varrho(\boldsymbol{\varphi})}{\partial \boldsymbol{\varphi}} \right]^{\top}, \quad \mathcal{R}(\boldsymbol{\varphi}) := \frac{\partial \boldsymbol{r}(\boldsymbol{\varphi})}{\partial \boldsymbol{\varphi}}, \quad \varrho(\boldsymbol{\varphi}) := \varsigma(\boldsymbol{\varphi}) + \frac{1}{2} \boldsymbol{\beta}(\boldsymbol{g}(\boldsymbol{\varphi}))^{\top} \boldsymbol{\beta}(\boldsymbol{g}(\boldsymbol{\varphi})) \quad (24c)$$

and that $\boldsymbol{\varphi}^{[k]}$ converges to $\boldsymbol{\varphi}^{\circledast}$ as $k \in \mathbb{N}$ increases.

Expanding (24) yields

$$\boldsymbol{\phi}^{[k+1]}(n\delta t) = \boldsymbol{\phi}^{[k]}(n\delta t) + \boldsymbol{\eta}(n\delta t, \boldsymbol{\phi}^{[k]}(n\delta t), \boldsymbol{y}_{\text{ref}}(n\delta t)), \quad \forall n \in \mathbb{N}^+ \cap [1, N],$$

which exhibits the same iterative behavior as $\boldsymbol{\chi}^{[k]}(t)$, see (10). This leads to

$$\boldsymbol{\phi}^{\circledast} = \left[[\boldsymbol{\chi}^{\circledast}(1\delta t)]^{\top} \quad [\boldsymbol{\chi}^{\circledast}(2\delta t)]^{\top} \quad \cdots \quad [\boldsymbol{\chi}^{\circledast}(N\delta t)]^{\top} \right]^{\top},$$

and consequently,

$$\boldsymbol{\phi}^{\circledast}(t) = \boldsymbol{\chi}^{\circledast}(t), \quad \forall t \in \{t = n\delta t \mid n \in \mathbb{N}^+, \delta t > 0\}. \quad (25)$$

This discrete-time equivalency (25) makes the conclusion in Subsection *Exponential convergence*, cf. (22), applicable here, i.e., if $\exists D_\phi \geq 0$: $\|\dot{\boldsymbol{\phi}}^\otimes(t)\|_2 \leq D_\phi \forall t \geq 0$ then

$$\begin{aligned} \|\mathbf{x}(t) - \boldsymbol{\phi}^\otimes(t)\|_2 &\leq \|\mathbf{x}(0) - \boldsymbol{\phi}^\otimes(0)\|_2 \exp(-\kappa t) + \int_0^t \exp(-\kappa(t-\tau)) \|\dot{\boldsymbol{\phi}}^\otimes(\tau)\|_2 d\tau \\ &\leq \|\mathbf{x}(0) - \boldsymbol{\phi}^\otimes(0)\|_2 \exp(-\kappa t) + \kappa^{-1} D_\phi = \kappa^{-1} D_\phi, \end{aligned} \quad (26)$$

where \mathbf{x} is the state of (18) and $\kappa = \alpha K_x$ (SI, Theorem 4). Remember $\alpha \in (0, 0.5)$ accounts for the rate of convergence, see (21), and $\mathbf{x}(0) = \boldsymbol{\phi}^\otimes(0)$, cf. (3).

Conclusively, by inserting (17) into (14) and then into (12), we constitute the *optimal tracking controller* (OTC)

$$\mathbf{u} = \boldsymbol{\mu}(t, \mathbf{x}, \mathbf{y}_{\text{ref}}; K_x) = \mathbf{B}(\mathbf{x})^{-1} (-\mathbf{f}_A(\mathbf{x}) + K_x \boldsymbol{\eta}(t, \mathbf{x}, \mathbf{y}_{\text{ref}})) \quad (27)$$

with $K_x > 0$ and $\boldsymbol{\eta}$ in (11).

Systemic interpretation

The principal part $\boldsymbol{\eta}(t, \mathbf{x}, \mathbf{y}_{\text{ref}})$ (11) of OTC (27) is composed of two complementary components:

$$\boldsymbol{\eta}(t, \mathbf{x}, \mathbf{y}_{\text{ref}}) = \underbrace{\mathbf{H}(t, \mathbf{x}) \#_{\mathbf{R}(t, \mathbf{x})}}_{\text{Pseudoinverse}} (\mathbf{y}_{\text{ref}} - \mathbf{h}(t, \mathbf{x})) + \underbrace{(\mathbf{I} - \mathbf{H}(t, \mathbf{x}) \#_{\mathbf{R}(t, \mathbf{x})} \mathbf{H}(t, \mathbf{x}))}_{\text{Null-space projection}} \underbrace{(-\mathbf{R}(t, \mathbf{x})^{-1} \mathbf{r}(t, \mathbf{x}))}_{\text{Newton-Raphson step}}.$$

While Component I ensures the output tracking behavior, Component II guarantees the convergence towards a local minimizer of $\rho(t, \cdot)$ (by the Newton-Raphson step) without affecting the output tracking behavior (by the projection into a local null space of $\mathbf{h}(t, \cdot)$).

Similar complementarity structures are common in state of the art, including the differential-equation solutions [28, 29, 33] and the iterative algorithms [25, 31, 35]. However, these works did not take full advantage of the cost function's Hessian matrix. On the contrary, we incorporate the Hessian $\mathbf{R}(t, \mathbf{x})$ of augmented cost function in three spots:

1. as weighting in the pseudoinverse in Component I,
2. as weighting in the null-space projection in Component II,
3. to constitute a Newton-Raphson step $-\mathbf{R}(t, \mathbf{x})^{-1} \mathbf{r}(t, \mathbf{x})$ rather than the steepest descent $-\mathbf{r}(t, \mathbf{x})$ in Component II.

This enables OTC to achieve a rapid exponential convergence.

Computational complexity

The time complexity $\mathcal{T}(\text{OTC})$ of OTC can be determined by counting the number of arithmetic operations in (27), which is dominated by inverting $\mathbf{B}(\mathbf{x}) \in \mathbb{R}^{d_x \times d_x}$ and evaluating $\boldsymbol{\eta}(t, \mathbf{x}, \mathbf{y}_{\text{ref}})$. The function $\boldsymbol{\eta}$, due to its close relation with Newton-Raphson iteration, is dominated by constituting $\mathbf{r}(t, \mathbf{x})$ and $\mathbf{R}(t, \mathbf{x})$ and inverting a

$(d_x + d_y)$ -by- $(d_x + d_y)$ matrix. This means,

$$\mathcal{T}(\text{OTC}) = \mathcal{O}(d_x^3) + \mathcal{O}(d_c^2 d_x) + \mathcal{O}(d_c d_x^2) + \mathcal{O}((d_x + d_y)^3) \quad (28)$$

plus the operations required for evaluating functions of \mathbf{x} and their derivatives (e.g., \mathbf{h} and \mathbf{H}). The reader may refer to SI, Section 3 for a detailed deduction and expression.

The space complexity $\mathcal{S}(\text{OTC})$ of OTC is dominated by $\mathbf{R}(t, \mathbf{x}) \in \mathbb{R}^{d_x \times d_x}$, $\mathbf{H}(t, \mathbf{x}) \in \mathbb{R}^{d_y \times d_x}$, and an intermediate d_c -by- d_c matrix for constituting $\mathbf{R}(t, \mathbf{x})$ (see SI, Section 3). This means

$$\mathcal{S}(\text{OTC}) = \mathcal{O}(d_x^2) + \mathcal{O}(d_y d_x) + \mathcal{O}(d_c^2). \quad (29)$$

Traditional approaches solving the control problem for (1) and (2) involves iterative algorithms such as SQP [24, 25, 35]. A local optimum χ^{\otimes} , which results after sufficiently many iterations, is converted to \mathbf{u} by resolving (1a) (this involves inverting $\mathbf{B}(\mathbf{x})$) [6, 48, 49]. Under the best-case assumption, i.e.,

- (2) is a convex optimization problem and
- the initial guess $\chi^{[0]}(t)$ at every time instant $t \geq 0$ is sufficiently close to a local minimizer and satisfies all inequality and equality constraints,

the time complexity $\mathcal{T}(\text{SQP})$ of this SQP-based method is

$$\begin{aligned} \mathcal{T}(\text{SQP})(t) &= \mathcal{O}(d_x^3) + \sum_{k=1}^{\mathcal{O}(\sqrt{d_c} \log(d_c \ell(t)))} \left(\mathcal{O}(d_c d_x) + \mathcal{O}((d_x + d_y + d_a[k])^3) \right) \\ &= \underbrace{\mathcal{O}(d_x^3) + \mathcal{O}(\sqrt{d_c} \log(d_c \ell(t)))}_{\substack{\text{number of iterations} \\ [26, 27]}} \times \underbrace{\mathcal{O}((d_x + d_y + d_c)^3)}_{\substack{\text{number of operations} \\ \text{within an iteration [25, 35]}}} \end{aligned} \quad (30)$$

plus the operations required for evaluating functions of \mathbf{x} and their derivatives (e.g., \mathbf{h} and \mathbf{H}) within each iteration. Herein, $d_a[k] \in [0, d_c]$ is the number of active inequality constraints [24, 25, 35] at the k -th iteration, and the quantity $\ell(t)$ is time-variant due to the time-variant property of (2) and in general, $\ell(t) \gg 1$. The reader may refer to SI, Section 3 for an overview of SQP algorithm and a detailed deduction of $\mathcal{T}(\text{SQP})(t)$ including the formula of $\ell(t)$.

The space complexity $\mathcal{S}(\text{SQP})$ of SQP is dominated by the $(d_x + d_y + d_a[k])$ -by- $(d_x + d_y + d_a[k])$ coefficient matrix in any iteration (see SI, Section 3). This means

$$\mathcal{S}(\text{SQP}) = \mathcal{O}((d_x + d_y + d_c)^2). \quad (31)$$

It may become practically more usable if (28)–(31) are written in a more compact form. In fact, $d_y \ll d_x$ and $d_c \propto d_x$ is a valid assumption in most practical situations (see Section *Numerical examples*). This allows us to simplify (28)–(31) without losing practical meanings. As a result,

$$\mathcal{T}(\text{OTC}) = \mathcal{O}(d_x^3), \quad \mathcal{S}(\text{OTC}) = \mathcal{O}(d_x^2), \quad (32a)$$

$$\mathcal{T}(\text{SQP})(t) = \mathcal{O}(\sqrt{d_x} \log(d_x \ell(t))) \times \mathcal{O}(d_x^3), \quad \mathcal{S}(\text{SQP}) = \mathcal{O}(d_x^2). \quad (32b)$$

Analogously, the average time complexity of SQP per time step for solving (23) is $\frac{1}{N} \times \mathcal{O}(\sqrt{Nd_x} \log(Nd_x \ell)) \times \mathcal{O}((Nd_x)^3)$ and the space complexity is $\mathcal{O}((Nd_x)^2)$. They are way higher than those of OTC.

Numerical examples

In order to demonstrate OTC's behavior and performance, we select four examples: one comprehensive, purely mathematical example (Example M1) and three real-world problems covering autonomous systems (Example R1), neuromechanics (Example R2), and economics (Example R3). For Examples R1–R3, we apply, in addition to OTC (with $K_x = 500$), the state-of-the-art method SQP [35] as the reference for comparison. All examples are implemented and computed in MATLAB[®] R2020b (The MathWorks, Inc., USA) on a personal computer with Intel[®] Core™ i9-10900K CPU (10×3.70 GHz) and DDR4 RAM of 4×16 GB, where we use the classical Runge-Kutta (RK4) method to solve ordinary differential equations. Prior to the numerical computation, we built MATLAB executable (MEX) functions (for OTC and for SQP) to maximize the code execution efficiency. Parallel computing was not applied.

Example M1

In terms of the system and problem class (1)–(3), we construct this comprehensive example as follows:

$$\mathbf{x} = [x_1 \ x_2]^\top, \quad \mathbf{f}_A(\mathbf{x}) = \frac{1}{\mathbf{x}^\top \mathbf{x} + 0.001}, \quad \mathbf{B}(\mathbf{x}) = (\mathbf{x}^\top \mathbf{x} + 1)\mathbf{I}, \quad (33a)$$

$$h(t, \mathbf{x}) = -6t + (5x_1 + 25x_2^2 - 7)^2 + (25x_1^2 + 5x_2 - 11)^2 - 1, \quad y_{\text{ref}} = 0, \quad (33b)$$

$$\mathbf{g}(t, \mathbf{x}) = \begin{bmatrix} 1 & 0 \\ -1 & 0 \\ 0 & 1 \\ 0 & -1 \\ \frac{209}{100 \sin(\pi t/10) - 143} & 1 \\ \frac{\sin(\pi t/10)}{2} + \frac{73}{75} & 1 \\ \frac{77}{8(5 \sin(\pi t/10) + 7)} & -1 \\ \frac{15 \sin(\pi t/10)}{38} - \frac{67}{152} & -1 \end{bmatrix} \mathbf{x} + \begin{bmatrix} -\frac{19}{20} \\ -\frac{19}{20} \\ -\frac{19}{20} \\ -\frac{19}{20} \\ -\frac{209(3 \sin(\pi t/10) - 10)}{10(100 \sin(\pi t/10) - 143)} \\ -\frac{3 \sin(\pi t/10)}{10} - 1 \\ -\frac{77(\sin(\pi t/10) + 5)}{40(5 \sin(\pi t/10) + 7)} \\ \frac{3 \sin(\pi t/10)}{10} - 1 \end{bmatrix}, \quad (33c)$$

$$\sigma(t, \mathbf{x}) = \sqrt{(\mathbf{x} - \mathbf{p}(t))^\top \mathbf{P}(t) (\mathbf{x} - \mathbf{p}(t)) + 0.001 + 0.001 (\mathbf{x} - \mathbf{p}(t))^\top (\mathbf{x} - \mathbf{p}(t))}, \quad (33d)$$

$$\mathbf{P}(t) = \begin{bmatrix} \frac{9t + 9t \cos(4\pi^2 \sin(\pi t/100)) + 40}{18t + 40} & \frac{9t \sin(4\pi^2 \sin(\pi t/100))}{18t + 40} \\ \frac{9t \sin(4\pi^2 \sin(\pi t/100))}{18t + 40} & \frac{9t \sin(2\pi^2 \sin(\pi t/100))^2 + 20}{9t + 20} \end{bmatrix}, \quad (33e)$$

$$\mathbf{p}(t) = \begin{bmatrix} -\frac{2 \sin(\pi t/5)}{3} - \frac{10 \sin(3\pi t/10)}{27} \\ \frac{2 \cos(\pi t/5)}{3} - \frac{10 \cos(3\pi t/10)}{27} \end{bmatrix}. \quad (33f)$$

This example is constructed to have high degrees of nonlinearity in the state, output, and cost functions, along with time-variance in these functions and the boundary constraints. These features make it a suitable lowest-dimensional representative of the system and problem class (1)–(3). The time evolution of the cost function $\sigma(t, \mathbf{x})$, equality constraint $\mathbf{y}_{\text{ref}} = \mathbf{h}(t, \mathbf{x})$, and inequality constraint $\mathbf{0} \geq \mathbf{g}(t, \mathbf{x})$ are illustrated in Figure 2.

Example R1: control allocation of multiple drones

The control allocation problem of drones (omnidirectional micro aerial vehicles) aims to determine the optimal distribution of control inputs among various actuators to achieve the desired wrench for flight, maneuverability, and/or interaction with the environment, while considering constraints such as payload capacity [49]. In this example, we establish scenarios in which n VoliroX drones [37] move a hollow sphere following a predefined trajectory. In each scenario, the sphere is of a different size and weight, and, correspondingly, there is a different number of drones ($n \in \{16, 36, 64, 100, 144, 196, 256, 400\}$). In terms of the system and problem class (1)–(2), we construct this example as follows:

- $\mathbf{x} = [\mathbf{x}_{(1)}^\top \ \mathbf{x}_{(2)}^\top \ \cdots \ \mathbf{x}_{(n)}^\top]^\top$, where $\mathbf{x}_{(i)} \in \mathbb{R}^{24}$ is the effective state of 12 tiltrotors [37]. This implies $d_x = 24n$.
- $\mathbf{f}_A(\mathbf{x}) = -100\mathbf{x}$ and $\mathbf{B}(\mathbf{x}) = 100\mathbf{I}$.
- $\mathbf{h}(t, \mathbf{x})$ and $\mathbf{y}_{\text{ref}}(t)$: by knowing the inverse-dynamics models of the object and drones, i.e., the wrench $\mathbf{h}_o(\mathbf{p}_o(t), \dot{\mathbf{p}}_o(t), \ddot{\mathbf{p}}_o(t))$ that is required to move the object along the trajectory $\mathbf{p}_o(t)$ and the wrench $\mathbf{h}_d(\mathbf{p}_{d(i)}(t), \dot{\mathbf{p}}_{d(i)}(t), \ddot{\mathbf{p}}_{d(i)}(t), \mathbf{x}_{(i)})$ that a moving drone (along the trajectory $\mathbf{p}_{d(i)}(t)$ for the i -th drone) is still able to exert to its environment [37], we are able to formulate

$$\mathbf{y} = \mathbf{h}_o(\mathbf{p}_o(t), \dot{\mathbf{p}}_o(t), \ddot{\mathbf{p}}_o(t)) + \sum_{i=1}^n \mathbf{h}_d(\mathbf{p}_{d(i)}(t), \dot{\mathbf{p}}_{d(i)}(t), \ddot{\mathbf{p}}_{d(i)}(t), \mathbf{x}_{(i)}) \quad (34)$$

as the deficient part $\mathbf{y} \in \mathbb{R}^6$ in wrench for moving the complexity composed of the object and all n drones following predefined trajectories. This implies $\mathbf{y}_{\text{ref}} = \mathbf{0}$. All wrenches and poses are expressed in the same inertial frame of reference. We further assume that there is no relative movement between any drone and the object, i.e., there exists a fixed relation

$$\mathbf{p}_{d(i)} = \boldsymbol{\psi}_{d(i)}(\mathbf{p}_o) \quad (35)$$

between any $\mathbf{p}_{d(i)}$ and \mathbf{p}_o . Provided that $\mathbf{p}_o(t)$ is given explicitly as a function of t (see below), inserting it and (35) into (34) yields the linear time-variant output function

$$\mathbf{y} = \mathbf{h}(t, \mathbf{x}) = \mathbf{H}(t)\mathbf{x} + \mathbf{b}(t)$$

- The object’s pose $\mathbf{p}_o(t)$ is a minimum-jerk trajectory [50] predefined for $t \in [0\text{s}, 1.5\text{s}]$ subject to boundary conditions

$$\mathbf{p}_o(t \leq 0.25\text{s}) = [0\text{m} \ 0\text{m} \ 0\text{m} \ 0\text{rad} \ 0\text{rad} \ 0\text{rad}]^\top,$$

$$\mathbf{p}_o(t \geq 1.25 \text{ s}) = [2 \text{ m} \ 2 \text{ m} \ 2 \text{ m} \ 0 \text{ rad} \ 0 \text{ rad} \ 0 \text{ rad}]^\top.$$

The trajectory is created numerically at 2000 samples/second.

- $\mathbf{g}(t, \mathbf{x})$: the drones' actuator state \mathbf{x} must be such that ^{a)}every drone is allowed to push, but not pull, the object with a normal force $\geq 1 \text{ N}$ (i.e., drones and object are always in contact and no relative sliding between them). Further, ^{b)}every actuator must operate within its payload capacity. This means in total $d_c = n + 2d_x$ inequality constraints. The resulting formula is a function of \mathbf{x} as well as $\mathbf{p}_{d(i)}$ (meaning, of \mathbf{p}_o , cf. (35), and ultimately, of t).
- $\sigma(t, \mathbf{x}) := \mathbf{x}^\top \mathbf{I} \mathbf{x}$ is chosen according to the state of the art [37, 49].

Other details about this established example are:

- The contact points between the object and the drones are equidistant on the object's spherical surface.
- The number n of drones is chosen corresponding to the object's radius such that there is adequate spacing between each two adjacent drones.
- The object's mass is chosen realistically in accordance with the its radius.

Example R2: muscle-force distribution

In biomechanics, the muscle-force distribution problem deals with the determination of muscle activations and/or ligament forces—within their physiological boundaries—that produce a multijoint limb movement while resisting possible external forces [1, 34, 51]. In this example, we establish scenarios based on the human shoulder-arm model [34] ($d_y = 12$ joints, 42 muscles, and 2 ligamentous elements). We extend this model such that each muscle is composed of $2^n - 1$ actuators with different sizes of physiological cross-section area (PCSA), while the combined force producing capability and characteristics of each muscle remain unchanged. This results in altogether $d_x = 2 + 42 \times (2^n - 1)$ force producing elements. This extension combines in principle the muscle-force distribution [1, 34, 51] and the motor-unit recruitment [2]. In terms of the system and problem class (1)–(2), we summarize the model details as follows:

- the state is the activation level of $42 \times (2^n - 1)$ muscle actuators and the normalized force magnitude of 2 ligamentous elements.
- We obtain $\mathbf{f}_A(\mathbf{x})$ and $\mathbf{B}(\mathbf{x})$ from the nonaffine muscle-activation dynamics model in [34] with the aid of first-order Taylor expansion at $\mathbf{u} = \mathbf{0}$.
- $\mathbf{h}(t, \mathbf{x})$: a nonlinear function of \mathbf{x} , muscle lengths and the change rates, joint-space generalized coordinate produces the joint-space generalized force \mathbf{y} . We obtain the time-variant function $\mathbf{h}(t, \mathbf{x})$ by knowing the relevant quantities as functions of t . Details are provided in [34].
- We calculate the reference $\mathbf{y}_{\text{ref}}(t)$ for joint-space generalized force from a recorded human shoulder-arm movement in [52, 53] (duration $\approx 4.27 \text{ s}$, interpolated to 2000 samples/second) by using the joint-space inverse-dynamics model [34].
- $\mathbf{g}(t, \mathbf{x})$: time-invariant box constraint $\mathbf{x} \in [0, 1]^{d_x}$ ($\Rightarrow d_c = 2d_x$) accounting for the physiological boundaries.
- $\sigma(t, \mathbf{x}) := \mathbf{x}^\top \mathbf{Q} \mathbf{x}$ with different \mathbf{Q} : identity matrices [34], diagonal matrices of PCSA values (diag. n) [54], almost fully occupied SPD matrices reflecting muscle

synergies of the concerned movement (SPD1. n) and of a difference movement (SPD2. n) [52].

Example R3: portfolio optimization

As one of the fundamental frameworks for portfolio optimization, Markowitz mean-variance problem aims to find the optimal allocation of assets by considering the trade-off between expected return and risk, as measured by mean and covariance, respectively, of the historical market data [9]. In this example, we establish scenarios for *the mean-variance problem with prescribed reward* [9]. We deploy real-world data of weekly returns on 6 markets with $d_x \in \{28, 49, 82, 83, 442, 1203\}$ assets over > 10 years until 2015/2016 [55]. We apply moving-average filter (window size 52 weeks) to obtain time-varying expected returns $\mathbf{p}(t) \in \mathbb{R}^{d_x}$ of and covariance matrix $\mathbf{Q}(t)$ among d_x assets. We select the data of the latest year where the established time-variant optimization problem (2) is feasible and interpolated them to 2000 samples/year. In terms of the system and problem class problem class (1)–(2), we summarize this example as follows:

$$\begin{aligned} f_A(\mathbf{x}) &= -100\mathbf{x}, & \mathbf{B}(\mathbf{x}) &= 100\mathbf{I}, \\ \mathbf{h}(t, \mathbf{x}) &= \begin{bmatrix} \mathbf{p}(t)^\top \mathbf{x} \\ \sum_{i=1}^{d_x} x_i \end{bmatrix}, & \mathbf{y}_{\text{ref}}(t) &= \begin{cases} [0 \ 0]^\top & \text{if } \exists i : p_i(t) > 0 \\ [p_{\text{am}}(t) \ 1]^\top & \text{otherwise} \end{cases}, \\ \mathbf{g}(t, \mathbf{x}) &= \begin{bmatrix} \mathbf{x} - 1 \\ -\mathbf{x} \end{bmatrix}, & \sigma(t, \mathbf{x}) &= \mathbf{x}\mathbf{Q}(t)\mathbf{x}, \end{aligned}$$

where $p_{\text{am}}(t)$ is the arithmetic mean of the positive elements in $\mathbf{p}(t)$.

Evaluation

In order to quantitatively assess the accuracy of OTC in comparison to that of SQP, we define the following *accuracy metrics*:

$$\begin{aligned} E_x &= \frac{1}{t_f} \int_0^{t_f} \frac{1}{d_x} \|\mathbf{x}(t) - \boldsymbol{\chi}^\circledast(t)\|_1 dt, \\ E_\sigma &= \frac{\int_0^{t_f} \sigma(t, \mathbf{x}(t)) dt}{\int_0^{t_f} \sigma(t, \boldsymbol{\chi}^\circledast(t)) dt}, \end{aligned}$$

where t_f is the final time instant of $\mathbf{x}(t)$ and $\boldsymbol{\chi}^\circledast(t)$. These two metrics measure the closeness of the OTC’s trajectory $\mathbf{x}(t)$ to the optimal one $\boldsymbol{\chi}^\circledast(t)$. Specifically, the closer E_x is to zero and E_σ is to one, the more accurate OTC is.

For evaluating the computation time, we measure the time duration $\tau_{\text{C,OTC}}(t)$ ($\tau_{\text{C,SQP}}(t)$) needed to complete computation for the sample at time instant t with OTC (SQP). This time-variant quantity allows us to compare probability distribution of OTC’s and SQP’s computation time duration. Besides, we analyze the growth of

average computation time

$$\bar{\tau}_{C,\square} := \frac{1}{t_f} \int_0^{t_f} \tau_{C,\square}(t) dt$$

with problem size d_x by using the trendlines

$$\begin{aligned} \bar{\tau}_{C,\text{OTC}} &= (p_1 d_x + p_2)^3, \\ \bar{\tau}_{C,\text{SQP}} &= (p_4 d_x + p_5)^{3.5} \log(p_6 (p_4 d_x + p_5)), \end{aligned}$$

corresponding to \mathcal{T} (OTC) and \mathcal{T} (SQP) in (32), respectively, Note that $d_y \ll d_x$ and $d_c \propto d_x$ in Examples R1–R3.

Outlook into state-constrained control

In absence of cost function σ the system and problem class (1)–(3) can be considered as a state-constrained system

$$\dot{\mathbf{x}} = \mathbf{f}_A(\mathbf{x}) + \mathbf{B}(\mathbf{x})\mathbf{u}, \quad \mathbf{x}(t) \in \mathcal{X}(t) := \{ \boldsymbol{\varphi} \in \mathbb{R}^{d_x} \mid \mathbf{h}(t, \boldsymbol{\varphi}) = \mathbf{0} \wedge \mathbf{g}(t, \boldsymbol{\varphi}) \leq \mathbf{0} \}. \quad (36)$$

Given the state-constraining nature of OTC, we conclude that the controller

$$\mathbf{u} = \boldsymbol{\omega}(t, \mathbf{x}, \mathbf{v}) := \mathbf{B}(\mathbf{x})^{-1} \left(-\mathbf{f}_A(\mathbf{x}) + K_x \boldsymbol{\omega}_A(t, \mathbf{x}) + \boldsymbol{\Omega}_B(t, \mathbf{x})\mathbf{v} \right) \quad (37)$$

with a new input $\mathbf{v} \in \mathbb{R}^{d_x}$ provides an admissible control \mathbf{u} . Herein, $\boldsymbol{\omega}_A$ is a variant of $\boldsymbol{\eta}$ (11) in absence of cost function σ and when $\mathbf{y}_{\text{ref}} = \mathbf{0}$, and the matrix $\boldsymbol{\Omega}_B(t, \mathbf{x})$ projects \mathbf{v} into a local null space of $\mathbf{h}(t, \cdot)$ and $\mathbf{g}(t, \cdot)$. This means, $\mathbf{x}(t)$ of (36) with (37) converges exponentially to $\mathcal{X}(t)$ as $t \geq 0$ increases, regardless of \mathbf{v} 's value. The reader may refer to SI, Section 6 for the formulae of $\boldsymbol{\omega}_A$ and $\boldsymbol{\Omega}_B$ (see SI (74)).

By inserting the admissible control \mathbf{u} (37) into (36), the state-constrained control problem is reduced to the simpler unconstrained one; that is

$$\dot{\mathbf{x}} = K_x \boldsymbol{\omega}_A(t, \mathbf{x}) + \boldsymbol{\Omega}_B(t, \mathbf{x})\mathbf{v}.$$

One can use standard control methods [47] such as feedback linearization, sliding mode control, or, when applicable, linear-quadratic regulator (LQR) [41] to find \mathbf{v} . This means, OTC provides a way for generalizing a wide spectrum of control methods to accommodate state constraints. In SI, Section 6, we present a state-constrained LQR with both mathematical derivation and numerical example. We leave generalization of other control methods for future work.

Moreover, (36) is commonly accompanied with an output function

$$\mathbf{z} = \mathbf{f}_C(t, \mathbf{x})$$

and it has been a challenge to find an optimal trajectory for constrained systems such that the output \mathbf{z} eventually reaches a goal \mathbf{z}_g . If \mathbf{z}_g is somehow on the path that is generated by a state-constrained optimal control, then the latter is the optimal

trajectory planner (see SI, Section 6 for exemplary illustration). This insight points to a promising direction in solving optimal trajectory planning problems using closed-form feedback controllers.

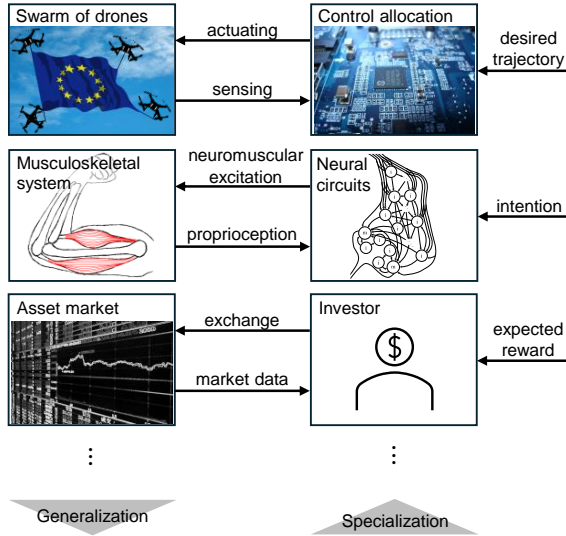
Supplementary information. Mathematical deduction and derivation of OTC, analysis of OTC's convergence behavior and computational complexity, extended numerical results, and preliminary deduction of state-constrained optimal control.

Code availability. We provide the MATLAB codes of all numerical examples, including M1, R1, R2, R3, and the one for state-constrained LQR. These codes are accessible for download at this link.

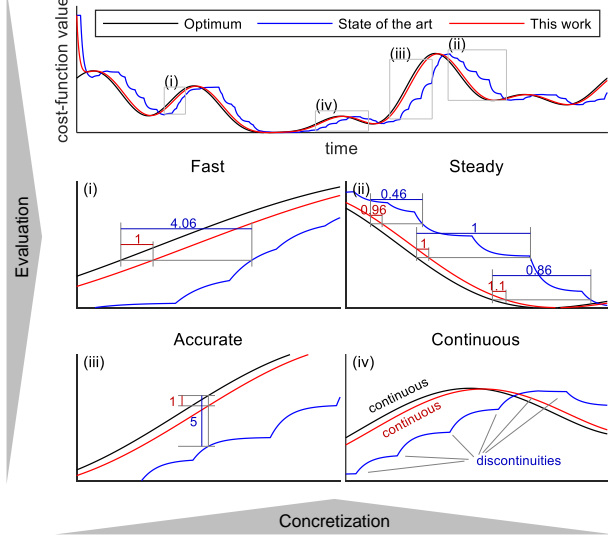
Acknowledgements. The authors gratefully acknowledge the funding of this work by the Alfred Krupp von Bohlen und Halbach Foundation, the European Union's Horizon 2020 research and innovation programme as part of the project SoftPro (grant no. 688857), the Lighthouse Initiative Geriatrics by StMWi Bayern (Project X, grant no. 5140951), and LongLeif GaPa gGmbH (Project Y, grant no. 5140953), as well as the German Federal Ministry of Education and Research (BMBF) funding as part of the project ALD (grant no. 16ME0539K).

Author contributions. T. Hu and S. Haddadin developed the theory and methods. T. Hu developed and conducted the numerical experiments. Both authors interpreted the results. Both authors conceptualized, T. Hu wrote, and S. Haddadin edited the manuscript. Both authors read and approved the final paper.

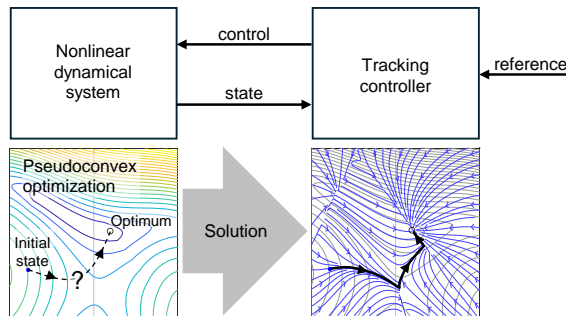
Physical systems and real-world problems



Performance



General system and problem class



System behavior

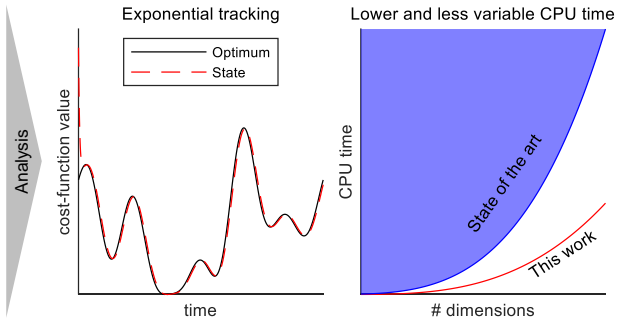


Fig. 1 This work aims at solving pseudoconvex optimization problems for nonlinear dynamical systems by a closed-form tracking controller. Its efficiency and superior performance over state-of-the-art methods are proven by rigorous mathematical analysis as well as demonstrated by solving challenging high-dimensional real-world problems.

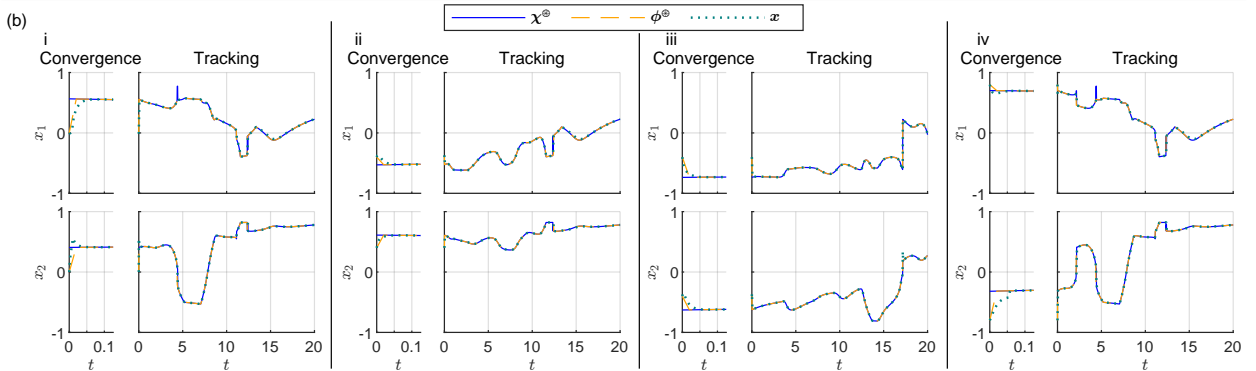
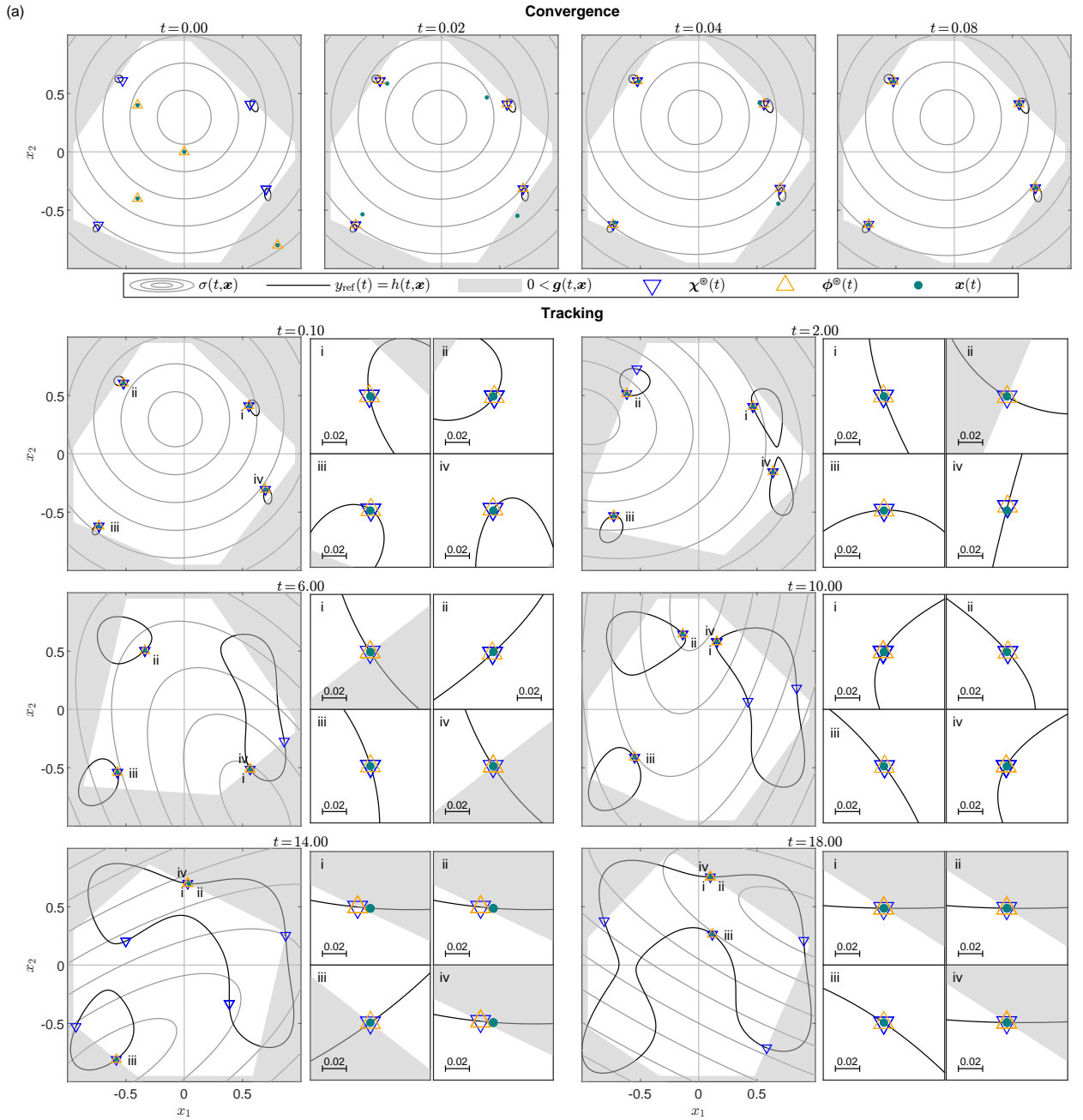


Fig. 2 Example M1: A two-dimensional system (33) controlled by the OTC with $K_x = 100$. The trajectories $\mathbf{x}(t)$ (marked as i, ii, iii, iv) starting from different initial conditions $\mathbf{x}(0)$ follow the corresponding $\chi^\circ(t)$ and $\phi^\circ(t)$ over time t . (a) Trajectories of $\mathbf{x}(t)$ (teal), $\chi^\circ(t)$ (blue), and $\phi^\circ(t)$ (orange) in the two-dimensional space along with cost function and constraints. Each subplot corresponds to a snapshot at time instant t as indicated. An animation is available in the Supplementary Video. (b) Exponentially convergent tracking of $\mathbf{x}(t)$ to the closest $\chi^\circ(t)$ and $\phi^\circ(t)$. Each column represents the time evolution starting from a different initial condition. A zoomed-in perspective to the initial transient phase is provided on the left in each column.

Table 1 Computational behavior of all real-world examples. Refer to Subsection *Numerical examples* for detailed description.

n	$\min_{\chi} \sigma(t, \chi)$ s.t. $\mathbf{0} = \mathbf{h}(t, \chi) - \mathbf{y}_{\text{ref}}(t) \wedge \mathbf{0} \geq \mathbf{g}(t, \chi)$						Solvers		Remark
	d_x	d_y	d_c	Hessian $\mathbf{Q} := \frac{\partial}{\partial \chi} \frac{\partial \sigma(t, \chi)}{\partial \chi}$	Equality constraint	Inequality constraint	OTC	SQP	
Example R1: control allocation among n drones moving a spherical object									
16	384	6	784	identity matrices	time-variant linear	time-variant linear	✓	✓	1.0 m, 33.90 kg
36	864		1764				✓	✓	1.5 m, 76.29 kg
64	1536		3136				✓	✓	2.0 m, 135.65 kg
100	2400		4900				✓	✓	2.5 m, 211.97 kg
144	3456		7056				✓	✓	3.0 m, 305.26 kg
196	4704		9604				✓	✓	3.5 m, 415.51 kg
256	6144		12544				✓	✓	4.0 m, 542.73 kg
400	9600	19600	✓	✓ [†]	5.0 m, 848.06 kg				
Example R2: muscle-force distribution among $\approx d_x$ muscle actuators for performing a limb movement									
1	44	12	88	identity matrices	time-variant nonlinear	time-invariant box	✓	✓	
2	128		256				✓	✓	
3	296		592				✓	✓	
4	632		1264				✓	✓	
5	1304		2608				✓	✓	
1	44		88	time-invariant diagonal matrices			✓	✓	
2	128		256				✓	✓	
3	296		592				✓	✓	
4	632		1264				✓	✓	
5	1304		2608				✓	✓	
1	44		88	time-invariant symmetric and positive definite matrices [§]			✓	✓	
2	128		256				✓	✓	
3	296		592				✓	✓	
4	632		1264				✓	✓	
5	1304		2608				✓	✓	
1	44	88	time-invariant symmetric and positive definite matrices [§]	✓	✓				
2	128	256		✓	✓				
3	296	592		✓	✓				
4	632	1264		✓	✓				
5	1304	2608		✓	✓				
Example R3: portfolio optimization for d_x assets									
1	28	2	56	time-variant symmetric and positive definite matrices	time-variant linear	time-invariant box	✓	✓	
2	49		98				✓	✓	
3	82		164				✓	✓	
4	83		166				✓	✓	
5	442		884				✓	✓	
6	1203		2406				✓ [‡]	✓ [‡]	

All input data were created at or interpolated to 2000 samples per second (Examples R1 and R2) or per year (Example R3), except those with [†]500 samples/second and [‡]1000 samples/year due to practical limitations.

[§] These two types of time-invariant symmetric and positive definite matrices reflect different muscle-coactivation pattern.

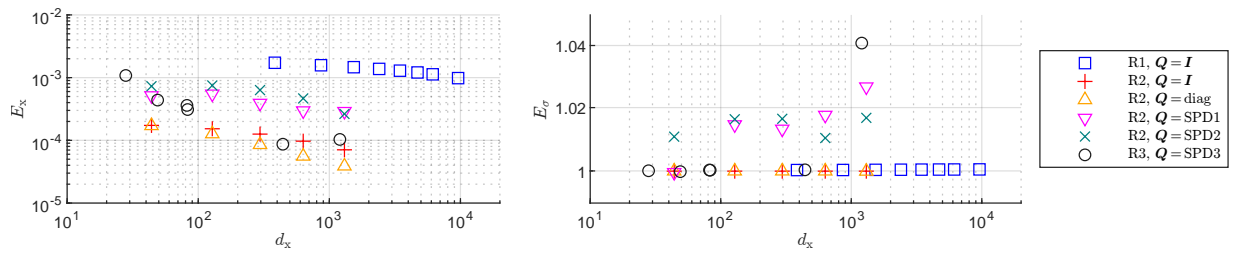


Fig. 3 Values of accuracy metrics E_x (absolute accuracy) and E_σ (relative accuracy) of OTC for Examples R1–R3 of real-world problems. Each data point represents a numerical scenario characterized by the system’s dimension d_x and the cost function’s Hessian matrix \mathbf{Q} (identity matrices \mathbf{I} , dagonal matrices, and three different types of symmetric and positive definite matrices).

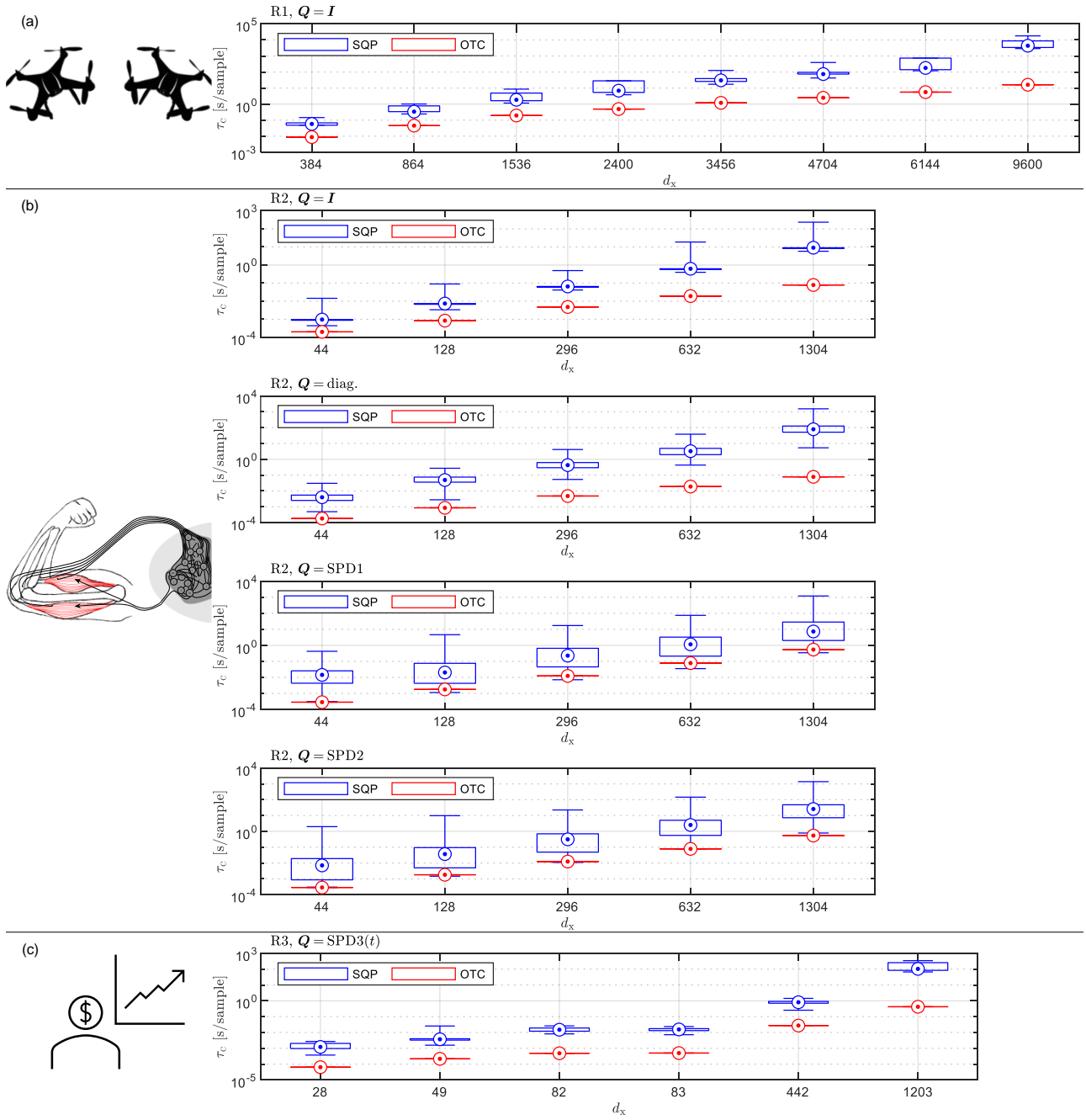


Fig. 4 The box plots of the time duration τ_C needed to compute each sample using SQP (blue) and OTC (red). Each plot represents a numerical scenario characterized by the system's dimension d_x and the cost function's Hessian matrix Q (identity matrices I , diagonal matrices, and three different types of symmetric and positive definite matrices). In each plot, the data are presented as median values (the circled dot inside each box) along with the 25th and 75th percentiles (the bottom and top edges of each box) as well as minima and maxima (the whiskers attached to each box). (a) Example R1 (control allocation among multiple drones). (b) Example R2 (muscle-force distribution). (c) Example R3 (portfolio optimization).

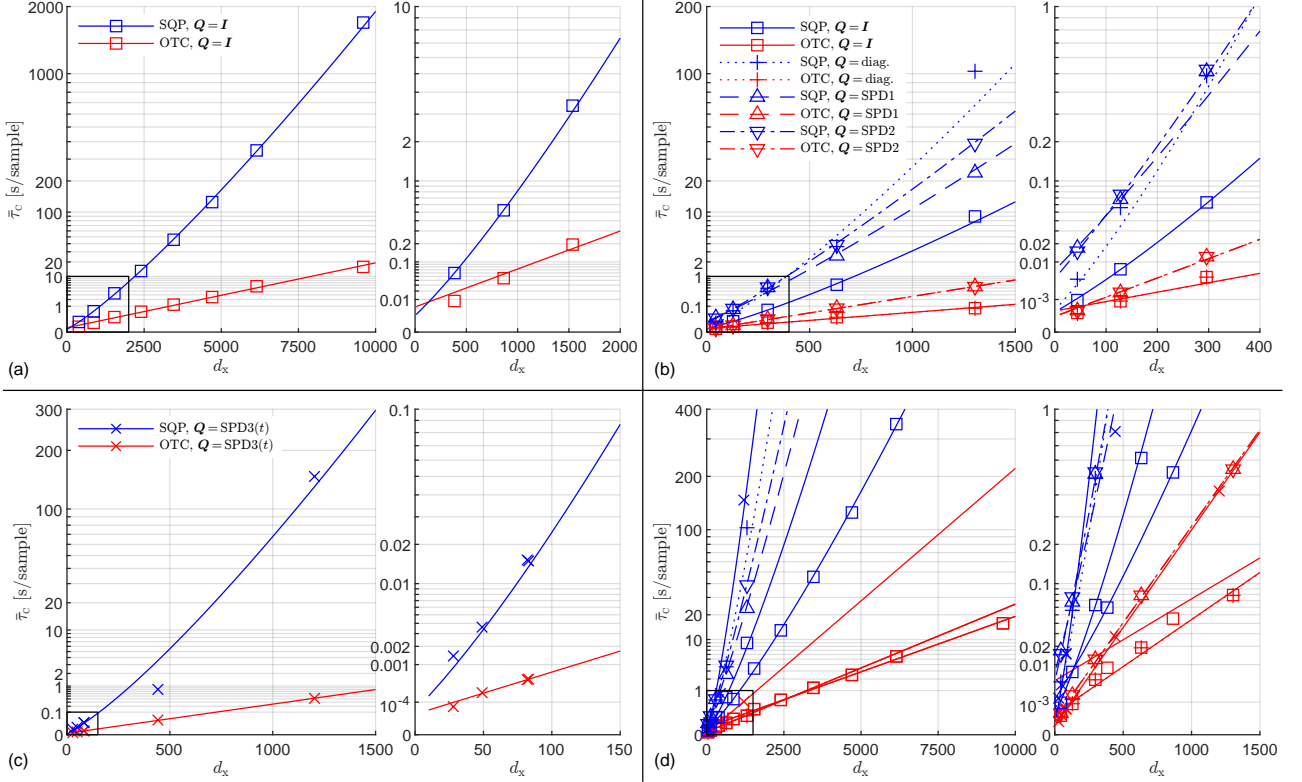


Fig. 5 The average time duration $\bar{\tau}_C$ required to compute each sample as a function of the system's dimension d_x . (a) Example R1 (control allocation among multiple drones). (b) Example R2 (muscle-force distribution). (c) Example R3 (portfolio optimization). (d) Examples R1–R3, sharing the same color/line/marker scheme as Subfigures (a)–(c); refer to them for legends. The quantity $\bar{\tau}_C$ is displayed on the cube-root scale, while d_x on a linear scale. Each marker represents a scenario characterized by the system's dimension d_x and the cost function's Hessian matrix \mathbf{Q} (identity matrices \mathbf{I} , diagonal matrices, and three different types of symmetric and positive definite matrices). In each subfigure, the right plot provides a zoomed-in perspective of the region outlined by a black box in the left plot. The trendlines are the best-fit curves according to (5) and (6).

References

- [1] Erdemir, A., McLean, S., Herzog, W., Bogert, A.J.: Model-based estimation of muscle force exerted during movements. *Clin. Biomech.* **22**, 131–154 (2007)
- [2] Marshall, N., Glaser, J., Trautmann, E., Amematsro, E., Perkins, S., Shadlen, M., Abbott, L., Cunningham, J., Churchland, M.: Flexible neural control of motor units. *Nature Neuroscience* **25**, 1–13 (2022) <https://doi.org/10.1038/s41593-022-01165-8>
- [3] Orth, J., Thiele, I., Palsson, B.: What is flux balance analysis? *Nature biotechnology* **28**, 245–8 (2010) <https://doi.org/10.1038/nbt.1614>
- [4] Schuetz, R., Zamboni, N., Zampieri, M., Heinemann, M., Sauer, U.: Multidimensional optimality of microbial metabolism. *Science* **336**(6081), 601–604 (2012) <https://doi.org/10.1126/science.1216882>
- [5] Naseri, G., Koffas, M.: Application of combinatorial optimization strategies in synthetic biology. *Nature Communications* **11** (2020) <https://doi.org/10.1038/s41467-020-16175-y>
- [6] Allenspach, M., Bodie, K., Brunner, M., Rinsoz, L., Taylor, Z., Kamel, M., Siegwart, R., Nieto, J.: Design and optimal control of a tiltrotor micro-aerial vehicle for efficient omnidirectional flight. *The International Journal of Robotics Research* **39**(10-11), 1305–1325 (2020) <https://doi.org/10.1177/0278364920943654>
- [7] Jaleel, H., Shamma, J.S.: Distributed optimization for robot networks: From real-time convex optimization to game-theoretic self-organization. *Proceedings of the IEEE* **108**(11), 1953–1967 (2020) <https://doi.org/10.1109/JPROC.2020.3028295>
- [8] Izzo, D., Blazquez, E., Ferede, R., Origer, S., De Wagter, C., Croon, G.C.: Optimality principles in spacecraft neural guidance and control. *Science Robotics* **9**(91), 6421 (2024)
- [9] Steinbach, M.: Markowitz revisited: Mean-variance models in financial portfolio analysis. *Society for Industrial and Applied Mathematics* **43**, 31–85 (2001) <https://doi.org/10.1137/S0036144500376650>
- [10] Abdi, H., Beigvand, S.D., Scala, M.L.: A review of optimal power flow studies applied to smart grids and microgrids. *Renewable and Sustainable Energy Reviews* **71**, 742–766 (2017) <https://doi.org/10.1016/j.rser.2016.12.102>
- [11] Wei, W., Wang, J., Li, N., Mei, S.: Optimal power flow of radial networks and its variations: A sequential convex optimization approach. *IEEE Transactions on Smart Grid* **8**(6), 2974–2987 (2017) <https://doi.org/10.1109/TSG.2017.2684183>
- [12] Jha, R.R., Inaolaji, A., Biswas, B.D., Suresh, A., Dubey, A., Paudyal, S.,

- Kamalasadan, S.: Distribution grid optimal power flow (D-OPF): Modeling, analysis, and benchmarking. *IEEE Transactions on Power Systems* **38**(4), 3654–3668 (2023) <https://doi.org/10.1109/TPWRS.2022.3204227>
- [13] Gershman, A., Sidiropoulos, N.D., Shahbazpanahi, S., Bengtsson, M., Ottersten, B.: Convex optimization-based beamforming **27**, 62–75 <https://doi.org/10.1109/MSP.2010.936015>
- [14] Matai, R., Singh, S., Mittal, M.L.: Traveling salesman problem: an overview of applications, formulations, and solution approaches. In: Davendra, D. (ed.) *Traveling Salesman Problem*. IntechOpen, Rijeka (2010). Chap. 1. <https://doi.org/10.5772/12909>
- [15] Bouajaja, S., Dridi, N.: A survey on human resource allocation problem and its applications. *Operational Research* **17**, 339–369 (2017)
- [16] Morone, F., Makse, H.A.: Influence maximization in complex networks through optimal percolation. *Nature* **524**, 65–68 (2015)
- [17] Kleidon, A.: Working at the limit: a review of thermodynamics and optimality of the earth system. *Earth System Dynamics* **14**(4), 861–896 (2023) <https://doi.org/10.5194/esd-14-861-2023>
- [18] Leine, R.: The historical development of classical stability concepts: Lagrange, Poisson and Lyapunov stability. *Nonlinear Dynamics* **59**, 173–182 (2010) <https://doi.org/10.1007/s11071-009-9530-z>
- [19] Mironchenko, A.: *Input-to-State Stability: Theory and Applications*. Communications and Control Engineering. Springer, Cham, Switzerland (2023)
- [20] Liu, Y.-Y., Slotine, J.-J., Barabasi, A.-L.: Controllability of complex networks. *Nature* **473**, 167–73 (2011) <https://doi.org/10.1038/nature10011>
- [21] Klamka, J.: Controllability of dynamical systems. a survey. *Bulletin of the Polish Academy of Sciences Technical Sciences* **61**(No 2), 335–342 (2013) <https://doi.org/10.2478/bpasts-2013-0031>
- [22] Montanari, A., Aguirre, L.: Observability of network systems: A critical review of recent results (2020) <https://doi.org/10.1007/s40313-020-00633-5>
- [23] Bernard, P., Andrieu, V., Astolfi, D.: Observer design for continuous-time dynamical systems. *Annual Reviews in Control* **53**, 224–248 (2022) <https://doi.org/10.1016/j.arcontrol.2021.11.002>
- [24] Fletcher, R.: *Practical Methods of Optimization*, 2nd edn. John Wiley & Sons, Chichester, West Sussex, England (1987)
- [25] Nocedal, J., Wright, S.J.: *Numerical Optimization*. Springer, New York, NY, USA

(2006)

- [26] Potra, S.J. F. A.; Wright: Interior-point methods. *J. Comput. Appl. Math.* **124**, 281–302 (2000)
- [27] Boyd, S., Vandenberghe, L.: *Convex Optimization*. Cambridge University Press
- [28] Yamashita, H.: A differential equation approach to nonlinear programming. *Mathematical Programming* **18**, 155–168 (1980)
- [29] Zhou, Z., Shi, Y.: An ODE method of solving nonlinear programming. *Computers & Mathematics with Applications* **34**(1), 97–102 (1997) [https://doi.org/10.1016/S0898-1221\(97\)00101-6](https://doi.org/10.1016/S0898-1221(97)00101-6)
- [30] Xia, Y., Feng, G.: An improved neural network for convex quadratic optimization with application to real-time beamforming. *Neurocomputing* **64**, 359–374 (2005)
- [31] Feppon, F., Allaire, G., Dapogny, C.: Null space gradient flows for constrained optimization with applications to shape optimization. *ESAIM: Control, Optimisation and Calculus of Variations* **26**, 90 (2020) <https://doi.org/10.1051/cocv/2020015>
- [32] Raveendran, R., Mahindrakar, A.D., Vaidya, U.: Dynamical System Approach for Time-Varying Constrained Convex Optimization Problems (2023)
- [33] Allibhoy, A., Cortés, J.: Control Barrier Function Based Design of Gradient Flows for Constrained Nonlinear Programming (2023)
- [34] Hu, T., Kühn, J., Haddadin, S.: Forward and inverse dynamics modeling of human shoulder-arm musculoskeletal system with scapulothoracic constraint. *Computer Methods in Biomechanics and Biomedical Engineering* (2020)
- [35] Optimization Toolbox™ User’s Guide, R2020b edn. The MathWorks, Inc. (2020)
- [36] Bogert, A.J., Geijtenbeek, T., Even-Zohar, O., Steenbrink, F., Hardin, E.C.: A real-time system for biomechanical analysis of human movement and muscle function. *Medical & biological engineering & computing* **51**(10), 1069–1077 (2013)
- [37] Bodie, K., Taylor, Z., Kamel, M., Siegart, R.: Towards efficient full pose omnidirectionality with overactuated mavs. In: Xiao, J., Kröger, T., Khatib, O. (eds.) *Proceedings of the 2018 International Symposium on Experimental Robotics*, pp. 85–95. Springer, Cham (2020)
- [38] Mayne, D.Q., Rawlings, J.B., Rao, C.V., Scokaert, P.O.M.: Constrained model predictive control: Stability and optimality. *Automatica* **36**(6), 789–814 (2000) [https://doi.org/10.1016/S0005-1098\(99\)00214-9](https://doi.org/10.1016/S0005-1098(99)00214-9)

- [39] Schwenzer, M., Ay, M., Bergs, T., Abel, D.: Review on model predictive control: an engineering perspective. *The International Journal of Advanced Manufacturing Technology* **117**, 1327–1349 (2021)
- [40] Eren, U., Prach, A., Kocer, B., Raković, S.V., Kayacan, E., Açıkmeşe, B.: Model predictive control in aerospace systems: Current state and opportunities. *Journal of Guidance, Control, and Dynamics* **40**, 1541–1566 (2017) <https://doi.org/10.2514/1.G002507>
- [41] Mehrmann, V.: *The autonomous linear quadratic control problem: Theory and numerical solution.* (1991)
- [42] Cortes, J.: Discontinuous dynamical systems. *IEEE Control Systems Magazine* **28**(3), 36–73 (2008) <https://doi.org/10.1109/MCS.2008.919306>
- [43] Binazadeh, T., Rahgoshay, M.A.: Robust output tracking of a class of non-affine systems. *Systems Science & Control Engineering* **5**(1), 426–433 (2017) <https://doi.org/10.1080/21642583.2017.1376296>
- [44] Chen, Z., Bai, W., Kong, L.: Robust output tracking control of uncertain non-affine systems with guaranteed tracking error bounds. *International Journal of Control, Automation and Systems* **22**, 1–13 (2024) <https://doi.org/10.1007/s12555-021-0974-3>
- [45] LaSalle, J.: Some extensions of Liapunov’s second method. *IRE Transactions on Circuit Theory* **7**(4), 520–527 (1960) <https://doi.org/10.1109/TCT.1960.1086720>
- [46] Gronwall, T.H.: Note on the derivatives with respect to a parameter of the solutions of a system of differential equations. *Annals of Mathematics* **20**(4), 292–296 (1919)
- [47] Khalil, H.K.: *Nonlinear Systems*, 3rd edn. Prentice-Hall, Inc., Upper Saddle River, NJ, USA (2002)
- [48] Thelen, D.G., Anderson, F.C.: Using computed muscle control to generate forward dynamic simulation of human walking from experimental data. *J. Biomech.* **39**, 1107–1115 (2006)
- [49] Kirchengast, M., Steinberger, M., Horn, M.: Control allocation under actuator saturation: An experimental evaluation. *IFAC-PapersOnLine* **51**(25), 48–54 (2018). 9th IFAC Symposium on Robust Control Design ROCOND 2018
- [50] Ghazaei Ardakani, M.M., Robertsson, A., Johansson, R.: Online minimum-jerk trajectory generation. In: *IMA Conference on Mathematics of Robotics*, Oxford, UK (2015)
- [51] Herzog, W.: Distribution problem in biomechanics. In: Binder, M.D., Hirokawa,

- N., Windhorst, U. (eds.) *Encyclopedia of Neuroscience*, pp. 983–985. Springer, Heidelberg, Germany (2009)
- [52] Hu, T., Kuehn, J., Haddadin, S.: Identification of human shoulder-arm kinematic and muscular synergies during daily-life manipulation tasks. In: *IEEE Int. Conf. Bio. Rob.*, Enschede, the Netherlands, pp. 1011–1018 (2018)
- [53] Averta, G., Barontini, F., Catrambone, V., Haddadin, S., Handjaras, G., Held, J.P.O., Hu, T., Jakubowitz, E., Kanzler, C.M., Kühn, J., Lambercy, O., Leo, A., Obermeier, A., Ricciardi, E., Schwarz, A., Valenza, G., Bicchi, A., Bianchi, M.: U-Limb: A multi-modal, multi-center database on arm motion control in healthy and post-stroke conditions. *GigaScience* **10**(6) (2021) <https://doi.org/10.1093/gigascience/giab043>
- [54] Terrier, A., Aeberhard, M., Michellod, Y., Mullhaupt, P., Gillet, D., Farron, A., Pioletti, D.P.: A musculoskeletal shoulder model based on pseudo-inverse and null-space optimization. *Med. Eng. Phys.* **32**, 1050–1056 (2010)
- [55] Bruni, R., Cesarone, F., Scozzari, A., Tardella, F.: Real-world datasets for portfolio selection and solutions of some stochastic dominance portfolio models **8**, 858–862 <https://doi.org/10.1016/j.dib.2016.06.031>

Supplementary Information

for

Feedback control solves pseudoconvex optimal tracking problems in nonlinear dynamical systems

Tingli Hu and Sami Haddadin*

Chair of Robotics and Systems Intelligence,
MIRMI - Munich Institute of Robotics and Machine Intelligence,
Technical University of Munich,
Georg-Brauchle-Ring 60/62, 80992 München, Germany.

*To whom correspondence should be addressed; E-mail: haddadin@tum.de.

Contents

1	System and problem class	5
2	Feedback controller for optimality	7
2.1	Interior-point iteration	7
2.2	Output tracking controller with full-state feedback	12
2.3	Exponential convergence	14
2.4	Optimal tracking controller	20
3	Computational complexity	25
3.1	Optimal tracking controller	25
3.2	Interior-point algorithm	25
3.3	Sequential quadratic programming	26
3.4	Discussion	28
4	Implementation remark	29
5	Extended numerical results of Examples R1–R3	32

6	State-constrained systems	34
6.1	State-constrained linear-quadratic regulator	35
6.2	Outlook into optimal trajectory planner	35
6.3	Numerical example and result	36
7	Background material	39
7.1	Newton-Raphson method	39
7.2	Stability of slowly varying systems	39

Notation	Description
General	
\mathbb{R}	set of real numbers
$\mathbb{R}_{\geq 0} \subset \mathbb{R}$	set of nonnegative real numbers
$\mathbb{R}_{> 0} \subset \mathbb{R}_{\geq 0}$	set of positive real numbers
$\mathbb{N} \subset \mathbb{R}$	set of natural numbers
$\mathbf{0}$	conformable vector of zeros
\mathbf{O}	conformable matrix of zeros
\mathbf{I}	conformable identity matrix
$t \in \mathbb{R}_{\geq 0}$	time
$\boldsymbol{x} \in \mathbb{R}^{d_x}$	d_x -dimensional general argument of functions
$s \in \mathbb{R}^{d_c}$	d_c -dimensional general argument of functions
$\boldsymbol{x}^\oplus \in \mathbb{R}^{d_x}$	root of system of equations
$\boldsymbol{x}^* \in \mathbb{R}^{d_x}$	equilibrium point
$\dot{\boldsymbol{x}}$	time derivative of $\boldsymbol{x}(t)$, i.e., $\dot{\boldsymbol{x}}(t) := d\boldsymbol{x}(t)/dt$
$(a, b) \subset \mathbb{R}$	$:= \{ \boldsymbol{x} \in \mathbb{R} \mid a < \boldsymbol{x} < b \}$
$[a, b) \subset \mathbb{R}$	$:= \{ \boldsymbol{x} \in \mathbb{R} \mid a \leq \boldsymbol{x} < b \}$
$(a, b] \subset \mathbb{R}$	$:= \{ \boldsymbol{x} \in \mathbb{R} \mid a < \boldsymbol{x} \leq b \}$
$[a, b] \subset \mathbb{R}$	$:= \{ \boldsymbol{x} \in \mathbb{R} \mid a \leq \boldsymbol{x} \leq b \}$
$\mathcal{N}(\boldsymbol{x}^*, \delta) \subset \mathbb{R}^{d_x}$	$:= \{ \boldsymbol{x} \in \mathbb{R}^{d_x} \mid \ \boldsymbol{x} - \boldsymbol{x}^*\ _2 < \delta \}$
$\ \boldsymbol{x}\ , \ \mathbf{A}\ $	norm of vector \boldsymbol{x} or induced norm of matrix \mathbf{A}
$\ \boldsymbol{x}\ _2, \ \mathbf{A}\ _2$	(induced) Euclidean norm
$\mathbf{A}_W^\#$	\mathbf{W} -weighted right pseudoinverse of \mathbf{A}
$K_x, K_y \in \mathbb{R}_{> 0}$	control gain
Dynamical system	
$\boldsymbol{x} \in \mathbb{R}^{d_x}$	state
$\boldsymbol{u} \in \mathbb{R}^{d_x}$	input
$\boldsymbol{y} \in \mathbb{R}^{d_y}$	output
$\boldsymbol{y}_{\text{ref}} \in \mathbb{R}^{d_y}$	reference for \boldsymbol{y}
$\boldsymbol{f}_A : \mathbb{R}^{d_x} \rightarrow \mathbb{R}^{d_x}$	state and input function as in $\dot{\boldsymbol{x}} = \boldsymbol{f}_A(\boldsymbol{x}) + \mathbf{B}(\boldsymbol{x})\boldsymbol{u}$
$\mathbf{B} : \mathbb{R}^{d_x} \rightarrow \mathbb{R}^{d_x \times d_x}$	
$\boldsymbol{h} : \mathbb{R}_{\geq 0} \times \mathbb{R}^{d_x} \rightarrow \mathbb{R}^{d_y}$	time-variant output function as in $\boldsymbol{y} = \boldsymbol{h}(t, \boldsymbol{x})$
$\mathbf{H} : \mathbb{R}_{\geq 0} \times \mathbb{R}^{d_x} \rightarrow \mathbb{R}^{d_y \times d_x}$	Jacobian of $\boldsymbol{h}(t, \cdot)$
$V, U : \mathbb{R}^{d_x} \rightarrow \mathbb{R}_{\geq 0}$	Lyapunov function
Optimization	
$\boldsymbol{\chi} \in \mathbb{R}^{d_x}$	candidate of decision variables
$\boldsymbol{\chi}^{[k]} \in \mathbb{R}^{d_x}$	$\boldsymbol{\chi}$ at the k -th iteration
$\boldsymbol{\chi}^\ominus \in \mathbb{R}^{d_x}$	locally optimal $\boldsymbol{\chi}$
$\sigma : \mathbb{R}_{\geq 0} \times \mathbb{R}^{d_x} \rightarrow \mathbb{R}$	time-variant cost function as in $\min_{\boldsymbol{\chi}} \sigma(t, \boldsymbol{\chi})$
$\boldsymbol{q} : \mathbb{R}_{\geq 0} \times \mathbb{R}^{d_x} \rightarrow \mathbb{R}^{d_x}$	gradient of $\sigma(t, \cdot)$
$\boldsymbol{Q} : \mathbb{R}_{\geq 0} \times \mathbb{R}^{d_x \times d_x} \rightarrow \mathbb{R}^{d_x}$	Hessian of $\sigma(t, \cdot)$

$\mathbf{g}(t, \boldsymbol{\chi}) = \mathbf{G}(t)\boldsymbol{\chi} + \mathbf{c}(t)$ $\mathbf{G}(t) \in \mathbb{R}^{d_c \times d_x}$ $\mathbf{c}(t) \in \mathbb{R}^{d_c}$	time-variant inequality constraint as in $\mathbf{0} \geq \mathbf{g}(t, \boldsymbol{\chi})$
$\beta : \mathbb{R} \rightarrow \mathbb{R}$ $\boldsymbol{\beta} : \mathbb{R}^{d_c} \rightarrow \mathbb{R}^{d_c}$	barrier function
$\rho : \mathbb{R}_{\geq 0} \times \mathbb{R}^{d_x} \rightarrow \mathbb{R}$ $\mathbf{r} : \mathbb{R}_{\geq 0} \times \mathbb{R}^{d_x} \rightarrow \mathbb{R}^{d_x}$ $\mathbf{R} : \mathbb{R}_{\geq 0} \times \mathbb{R}^{d_x} \rightarrow \mathbb{R}^{d_x \times d_x}$	augmented σ gradient of $\rho(t, \cdot)$ Hessian of $\rho(t, \cdot)$
$\boldsymbol{\zeta} \in \mathbb{R}^{d_y}$ $L : \mathbb{R}_{\geq 0} \times \mathbb{R}^{d_x} \times \mathbb{R}^{d_y} \rightarrow \mathbb{R}$ $\boldsymbol{\lambda} : \mathbb{R}_{\geq 0} \times \mathbb{R}^{d_x} \times \mathbb{R}^{d_y} \rightarrow \mathbb{R}^{1 \times (d_x + d_y)}$ $\boldsymbol{\Lambda} : \mathbb{R}_{\geq 0} \times \mathbb{R}^{d_x} \times \mathbb{R}^{d_y} \rightarrow \mathbb{R}^{(d_x + d_y) \times (d_x + d_y)}$ $\boldsymbol{\Lambda}_{xx} : \mathbb{R}_{\geq 0} \times \mathbb{R}^{d_x} \times \mathbb{R}^{d_y} \rightarrow \mathbb{R}^{d_x \times d_x}$	vector of Lagrange multipliers time-variant Lagrange function $L(t, \boldsymbol{\chi}, \boldsymbol{\zeta})$ Jacobian of $L(t, \cdot, \cdot)$ Hessian of $L(t, \cdot, \cdot)$ Hessian of $L(t, \cdot, \boldsymbol{\zeta})$ (w.r.t. the second argument)
$\boldsymbol{\eta} : \mathbb{R}_{\geq 0} \times \mathbb{R}^{d_x} \times \mathbb{R}^{d_y} \rightarrow \mathbb{R}^{d_x}$	iterated function as in $\boldsymbol{\chi}[k+1] = \boldsymbol{\chi}[k] + \boldsymbol{\eta}(t, \boldsymbol{\chi}[k], \mathbf{y}_{\text{ref}})$
Optimal tracking control	
$t_f \in \mathbb{R}_{> 0}$ $\boldsymbol{\phi} : \mathbb{R}_{\geq 0} \rightarrow \mathbb{R}^{d_x}$ $\boldsymbol{\phi}^{\otimes} : \mathbb{R}_{\geq 0} \rightarrow \mathbb{R}^{d_x}$ $\boldsymbol{\varphi} \in \mathbb{R}^{d_x N}$ $\boldsymbol{\varphi}^{\otimes} \in \mathbb{R}^{d_x N}$	final time instant candidate trajectory locally optimal $\boldsymbol{\phi}$ discrete-time representation of $\boldsymbol{\phi}$ for the first N time instants discrete-time representation of $\boldsymbol{\phi}^{\otimes}$ for the first N time instants
$\boldsymbol{y}_{\text{ref}} \in \mathbb{R}^{d_y N}$ $\boldsymbol{\varsigma} : \mathbb{R}^{d_x N} \rightarrow \mathbb{R}$ $\boldsymbol{q} : \mathbb{R}^{d_x N} \rightarrow \mathbb{R}^{d_x N}$ $\boldsymbol{Q} : \mathbb{R}^{d_x N} \rightarrow \mathbb{R}^{(d_x N) \times (d_x N)}$ $\boldsymbol{g} : \mathbb{R}^{d_x N} \rightarrow \mathbb{R}^{d_c N}$ $\boldsymbol{g} : \mathbb{R}^{d_x N} \rightarrow \mathbb{R}^{(d_c N) \times (d_c N)}$ $\boldsymbol{h} : \mathbb{R}^{d_x N} \rightarrow \mathbb{R}^{d_y N}$ $\boldsymbol{H} : \mathbb{R}^{d_x N} \rightarrow \mathbb{R}^{(d_y N) \times (d_y N)}$ $\boldsymbol{\varrho} : \mathbb{R}^{d_x N} \rightarrow \mathbb{R}$ $\boldsymbol{r} : \mathbb{R}^{d_x N} \rightarrow \mathbb{R}^{d_x N}$ $\boldsymbol{R} : \mathbb{R}^{d_x N} \rightarrow \mathbb{R}^{(d_x N) \times (d_x N)}$	discrete-time representation of $\mathbf{y}_{\text{ref}}(t)$ for the first N time instants sum of cost $\sigma(t, \boldsymbol{\phi})$ for the first N discrete time instants gradient of $\boldsymbol{\varsigma}$ Hessian of $\boldsymbol{\varsigma}$ discrete-time representation of $\mathbf{g}(t, \cdot)$ for the first N time instants Jacobian of \boldsymbol{g} discrete-time representation of $\mathbf{h}(t, \cdot)$ for the first N time instants Jacobian of \boldsymbol{h} augmented $\boldsymbol{\varsigma}$ gradient of $\boldsymbol{\varrho}$ Hessian of $\boldsymbol{\varrho}$
Computational complexity	
$\mathcal{T}(\omega)$ $\mathcal{S}(\omega)$ \mathcal{O}	time complexity of operation or procedure ω space complexity of operation or procedure ω Bachmann-Landau big \mathcal{O} notation

1 System and problem class

In this work, we study the time-variant nonlinear input-affine system

$$\dot{\mathbf{x}} = \mathbf{f}_A(\mathbf{x}) + \mathbf{B}(\mathbf{x})\mathbf{u}, \quad (1a)$$

$$\mathbf{y} = \mathbf{h}(t, \mathbf{x}), \quad (1b)$$

where $\mathbf{u} \in \mathbb{R}^{d_x}$ denotes the control input, $\mathbf{x} \in \mathbb{R}^{d_x}$ the state, and $\mathbf{y} \in \mathcal{Y} \subset \mathbb{R}^{d_y}$ the output. The functions $\mathbf{f}_A : \mathbb{R}^{d_x} \rightarrow \mathbb{R}^{d_x}$ and $\mathbf{B} : \mathbb{R}^{d_x} \rightarrow \mathbb{R}^{d_x \times d_x}$ are such that (1a) satisfies existence and uniqueness theorem, i.e., there exists one and only one trajectory $\mathbf{x} : \mathbb{R}_{>0} \rightarrow \mathbb{R}^{d_x}$ for any $\mathbf{u} : \mathbb{R}_{\geq 0} \rightarrow \mathbb{R}^{d_x}$ and any $\mathbf{x}(0) \in \mathbb{R}^{d_x}$. The input matrix $\mathbf{B}(\mathbf{x}) \in \mathbb{R}^{d_x \times d_x}$ is invertible $\forall \mathbf{x} \in \mathbb{R}^{d_x}$. The output function $\mathbf{h} : \mathbb{R}_{>0} \times \mathbb{R}^{d_x} \rightarrow \mathcal{Y}$ is continuous in t and twice continuously differentiable (differentiability class C^2) and surjective in \mathbf{x} , for all $t \geq 0$ and all $\mathbf{x} \in \mathbb{R}^{d_x}$. Due to the surjection \mathbf{h} , for any reference output \mathbf{y}_{ref} , there exist infinitely many possible solutions for the control \mathbf{u} such that $\lim_{t \rightarrow +\infty} \|\mathbf{y}(t) - \mathbf{y}_{\text{ref}}(t)\|_2 = 0$. This motivates us to find the optimal solution among all these possible ones. The optimality may be specified by the pseudoconvex optimization problem

$$\begin{aligned} \min_{\boldsymbol{\chi}} \sigma(t, \boldsymbol{\chi}) \quad \text{subject to } & \mathbf{0} = \mathbf{h}(t, \boldsymbol{\chi}) - \mathbf{y}_{\text{ref}}(t), \\ & \mathbf{0} \geq \mathbf{g}(t, \boldsymbol{\chi}) := \mathbf{G}(t)\boldsymbol{\chi} + \mathbf{c}(t) \end{aligned} \quad (2)$$

for every time instant $t \geq 0$ or the optimal tracking control problem

$$\begin{aligned} \min_{\boldsymbol{\phi}} \int_0^{t_f} \sigma(t, \boldsymbol{\phi}(t)) dt \quad \text{subject to } & \mathbf{0} = \mathbf{h}(t, \boldsymbol{\phi}(t)) - \mathbf{y}_{\text{ref}}(t) \quad \forall t \in (0, t_f], \\ & \mathbf{0} \geq \mathbf{g}(t, \boldsymbol{\phi}(t)) \quad \forall t \in (0, t_f], \\ & \mathbf{x}(0) = \boldsymbol{\phi}(0) \end{aligned} \quad (3)$$

for the time period $[0, t_f]$. Herein, $\boldsymbol{\chi} \in \mathbb{R}^{d_x}$ denotes candidate variable and $\boldsymbol{\phi} : \mathbb{R}_{>0} \rightarrow \mathbb{R}^{d_x}$ candidate trajectory; both are to be determined. The function $\sigma : \mathbb{R}_{>0} \times \mathbb{R}^{d_x} \rightarrow \mathbb{R}$ or its time-integral is the cost, the time-variant equality constraint $\mathbf{h}(t, \boldsymbol{\chi}) - \mathbf{y}_{\text{ref}}(t)$ reflects the desired output tracking behavior, and $\mathbf{g} : \mathbb{R}_{>0} \times \mathbb{R}^{d_x} \rightarrow \mathbb{R}^{d_c}$ accounts for the time-variant linear inequality constraint. The notation $\mathbf{0}$ denotes conformable zero vector. In order to ensure that the constrained optimization problem (2) is feasible and also to facilitate derivations and deductions, we impose the following assumptions:

Assumptions 1 *At any time instant $t \geq 0$,*

1. *the cost function $\sigma(t, \boldsymbol{\chi})$ is twice continuously differentiable and strongly convex in $\boldsymbol{\chi}$;*
2. *for (2), there exists at least one local minimizer;*
3. *if multiple local minimizers exist, they are isolated points in \mathbb{R}^{d_x} .*

Furthermore,

4. *there exists a differentiable $\boldsymbol{\chi}^\circ : \mathbb{R}_{>0} \rightarrow \mathbb{R}^{d_x}$ such that for any $t \geq 0$, $\boldsymbol{\chi}^\circ(t)$ is a local minimizer of (2).*

Herein, a *local minimizer* χ^\circledast of (2) refers to a point χ that a) satisfies all constraints and b) achieves the smallest value of $\sigma(t, \cdot)$ in its neighborhood [1], i.e.,

$$\exists D > 0 : \forall \chi \in \left\{ \chi \in \mathbb{R}^{d_x} \left| \begin{array}{l} \|\chi - \chi^\circledast\|_2 < D \\ \mathbf{0} = \mathbf{h}(t, \chi) - \mathbf{y}_{\text{ref}}(t) \\ \mathbf{0} \geq \mathbf{g}(t, \chi) \end{array} \right. \right\}, \sigma(t, \chi^\circledast) < \sigma(t, \chi).$$

Assumptions 1.2 and 1.3 are satisfied under conditions given in [1, 2] and [3], respectively. Intuitively, it seems to satisfy Assumption 1.4 if all time-variant functions $\sigma(t, \cdot)$, $\mathbf{h}(t, \cdot)$, $\mathbf{g}(t, \cdot)$ are differentiable in t . Practically, all these assumptions are easily satisfiable and concrete examples are shown in the main document.

Problem 1 Let $\chi^\circledast(t)$ be a local minimizer of the time-variant optimization problem (2) at time instant t . Given the reference $\mathbf{y}_{\text{ref}}(t)$ for the output of the time-variant system (1), find a control

$$\mathbf{u} = \boldsymbol{\mu}(t, \mathbf{x}, \mathbf{y}_{\text{ref}}; K_x)$$

with which $\mathbf{x}(t)$ converges, as $t \geq 0$ increases, exponentially to

1. $\chi^\circledast(t)$, if $\chi^\circledast(t) = \chi^\circledast(0) \forall t \geq 0$.
2. the interior of a moving ball centered at $\chi^\circledast(t)$ with a radius $\propto K_x^{-1}$.

Herein, $K_x > 0$ is a design parameter.

Problem 2 Let $\phi^\circledast : [0, t_f] \rightarrow \mathbb{R}^{d_x}$ be a local minimizer of (3) for the time period $[0, t_f]$. Given the reference $\mathbf{y}_{\text{ref}}(t)$ for the output of the time-variant system (1), find a control

$$\mathbf{u} = \boldsymbol{\mu}(t, \mathbf{x}, \mathbf{y}_{\text{ref}}; K_x)$$

with which $\mathbf{x}(t)$ converges, as $t \geq 0$ increases, exponentially to

1. $\phi^\circledast(t)$, if $\phi^\circledast(t) = \phi^\circledast(0) \forall t \geq 0$.
2. the interior of a moving ball centered at $\phi^\circledast(t)$ with a radius $\propto K_x^{-1}$.

Herein, $K_x > 0$ is a design parameter.

Definition 1 (Optimal tracking controller) Any function $\boldsymbol{\mu} : \mathbb{R}_{\geq 0} \times \mathbb{R}^{d_x} \times \mathbb{R}^{d_y} \rightarrow \mathbb{R}^{d_u}$ that solves Problem 2 is an optimal tracking controller (OTC).

2 Feedback controller for optimality

To approach hybrid Problems 1 and 2, we employ three workflows, each targeting the solution of pseudoconvex optimization, feedback control, and optimal tracking control, respectively (see Figure S1). These workflows, through their respective lemmata and theorems, complement each other and ultimately lead to the resulting OTC. The detailed deduction process is presented in the following subsections.

2.1 Interior-point iteration

For solving optimization problems with both equality and inequality constraints such as (2), one popular numerical method so far are the interior-point algorithms [1, 4, 5]. An interior-point algorithm iteratively updates the search direction toward a local minimizer while ensuring that the point χ at each iteration remain in the interior of the feasible region (hence the name). The key idea is to use *barrier functions* to penalize points that are outside the feasible region. Following this idea, we formulate an interior-point iteration, which provides useful insights in deriving an OTC (in Sections 2.3 and 2.4).

Definition 2 (Barrier function, augmented cost function) *A barrier function $\beta : \mathbb{R} \rightarrow \mathbb{R}_{\geq 0}$ for the open interval $(-\infty, 0]$ is a twice continuously differentiable function such that*

1. $\beta(z) \gg \beta(0) \geq \beta(s) \geq 0 \forall z > 0 \wedge s < 0$ and
2. for all $t \geq 0$ and any strongly convex $\sigma(t, \cdot)$, the augmented cost function

$$\rho(t, \chi) := \sigma(t, \chi) + \frac{1}{2} \boldsymbol{\beta}(\mathbf{g}(t, \chi))^\top \boldsymbol{\beta}(\mathbf{g}(t, \chi)), \quad (4)$$

is strongly convex in χ . Herein, $\boldsymbol{\beta}(\mathbf{s})$ applies β on each element of \mathbf{s} .

One example of barrier function β according to Definition 2 is

$$\beta(s) = \frac{p_2}{p_1} \ln(1 + \exp(p_1 s)), \quad p_1 \gg 1, \quad p_2 \gg 1. \quad (5)$$

Figure S2 illustrates the graph of $\beta(s)/p_2$ with different values of p_1 .

The barrier function and the augmented cost function transform (2) to the following time-variant optimization problem

$$\min_{\chi} \rho(t, \chi) \quad \text{subject to} \quad \mathbf{0} = \mathbf{h}(t, \chi) - \mathbf{y}_{\text{ref}}(t). \quad (6)$$

Although (6) is not equivalent to the original (2), the error occurs only for the local minimizers close to the boundary, given Definition 2 of $\boldsymbol{\beta}$ and ρ .

Lemma 1 (Bound constraint as penalty) *Let $\mathcal{E}^{\circledast}(t) \subset \mathbb{R}^{d_x}$ be the set of all local minimizers of (2) at instant t , and $\mathcal{E}_B^{\circledast}(t)$ the set of all local minimizers (6) at instant t . At any instant $t \geq 0$, for any $\chi \in \mathcal{E}^{\circledast}(t)$, there exists $\chi_B \in \mathcal{E}_B^{\circledast}(t)$ such that $\|\chi - \chi_B\|_2 < 10^{-n}$ with $n \gg 1$, and vice versa. Moreover, if (5) is chosen as the barrier function (Definition 2), then $n \rightarrow +\infty$ as $p_1 \rightarrow +\infty$.*

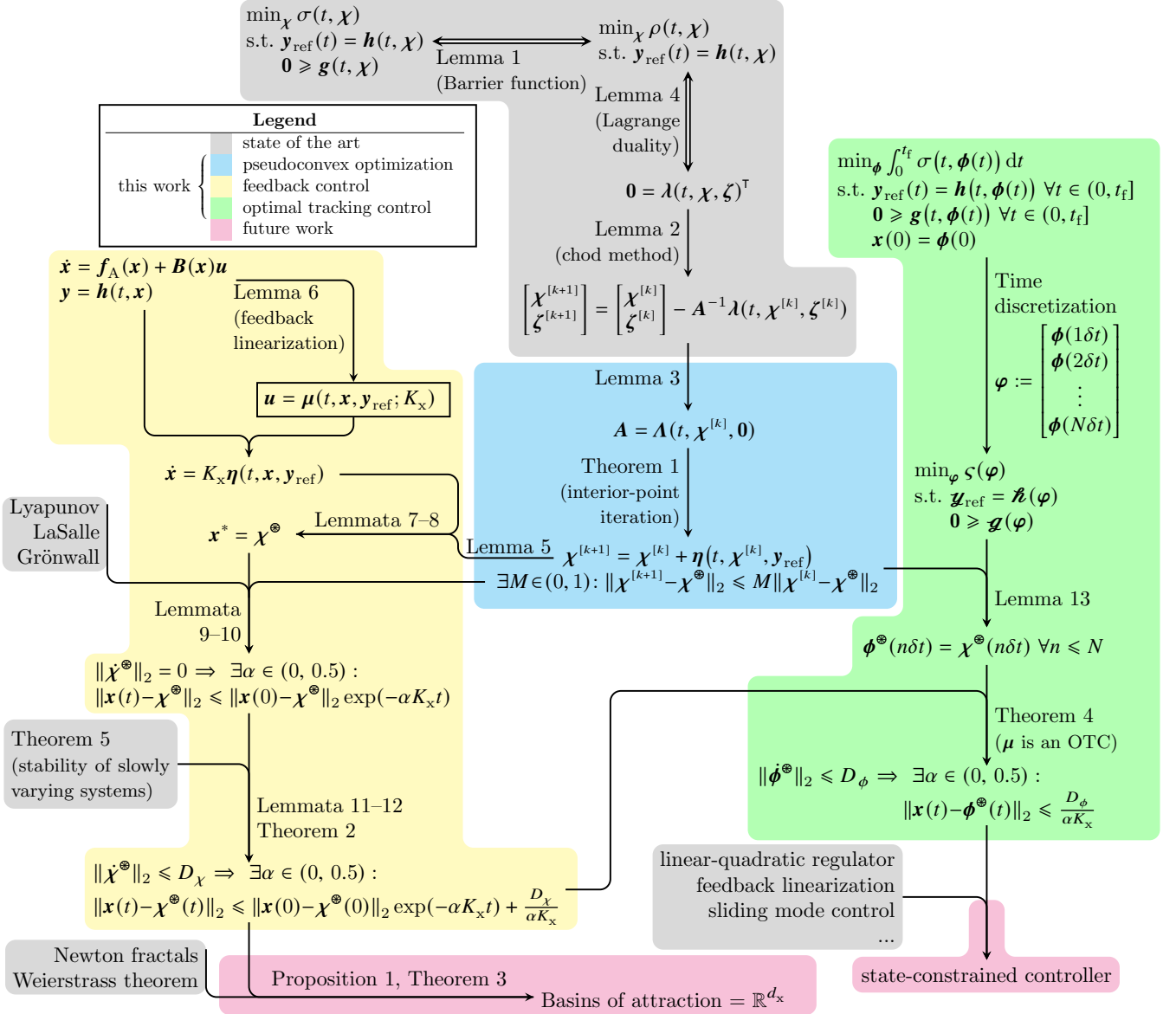


Fig. S1 The workflow of deriving the OTC by addressing three interrelated aspects: pseudoconvex optimization (cyan), feedback control (yellow), and optimal tracking control (green). Each aspect contributes through a series of deductions, lemmata, and theorems, ultimately revealing $\boldsymbol{\mu}$ as an optimal tracking controller.

Since p_1 and p_2 can be chosen arbitrarily large, the optimization problem (6) with (5) is essentially (2). We will show later in Section 4 that it is manageable to set p_1 to $+\infty$ and to choose p_2 to be sufficiently large.

In order to solve (6) at one arbitrary time instant, we apply the method of Lagrange multipliers [1]. The Lagrangian function is

$$L(t, \boldsymbol{\chi}, \boldsymbol{\zeta}) = \rho(t, \boldsymbol{\chi}) + \boldsymbol{\zeta}^\top (-\mathbf{h}(t, \boldsymbol{\chi}) + \mathbf{y}_{\text{ref}}(t))$$

with Lagrange multipliers $\boldsymbol{\zeta} \in \mathbb{R}^{d_y}$. The saddle points of $L(t, \boldsymbol{\chi}, \boldsymbol{\zeta})$ with respect to $\boldsymbol{\chi}$ and $\boldsymbol{\zeta}$ are the roots of

$$\mathbf{0} = \boldsymbol{\lambda}(t, \boldsymbol{\chi}, \boldsymbol{\zeta})^\top := \left[\frac{\partial L(t, \boldsymbol{\chi}, \boldsymbol{\zeta})}{\partial \boldsymbol{\chi}} \quad \frac{\partial L(t, \boldsymbol{\chi}, \boldsymbol{\zeta})}{\partial \boldsymbol{\zeta}} \right]^\top = \begin{bmatrix} \mathbf{r}(t, \boldsymbol{\chi}) - \mathbf{H}(t, \boldsymbol{\chi})^\top \boldsymbol{\zeta} \\ -\mathbf{h}(t, \boldsymbol{\chi}) + \mathbf{y}_{\text{ref}}(t) \end{bmatrix}, \quad (7a)$$

where $\boldsymbol{\lambda}(t, \boldsymbol{\chi}, \boldsymbol{\zeta}) \in \mathbb{R}^{d_x + d_y}$ is the Jacobian of the Lagrangian function $L(t, \boldsymbol{\chi}, \boldsymbol{\zeta})$, and

$$\mathbf{r}(t, \boldsymbol{\mathbf{x}}) := \left[\frac{\partial \rho(t, \boldsymbol{\mathbf{x}})}{\partial \boldsymbol{\mathbf{x}}} \right]^\top = \mathbf{q}(t, \boldsymbol{\mathbf{x}}) + \mathbf{G}(t)^\top \boldsymbol{\xi}(\mathbf{G}(t)\boldsymbol{\mathbf{x}} + \mathbf{c}(t)), \quad (7b)$$

$$\mathbf{q}(t, \boldsymbol{\mathbf{x}}) := \left[\frac{\partial \sigma(t, \boldsymbol{\mathbf{x}})}{\partial \boldsymbol{\mathbf{x}}} \right]^\top, \quad \boldsymbol{\xi}(s) := \frac{\partial \boldsymbol{\beta}(s)^\top}{\partial s} \boldsymbol{\beta}(s), \quad (7c)$$

$$\mathbf{H}(t, \boldsymbol{\mathbf{x}}) := \frac{\partial \mathbf{h}(t, \boldsymbol{\mathbf{x}})}{\partial \boldsymbol{\mathbf{x}}}. \quad (7d)$$

Here, $\boldsymbol{\mathbf{x}} \in \mathbb{R}^{d_x}$ and $s \in \mathbb{R}^{d_c}$ denote general arguments of functions. The nonlinear equation (7a) may be solved by the Newton-Raphson method (see Section 7.1), if the Jacobian of $\boldsymbol{\lambda}(t, \boldsymbol{\chi}, \boldsymbol{\zeta})$ (i.e, the Hessian of $L(t, \boldsymbol{\chi}, \boldsymbol{\zeta})$)

$$\begin{aligned} \boldsymbol{\Lambda}(t, \boldsymbol{\chi}, \boldsymbol{\zeta}) &:= \begin{bmatrix} \frac{\partial \boldsymbol{\lambda}(t, \boldsymbol{\chi}, \boldsymbol{\zeta})}{\partial \boldsymbol{\chi}} & \frac{\partial \boldsymbol{\lambda}(t, \boldsymbol{\chi}, \boldsymbol{\zeta})}{\partial \boldsymbol{\zeta}} \end{bmatrix} \\ &= \begin{bmatrix} \frac{\partial}{\partial \boldsymbol{\chi}} \frac{\partial L(t, \boldsymbol{\chi}, \boldsymbol{\zeta})}{\partial \boldsymbol{\chi}} & \frac{\partial}{\partial \boldsymbol{\zeta}} \frac{\partial L(t, \boldsymbol{\chi}, \boldsymbol{\zeta})}{\partial \boldsymbol{\chi}} \\ \frac{\partial}{\partial \boldsymbol{\chi}} \frac{\partial L(t, \boldsymbol{\chi}, \boldsymbol{\zeta})}{\partial \boldsymbol{\zeta}} & \frac{\partial}{\partial \boldsymbol{\zeta}} \frac{\partial L(t, \boldsymbol{\chi}, \boldsymbol{\zeta})}{\partial \boldsymbol{\zeta}} \end{bmatrix} = \begin{bmatrix} \boldsymbol{\Lambda}_{\text{xx}}(t, \boldsymbol{\chi}, \boldsymbol{\zeta}) & -\mathbf{H}(t, \boldsymbol{\chi})^\top \\ -\mathbf{H}(t, \boldsymbol{\chi}) & \mathbf{O} \end{bmatrix} \end{aligned} \quad (8a)$$

is invertible, where \mathbf{O} denotes the conformable zero matrix, and

$$\boldsymbol{\Lambda}_{\text{xx}}(t, \boldsymbol{\mathbf{x}}, \boldsymbol{\zeta}) := \frac{\partial}{\partial \boldsymbol{\mathbf{x}}} \frac{\partial L(t, \boldsymbol{\mathbf{x}}, \boldsymbol{\zeta})}{\partial \boldsymbol{\mathbf{x}}} = \mathbf{R}(t, \boldsymbol{\mathbf{x}}) + \frac{\partial (\mathbf{H}(t, \boldsymbol{\mathbf{x}})^\top \boldsymbol{\zeta})}{\partial \boldsymbol{\mathbf{x}}}, \quad (8b)$$

$$\mathbf{R}(t, \boldsymbol{\mathbf{x}}) := \frac{\partial \mathbf{r}(t, \boldsymbol{\mathbf{x}})}{\partial \boldsymbol{\mathbf{x}}} = \mathbf{Q}(t, \boldsymbol{\mathbf{x}}) + \mathbf{G}(t)^\top \boldsymbol{\Xi}(\mathbf{G}(t)\boldsymbol{\mathbf{x}} + \mathbf{c}(t))\mathbf{G}(t), \quad (8c)$$

$$\mathbf{Q}(t, \boldsymbol{\mathbf{x}}) := \frac{\partial}{\partial \boldsymbol{\mathbf{x}}} \frac{\partial \sigma(t, \boldsymbol{\mathbf{x}})}{\partial \boldsymbol{\mathbf{x}}}, \quad \boldsymbol{\Xi}(s) := \frac{\partial}{\partial s} \left(\frac{\partial \boldsymbol{\beta}(s)^\top}{\partial s} \boldsymbol{\beta}(s) \right). \quad (8d)$$

From the strong convexity of $\rho(t, \boldsymbol{\mathbf{x}})$ (Definition 2), one concludes that $\mathbf{R}(t, \boldsymbol{\mathbf{x}})$ is symmetric and positive definite (SPD). Consequently, one can conclude that

1. $\boldsymbol{\Lambda}_{\text{xx}}(t, \boldsymbol{\mathbf{x}}, \boldsymbol{\zeta})$ is SPD if $\mathbf{H}(t, \boldsymbol{\mathbf{x}}) = \mathbf{H}(t, \mathbf{0})$, and

2. $\Lambda_{\text{xx}}(t, \boldsymbol{x}, \boldsymbol{\zeta})|_{\boldsymbol{H}(t, \boldsymbol{x})=\boldsymbol{H}(t, \mathbf{0})} = \Lambda_{\text{xx}}(t, \boldsymbol{x}, \mathbf{0}) = \boldsymbol{R}(t, \boldsymbol{x})$ is SPD.

Therefore, for solving (7a), we apply a quasi-Newton method, where the Hessian $\boldsymbol{\Lambda}(t, \boldsymbol{\chi}, \boldsymbol{\zeta})$ is approximated by the invertible $\boldsymbol{\Lambda}(t, \boldsymbol{\chi}, \mathbf{0})$. This results in the following iteration

$$\begin{bmatrix} \boldsymbol{\chi}[k+1] \\ \boldsymbol{\zeta}[k+1] \end{bmatrix} = \begin{bmatrix} \boldsymbol{\chi}[k] \\ \boldsymbol{\zeta}[k] \end{bmatrix} - \boldsymbol{\Lambda}(t, \boldsymbol{\chi}[k], \mathbf{0})^{-1} \boldsymbol{\lambda}(t, \boldsymbol{\chi}[k], \boldsymbol{\zeta}[k])^\top \quad (9a)$$

\Leftrightarrow

$$\boldsymbol{\chi}[k+1] = \boldsymbol{\chi}[k] + \boldsymbol{\eta}_A(t, \boldsymbol{\chi}[k], \boldsymbol{y}_{\text{ref}}(t)) - \boldsymbol{\eta}_B(t, \boldsymbol{\chi}[k]) + \boldsymbol{\psi}_A(t, \boldsymbol{\chi}[k], \boldsymbol{\zeta}[k]), \quad (9b)$$

$$\boldsymbol{\zeta}[k+1] = \boldsymbol{\psi}_B(t, \boldsymbol{\chi}[k], \boldsymbol{y}_{\text{ref}}(t)) \quad (9c)$$

with

$$\boldsymbol{\eta}_A(t, \boldsymbol{x}, \boldsymbol{y}_{\text{ref}}) := \boldsymbol{H}(t, \boldsymbol{x}) \#_{\boldsymbol{R}(t, \boldsymbol{x})} (\boldsymbol{y}_{\text{ref}} - \boldsymbol{h}(t, \boldsymbol{x})), \quad (9d)$$

$$\boldsymbol{\eta}_B(t, \boldsymbol{x}) := \left(\boldsymbol{I} - \boldsymbol{H}(t, \boldsymbol{x}) \#_{\boldsymbol{R}(t, \boldsymbol{x})} \boldsymbol{H}(t, \boldsymbol{x}) \right) \boldsymbol{R}(t, \boldsymbol{x})^{-1} \boldsymbol{r}(t, \boldsymbol{x}), \quad (9e)$$

$$\boldsymbol{\psi}_A(t, \boldsymbol{x}, \boldsymbol{\zeta}) := \left(\boldsymbol{I} - \boldsymbol{H}(t, \boldsymbol{x}) \#_{\boldsymbol{R}(t, \boldsymbol{x})} \boldsymbol{H}(t, \boldsymbol{x}) \right) \boldsymbol{R}(t, \boldsymbol{x})^{-1} \boldsymbol{H}(t, \boldsymbol{x})^\top \boldsymbol{\zeta}, \quad (9f)$$

$$\boldsymbol{\psi}_B(t, \boldsymbol{x}, \boldsymbol{y}_{\text{ref}}) := \left(\boldsymbol{H}(t, \boldsymbol{x}) \boldsymbol{R}(t, \boldsymbol{x})^{-1} \boldsymbol{H}(t, \boldsymbol{x})^\top \right)^{-1} \left(\boldsymbol{y}_{\text{ref}} - \boldsymbol{h}(t, \boldsymbol{x}) + \boldsymbol{H}(t, \boldsymbol{x}) \boldsymbol{R}(t, \boldsymbol{x})^{-1} \boldsymbol{r}(t, \boldsymbol{x}) \right) \quad (9g)$$

and conformable identity matrix \boldsymbol{I} . The operation $\boldsymbol{A} \#_{\boldsymbol{W}}$ is the \boldsymbol{W} -weighted right pseudoinverse of a matrix \boldsymbol{A} , i.e.,

$$\boldsymbol{A} \#_{\boldsymbol{W}} = \boldsymbol{W}^{-1} \boldsymbol{A}^\top (\boldsymbol{A} \boldsymbol{W}^{-1} \boldsymbol{A}^\top)^{-1}. \quad (10)$$

Definition 3 (Quotient-linear convergence [1, 6, 7]) A convergent sequence $\boldsymbol{\chi}[0], \boldsymbol{\chi}[1], \boldsymbol{\chi}[2], \dots$ with $\boldsymbol{\chi}^* = \lim_{k \rightarrow +\infty} \boldsymbol{\chi}[k]$ is called quotient-linearly convergent if

$$\exists M = \text{const.} \in (0, 1) : \|\boldsymbol{\chi}[k+1] - \boldsymbol{\chi}^*\|_2 \leq M \|\boldsymbol{\chi}[k] - \boldsymbol{\chi}^*\|_2 \quad \forall k \in \mathbb{N}.$$

The constant M is known as the rate of convergence.

Lemma 2 (Chord method [6]) Let $[\boldsymbol{\chi}^{\oplus \top} \boldsymbol{\zeta}^{\oplus \top}]^\top$ denote a root of (7a). There exist $\delta_1 > 0$ and $\delta_2 > 0$ such that if

$$\left\| \begin{bmatrix} \boldsymbol{\chi}[0] - \boldsymbol{\chi}^{\oplus} \\ \boldsymbol{\zeta}[0] - \boldsymbol{\zeta}^{\oplus} \end{bmatrix} \right\|_2 < \delta_1 \quad \wedge \quad \|\boldsymbol{A} - \boldsymbol{\Lambda}(t, \boldsymbol{\chi}^{\oplus}, \boldsymbol{\zeta}^{\oplus})\|_2 < \delta_2 \quad (11)$$

then the iteration

$$\begin{bmatrix} \boldsymbol{\chi}[k+1] \\ \boldsymbol{\zeta}[k+1] \end{bmatrix} = \begin{bmatrix} \boldsymbol{\chi}[k] \\ \boldsymbol{\zeta}[k] \end{bmatrix} - \boldsymbol{A}^{-1} \boldsymbol{\lambda}(t, \boldsymbol{\chi}[k], \boldsymbol{\zeta}[k]) \quad (12)$$

converges quotient-linearly to $[\boldsymbol{\chi}^{\oplus\top} \boldsymbol{\zeta}^{\oplus\top}]^\top$ as $k \in \mathbb{N}$ increases. Moreover, the rate of convergence decreases proportionally as $\delta_1 + \delta_2$ decreases. Herein, $\|\cdot\|_2$ denotes the Euclidean norm (for vectors) or the matrix norm induced by the Euclidean norm.

Proof. See *chord method* in [6]. Note that t is considered constant since we are considering only *one* time instant and t does not depend on k . \square

Since (9) is a special case of (12) with $\mathbf{A} = \boldsymbol{\Lambda}(t, \boldsymbol{\chi}[k], \mathbf{0})$, Lemma 2 is valid for (9). Furthermore, we claim that the sufficient-closeness condition (11) can be further simplified in case $\mathbf{A} = \boldsymbol{\Lambda}(t, \boldsymbol{\chi}[k], \mathbf{0})$.

Lemma 3 *Let $[\boldsymbol{\chi}^{\oplus\top} \boldsymbol{\zeta}^{\oplus\top}]^\top$ denote a root of (7a). There exists $\delta > 0$ such that if*

$$\|\boldsymbol{\chi}[0] - \boldsymbol{\chi}^{\oplus}\|_2 < \delta \quad (13)$$

then the sequence $[\boldsymbol{\chi}[0]^\top \boldsymbol{\zeta}[0]^\top]^\top, [\boldsymbol{\chi}[1]^\top \boldsymbol{\zeta}[1]^\top]^\top, [\boldsymbol{\chi}[2]^\top \boldsymbol{\zeta}[2]^\top]^\top, \dots$ generated by (9) converges quotient-linearly to $[\boldsymbol{\chi}^{\oplus\top} \boldsymbol{\zeta}^{\oplus\top}]^\top$. Moreover, the rate of convergence decreases as δ decreases.

Proof. Since $\mathbf{r}(t, \boldsymbol{x})$ is of C^1 in \boldsymbol{x} and $\mathbf{h}(t, \boldsymbol{x})$ is of C^2 in \boldsymbol{x} , the functions $\boldsymbol{\Lambda}(t, \boldsymbol{x}, \boldsymbol{\zeta})$ and $\boldsymbol{\psi}_B(t, \boldsymbol{x}, \mathbf{y}_{\text{ref}})$ are locally Lipschitz continuous in \boldsymbol{x} . Furthermore, $\boldsymbol{\Lambda}(t, \boldsymbol{x}, \boldsymbol{\zeta})$ is linear in $\boldsymbol{\zeta}$ as defined in (8), i.e., $\boldsymbol{\Lambda}(t, \boldsymbol{x}, \boldsymbol{\zeta})$ is globally Lipschitz continuous in $\boldsymbol{\zeta}$. Hence, one obtains the following deduction:

$$\begin{aligned} \|\boldsymbol{\Lambda}(t, \boldsymbol{\chi}, \mathbf{0}) - \boldsymbol{\Lambda}(t, \boldsymbol{\chi}^{\oplus}, \boldsymbol{\zeta}^{\oplus})\|_2 &< \gamma_\Lambda(t) \left\| \begin{bmatrix} \boldsymbol{\chi} - \boldsymbol{\chi}^{\oplus} \\ \mathbf{0} - \boldsymbol{\zeta}^{\oplus} \end{bmatrix} \right\|_2 = \gamma_\Lambda(t) \sqrt{\|\boldsymbol{\chi} - \boldsymbol{\chi}^{\oplus}\|_2^2 + \|\mathbf{0} - \boldsymbol{\zeta}^{\oplus}\|_2^2} \\ &< \gamma_\Lambda(t) \sqrt{\delta^2 + \|\boldsymbol{\zeta}^{\oplus}\|_2^2}, \end{aligned} \quad (14a)$$

$$\begin{aligned} \|\boldsymbol{\zeta}[0] - \boldsymbol{\zeta}^{\oplus}\|_2 &= \|\boldsymbol{\psi}_B(t, \boldsymbol{\chi}[0], \mathbf{y}_{\text{ref}}) - \boldsymbol{\psi}_B(t, \boldsymbol{\chi}^{\oplus}, \mathbf{y}_{\text{ref}})\|_2 < \gamma_{\psi_B}(t, \mathbf{y}_{\text{ref}}) \|\boldsymbol{\chi} - \boldsymbol{\chi}^{\oplus}\|_2 \\ &= \gamma_{\psi_B}(t, \mathbf{y}_{\text{ref}}) \delta, \end{aligned} \quad (14b)$$

where $\gamma_\Lambda(t)$ is the Lipschitz constant of $\boldsymbol{\Lambda}(t, \cdot, \cdot)$ in the considered neighborhood of $\boldsymbol{\chi}^{\oplus}$, and $\gamma_{\psi_B}(t, \mathbf{y}_{\text{ref}})$ the Lipschitz constant of $\boldsymbol{\psi}_B(t, \cdot, \mathbf{y}_{\text{ref}})$ in the considered neighborhood of $\boldsymbol{\chi}^{\oplus}$. As mentioned before, t is considered constant, and so is \mathbf{y}_{ref} , since we are considering only *one* time instant and t does not depend on k . It is obvious that (13) and (14) together are (11). Therefore, the conclusion of Lemma 2 is applicable here. \square

Lemma 4 *The roots ($\boldsymbol{\chi}$ component) of (7a) are the local minimizers of (2).*

Proof. All roots ($\boldsymbol{\chi}$ component) of (7a) are the local minimizers of (6) (the Karush-Kuhn-Tucker conditions [1, 2, 8]), and the latter are the local minimizers of (2) (Lemma 1). \square

This means, all $\boldsymbol{\chi}^{\oplus}$ above can be replaced by $\boldsymbol{\chi}^{\otimes}$. For the sake of readability, we use the single notation $\boldsymbol{\chi}^{\otimes}$ for all these three notions (roots of (7a), local minimizers of (6), and local minimizers of (2)) from this point forth.

Since $\zeta[k]$ converges as k increases (Lemma 3), we apply $\zeta[k+1] = \zeta[k]$ to (9). By inserting (9c) into (9b), one obtains the *interior-point iteration*

$$\chi[k+1] = \chi[k] + \eta(t, \chi[k], \mathbf{y}_{\text{ref}}), \quad (15)$$

$$\eta(t, \boldsymbol{x}, \mathbf{y}_{\text{ref}}) := \boldsymbol{\eta}_A(t, \boldsymbol{x}, \mathbf{y}_{\text{ref}}) - \boldsymbol{\eta}_B(t, \boldsymbol{x}), \quad (16)$$

where $\boldsymbol{\eta}_A$ and $\boldsymbol{\eta}_B$ are defined in (9d) and (9e), respectively. Rigorously, (15) shall be written as

$$\chi^{[k+1]}(t) = \chi^{[k]}(t) + \eta(t, \chi^{[k]}(t), \mathbf{y}_{\text{ref}}(t)) \quad (17)$$

to reflect the time-variant property of (2).

Theorem 1 (Interior-point iteration) *For any local minimizer χ^\circledast of (2), there exists $\delta > 0$ such that if $\|\chi^{[0]}(t) - \chi^\circledast\|_2 < \delta$ then $\chi^{[k]}(t)$ of (17) converges quotient-linearly (Definition 3) to $\chi^\circledast(t)$ as $k \in \mathbb{N}$ increases, i.e.,*

$$\exists M \in (0, 1) : \|\chi^{[k+1]}(t) - \chi^\circledast(t)\|_2 \leq M \|\chi^{[k]}(t) - \chi^\circledast(t)\|_2 \quad \forall k \in \mathbb{N}. \quad (18)$$

Proof. As elaborated above, there is no difference between (9) and (15). Hence, one concludes the local convergence of $\chi[k]$ to a root χ^\oplus of (7a) as in Lemma 3, where χ^\oplus is as well a local minimizer χ^\circledast of (2) (Lemma 4). \square

Definition 4 (Equilibrium points at instant t) *A point $\chi^* \in \mathbb{R}^{d_x}$ is called an equilibrium point of (15) at instant t , if and only if*

$$\mathbf{0} = \eta(t, \chi^*, \mathbf{y}_{\text{ref}}) \Leftrightarrow \chi^* = \chi^* + \eta(t, \chi^*, \mathbf{y}_{\text{ref}}).$$

In other words, any

$$\chi^* \in \mathcal{E}_\chi(t, \mathbf{y}_{\text{ref}}) := \{ \boldsymbol{x} \in \mathbb{R}^{d_x} \mid \mathbf{0} = \eta(t, \boldsymbol{x}, \mathbf{y}_{\text{ref}}) \} \quad (19)$$

is an equilibrium point of (15) at instant t .

It is worth noting that

- the set $\mathcal{E}_\chi(t, \mathbf{y}_{\text{ref}})$ of equilibrium points is time-variant and depends on \mathbf{y}_{ref} , and
- $\mathcal{E}_\chi(t, \mathbf{y}_{\text{ref}}) \neq \emptyset$ as long as Assumptions 1.2 and 1.3 are satisfied.

Lemma 5 (Local minimizers) *A local minimizer of (2) is an asymptotically stable equilibrium point of (15).*

Proof. It can be concluded immediately from Lemma 4 and Theorem 1. \square

2.2 Output tracking controller with full-state feedback

Instead of considering the system (1) right away, we firstly consider a simple, yet, very special system that is

$$\dot{\boldsymbol{x}} = \boldsymbol{f}'_A(t, \boldsymbol{x}) + \boldsymbol{u}', \quad (20a)$$

$$\boldsymbol{y} = \boldsymbol{h}(t, \boldsymbol{x}), \quad (20b)$$

where $\mathbf{u}' \in \mathbb{R}^{d_x}$. The function $\mathbf{f}'_A : \mathbb{R}_{\geq 0} \times \mathbb{R}^{d_x} \rightarrow \mathbb{R}^{d_x}$ is of a certain form, which will be revealed later. It is easy to conclude that if

$$\mathbf{u} = \mathbf{B}(\mathbf{x})^{-1} \left(-\mathbf{f}_A(\mathbf{x}) + \mathbf{f}'_A(t, \mathbf{x}) + \mathbf{u}' \right), \quad (21)$$

is chosen, then (1) becomes (20).

To control the output \mathbf{y} of (20) to follow the reference \mathbf{y}_{ref} , we deploy a technique of feedback linearization.

Lemma 6 *Suppose $\mathbf{y}_{\text{ref}}(t) = \mathbf{y}_{\text{ref}}(0) \forall t \geq 0$ and $\mathbf{h}(t, \mathbf{x}) = \mathbf{h}(0, \mathbf{x})$ for all $t \geq 0$ and all $\mathbf{x} \in \mathbb{R}^{d_x}$. If*

$$\mathbf{u}' = \mathbf{H}(t, \mathbf{x}) \#_{\mathbf{Q}'} (K_y (\mathbf{y}_{\text{ref}} - \mathbf{h}(t, \mathbf{x})) - \mathbf{H}(t, \mathbf{x}) \mathbf{f}'_A(t, \mathbf{x})), \quad \mathbf{Q}' \text{ is SPD, } K_y > 0 \quad (22)$$

is chosen for (20), then $\mathbf{y}(t)$ converges exponentially to \mathbf{y}_{ref} as $t > 0$ increases.

Proof. Applying Lie derivative to (20b) results in

$$\dot{\mathbf{y}} = \frac{\partial \mathbf{h}(t, \mathbf{x})}{\partial t} + \mathbf{H}(t, \mathbf{x}) \dot{\mathbf{x}} = \frac{\partial \mathbf{h}(t, \mathbf{x})}{\partial t} + \mathbf{H}(t, \mathbf{x}) \mathbf{f}'_A(t, \mathbf{x}) + \mathbf{H}(t, \mathbf{x}) \mathbf{u}'. \quad (23)$$

One may propose

$$\mathbf{u}' = \mathbf{H}(t, \mathbf{x}) \#_{\mathbf{Q}'} \left(K_y (\mathbf{y}_{\text{ref}} - \mathbf{y}) + \dot{\mathbf{y}}_{\text{ref}} - \frac{\partial \mathbf{h}(t, \mathbf{x})}{\partial t} - \mathbf{H}(t, \mathbf{x}) \mathbf{f}'_A(t, \mathbf{x}) \right) \quad (24)$$

with an SPD matrix \mathbf{Q}' to globally linearize (23) via feedback of output. Note that $\mathbf{I} = \mathbf{H}(t, \mathbf{x}) \mathbf{H}(t, \mathbf{x}) \#_{\mathbf{Q}'}$, cf. (10). The resulting closed-loop system (23)(24) is the linear system

$$\dot{\mathbf{y}} - \dot{\mathbf{y}}_{\text{ref}} = -K_y (\mathbf{y} - \mathbf{y}_{\text{ref}}), \quad (25)$$

with negative eigenvalues ($\Leftrightarrow K_y > 0$). In case of constant \mathbf{y}_{ref} and time-invariant \mathbf{h} , equation (24) becomes (22). \square

Inserting (22) into (20) results in the closed-loop system

$$\dot{\mathbf{x}} = \mathbf{H}(t, \mathbf{x}) \#_{\mathbf{Q}'} K_y (\mathbf{y}_{\text{ref}} - \mathbf{h}(t, \mathbf{x})) + \left(\mathbf{I} - \mathbf{H}(t, \mathbf{x}) \#_{\mathbf{Q}'} \mathbf{H}(t, \mathbf{x}) \right) \mathbf{f}'_A(t, \mathbf{x}). \quad (26)$$

By comparing (26) and (15), it is easy to determine that with

$$\mathbf{Q}' = \mathbf{R}(t, \mathbf{x}), \quad (27a)$$

$$\mathbf{f}'_A(t, \mathbf{x}) = -K_x \mathbf{R}(t, \mathbf{x})^{-1} \mathbf{r}(t, \mathbf{x}), \quad K_x = K_y, \quad (27b)$$

(26) becomes

$$\dot{\mathbf{x}} = K_x \boldsymbol{\eta}(t, \mathbf{x}, \mathbf{y}_{\text{ref}}), \quad (28)$$

which shares certain similarities with (15) in equilibrium points and convergence behavior, which are outlined as follows.

Definition 5 (Equilibrium points at instant t) A point $\mathbf{x}^* \in \mathbb{R}^{d_x}$ is called an equilibrium point of (28) at instant t , if and only if

$$\mathbf{0} = K_x \boldsymbol{\eta}(t, \mathbf{x}^*, \mathbf{y}_{\text{ref}}).$$

In other words, any

$$\mathbf{x}^* \in \mathcal{E}_x(t, \mathbf{y}_{\text{ref}}) := \{ \boldsymbol{\alpha} \in \mathbb{R}^{d_x} \mid \mathbf{0} = K_x \boldsymbol{\eta}(t, \boldsymbol{\alpha}, \mathbf{y}_{\text{ref}}) \} \quad (29)$$

is an equilibrium point of (28) at instant t .

Lemma 7 The differential equation (28) and the difference equation (15) have the same equilibrium points, i.e.,

$$\mathcal{E}_x(t, \mathbf{y}_{\text{ref}}) = \mathcal{E}_\chi(t, \mathbf{y}_{\text{ref}}) \quad \forall t \geq 0.$$

Proof. It can be concluded immediately by comparing (19) and (29). \square

Lemma 8 (Local minimizers) A local minimizer of (2) is an asymptotically stable equilibrium point of (28).

Proof. It can be concluded immediately from Lemmata 5 and 7. \square

2.3 Exponential convergence

Lemma 9 Consider the system (28) with $K_x > 0$. Suppose $\mathbf{y}_{\text{ref}}(t) = \mathbf{y}_{\text{ref}}(0) \forall t \geq 0$. Suppose for all $t \geq 0$ and all $\mathbf{x} \in \mathbb{R}^{d_x}$, $\sigma(t, \mathbf{x}) = \sigma(0, \mathbf{x})$, $\mathbf{h}(t, \mathbf{x}) = \mathbf{h}(0, \mathbf{x})$, and $\mathbf{g}(t, \mathbf{x}) = \mathbf{g}(0, \mathbf{x})$. Let

$$\mathcal{N}(\mathbf{x}^*, \delta) := \{ \mathbf{x} \in \mathbb{R}^{d_x} \mid \|\mathbf{x} - \mathbf{x}^*\|_2 < \delta \}. \quad (30)$$

There exists $\delta : \mathbb{R}^{d_x} \rightarrow \mathbb{R}_{>0}$ and $\mathbf{x}^* \in \mathcal{E}_x$ such that if $\mathbf{x}(0) \in \mathcal{N}(\mathbf{x}^*, \delta(\mathbf{x}^*))$ then $\mathbf{x}(t)$ converges exponentially to \mathbf{x}^* as $t > 0$ increases.

Proof. We choose $\mathbf{x}^* = \boldsymbol{\chi}^\circledast$ (this is possible due to Lemma 8) and δ to be such that $\mathcal{N}(\mathbf{x}^*, \delta(\mathbf{x}^*)) \cap \mathcal{E}_x(0, \mathbf{y}_{\text{ref}}) = \{\mathbf{x}^*\}$ (such a $\delta(\mathbf{x}^*)$ exists due to Assumptions 1). Therefore, the time-invariant scalar function

$$V(\mathbf{x}) = \frac{1}{2}(\mathbf{x} - \mathbf{x}^*)^\top K_x^{-1}(\mathbf{x} - \mathbf{x}^*) \begin{cases} = 0 & \text{if } \mathbf{x} = \mathbf{x}^*, \\ > 0 & \text{if } \mathbf{x} \in \mathcal{N}(\mathbf{x}^*, \delta(\mathbf{x}^*)) \setminus \{\mathbf{x}^*\} \end{cases} \quad (31)$$

is a Lyapunov candidate function on $\mathcal{N}(\mathbf{x}^*, \delta(\mathbf{x}^*))$. Its time derivative is

$$\frac{d}{dt}V(\mathbf{x}) = \frac{\partial V(\mathbf{x})}{\partial \mathbf{x}} \dot{\mathbf{x}} = (\mathbf{x} - \mathbf{x}^*)^\top \boldsymbol{\eta}(t, \mathbf{x}, \mathbf{y}_{\text{ref}}). \quad (32)$$

Note that $\mathbf{x}^* = \text{const.}$ due to the time-invariant σ , \mathbf{h} , \mathbf{g} and constant \mathbf{y}_{ref} .

In order to analyze the bound of $dV(\mathbf{x})/dt$, we further let δ be such that if $\|\boldsymbol{\chi}[0] - \boldsymbol{\chi}^\circledast\|_2 < \delta(\boldsymbol{\chi}^\circledast)$ then $\boldsymbol{\chi}[k]$ of (15) converges quotient-linearly to a local minimizer $\boldsymbol{\chi}^\circledast$

of (2) as $k \in \mathbb{N}$ increases (Theorem 1). From this, with (15) and Definition 3, one concludes that $\exists M \in (0, 1)$:

$$\begin{aligned} \forall \chi &\in \mathcal{N}(\chi^\circledast, \delta(\chi^\circledast)), \\ (\chi + \boldsymbol{\eta}(t, \chi, \mathbf{y}_{\text{ref}}) - \chi^\circledast)^\top (\chi + \boldsymbol{\eta}(t, \chi, \mathbf{y}_{\text{ref}}) - \chi^\circledast) &\leq (\chi - \chi^\circledast)^\top M^2 (\chi - \chi^\circledast) \\ \Leftrightarrow (\chi - \chi^\circledast)^\top \boldsymbol{\eta}(t, \chi, \mathbf{y}_{\text{ref}}) &\leq -\frac{1}{2}(1 - M^2) \|\chi - \chi^\circledast\|_2^2 - \frac{1}{2} \|\boldsymbol{\eta}(t, \chi, \mathbf{y}_{\text{ref}})\|_2^2. \end{aligned} \quad (33)$$

Since $\mathbf{x}^* = \chi^\circledast$ has been chosen, inequality (33) can be written as

$$(\mathbf{x} - \mathbf{x}^*)^\top \boldsymbol{\eta}(t, \mathbf{x}, \mathbf{y}_{\text{ref}}) \leq -\frac{1}{2}(1 - M^2) \|\mathbf{x} - \mathbf{x}^*\|_2^2 - \frac{1}{2} \|\boldsymbol{\eta}(t, \mathbf{x}, \mathbf{y}_{\text{ref}})\|_2^2. \quad (34)$$

Inserting (34) into (32) results in

$$\frac{d}{dt} V(\mathbf{x}) \leq -\frac{1}{2}(1 - M^2) \|\mathbf{x} - \mathbf{x}^*\|_2^2 - \frac{1}{2} \|\boldsymbol{\eta}(t, \mathbf{x}, \mathbf{y}_{\text{ref}})\|_2^2 \quad (35)$$

and consequently, $dV(\mathbf{x})/dt \leq 0$. This concludes the Lyapunov stability. Furthermore, $dV(\mathbf{x})/dt$ reaches zero if and only if \mathbf{x} reaches \mathbf{x}^* , the only equilibrium point in $\mathcal{N}(\mathbf{x}^*, \delta(\mathbf{x}^*))$. Therefore, the asymptotic convergence of $\mathbf{x}(t)$ is concluded (LaSalle's invariance principle [9]).

Since (31) can be written as $2K_x V(\mathbf{x}) = \|\mathbf{x} - \mathbf{x}^*\|_2^2$, inequality (35) becomes

$$\frac{d}{dt} V(\mathbf{x}) \leq -\frac{1}{2}(1 - M^2) 2K_x V(\mathbf{x}) - \frac{1}{2} \|\boldsymbol{\eta}(t, \mathbf{x}, \mathbf{y}_{\text{ref}})\|_2^2 \leq -\frac{1}{2}(1 - M^2) 2K_x V(\mathbf{x}).$$

Solving this differential inequality using Grönwall's inequality [10] yields

$$\begin{aligned} V(\mathbf{x}(t)) &\leq V(\mathbf{x}(0)) \exp(-(1 - M^2)K_x t) \\ \Leftrightarrow \|\mathbf{x}(t) - \mathbf{x}^*\|_2 &\leq \|\mathbf{x}(0) - \mathbf{x}^*\|_2 \exp(-0.5(1 - M^2)K_x t). \end{aligned}$$

□

Since $\mathbf{x}^* = \chi^\circledast$ is chosen as an arbitrary local minimizer χ^\circledast explicitly in the proof of Lemma 9, one can replace \mathbf{x}^* with χ^\circledast in Lemma 9 and its proof. Also, it is worth noting that, in general, M in (33) depends on χ^\circledast , especially when there are multiple local minimizers. This results in the following lemma:

Lemma 10 *Consider the system (28) with $K_x > 0$. Suppose that the optimization problem (2) is time-invariant, i.e., for all $t \geq 0$ and all $\mathbf{x} \in \mathbb{R}^{d_x}$, $\sigma(t, \mathbf{x}) = \sigma(0, \mathbf{x})$, $\mathbf{h}(t, \mathbf{x}) = \mathbf{h}(0, \mathbf{x})$, $\mathbf{y}_{\text{ref}}(t) = \mathbf{y}_{\text{ref}}(0)$, and $\mathbf{g}(t, \mathbf{x}) = \mathbf{g}(0, \mathbf{x})$. There exists a pair $\delta : \mathbb{R}^{d_x} \rightarrow \mathbb{R}_{>0}$ and $M : \mathbb{R}^{d_x} \rightarrow (0, M_{\text{sup}}]$ with $M_{\text{sup}} < 1$ such that, for any local minimizer χ^\circledast , if $\mathbf{x}(0) \in \mathcal{N}(\chi^\circledast, \delta(\chi^\circledast))$ then*

$$\|\mathbf{x}(t) - \chi^\circledast\|_2 \leq \|\mathbf{x}(0) - \chi^\circledast\|_2 \exp\left(-0.5(1 - M(\chi^\circledast)^2)K_x t\right). \quad (36)$$

Besides, from (33) and (34), one concludes:

Lemma 11 *For the pair δ and M in Lemma 10 and any local minimizer $\chi^\circledast(t)$ of (2) at instant t , if $\|\mathbf{x} - \chi^\circledast(t)\|_2 < \delta(\chi^\circledast(t))$ then*

$$(\mathbf{x} - \chi^\circledast(t))^\top \boldsymbol{\eta}(t, \mathbf{x}, \mathbf{y}_{\text{ref}}(t)) \leq -\frac{1}{2}(1 - M(\chi^\circledast(t))^2) \|\mathbf{x} - \chi^\circledast(t)\|_2^2 - \frac{1}{2} \|\boldsymbol{\eta}(t, \mathbf{x}, \mathbf{y}_{\text{ref}}(t))\|_2^2$$

$\forall t \geq 0$.

Due to the exponential convergence stated in Lemma 10, one may infer that similar convergence behavior holds even in the presence of time-variant σ , \mathbf{h} , \mathbf{y}_{ref} , and \mathbf{g} , provided that $\chi^\circledast(t)$ remains band-limited in the frequency domain. To formalize this inference, we present the following lemma.

Lemma 12 *Consider the system (28) with $K_x > 0$. Consider an arbitrary local minimizer $\chi^\circledast : \mathbb{R}_{\geq 0} \rightarrow \mathbb{R}^{d_x}$ of (2). Suppose that*

$$\|\dot{\chi}^\circledast(t)\|_2 \leq D_\chi \quad \forall t \geq 0. \quad (37)$$

There exists $\delta : \mathbb{R}^{d_x} \rightarrow \mathbb{R}_{>0}$ and $M : \mathbb{R}^{d_x} \rightarrow (0, M_{\text{sup}}]$ with $M_{\text{sup}} < 1$ such that if

$$\|\mathbf{x}(0) - \chi^\circledast(0)\|_2 < \delta(\chi^\circledast(0)), \quad (38)$$

$$\|\mathbf{x}(0) - \chi^\circledast(0)\|_2 \exp(-\kappa t) + \kappa^{-1} D_\chi < \delta(\chi^\circledast(t)) \quad \forall t > 0 \quad (39)$$

then

$$\|\mathbf{x}(t) - \chi^\circledast(t)\|_2 \leq \|\mathbf{x}(0) - \chi^\circledast(0)\|_2 \exp(-\kappa t) + \int_0^t \exp(-\kappa(t-\tau)) \|\dot{\chi}^\circledast(\tau)\|_2 d\tau, \quad (40)$$

where

$$\kappa = \frac{1}{2}(1 - M_{\text{sup}}^2) K_x. \quad (41)$$

Proof. Let (28) be rewritten in terms of error dynamics; this results in

$$\tilde{\mathbf{x}} = \mathbf{x} - \chi^\circledast, \quad (42)$$

$$\dot{\tilde{\mathbf{x}}} = K_x \boldsymbol{\eta}(t, \tilde{\mathbf{x}} + \chi^\circledast, \mathbf{y}_{\text{ref}}) - \dot{\chi}^\circledast. \quad (43)$$

This system can be considered as the nominal system

$$\dot{\tilde{\mathbf{x}}} = K_x \boldsymbol{\eta}(t, \tilde{\mathbf{x}} + \chi^\circledast, \mathbf{y}_{\text{ref}}) \quad (44)$$

perturbed by the perturbation $\dot{\chi}^\circledast$ [11]. For the nominal system (44), we choose (31) as the Lyapunov function, which, with respect to (42), becomes

$$U(\tilde{\mathbf{x}}) = \frac{1}{2} \tilde{\mathbf{x}}^\top K_x^{-1} \tilde{\mathbf{x}}. \quad (45)$$

In order to proceed, we introduce an Ansatz

$$\|\tilde{\mathbf{x}}(t)\|_2 < \delta(\boldsymbol{\chi}^\otimes(t)) \quad \forall t > 0, \quad (46)$$

meaning that $\mathbf{x}(t) = \tilde{\mathbf{x}}(t) + \boldsymbol{\chi}^\otimes(t)$ is always within the ball $\mathcal{N}(\boldsymbol{\chi}^\otimes(t), \delta(\boldsymbol{\chi}^\otimes(t)))$ around $\boldsymbol{\chi}^\otimes(t)$. At the end of this proof, we will show that this Ansatz is satisfied.

With (38) and Ansatz (46), one can apply Lemma 11 and obtains

$$\tilde{\mathbf{x}}^\top \boldsymbol{\eta}(t, \tilde{\mathbf{x}} + \boldsymbol{\chi}^\otimes, \mathbf{y}_{\text{ref}}) \leq -\frac{1}{2}(1 - M(\boldsymbol{\chi}^\otimes)^2) \|\tilde{\mathbf{x}}\|_2^2 - \frac{1}{2} \|\boldsymbol{\eta}(t, \tilde{\mathbf{x}} + \boldsymbol{\chi}^\otimes, \mathbf{y}_{\text{ref}})\|_2^2. \quad (47)$$

Consequently, the time derivative

$$\frac{d}{dt} U(\tilde{\mathbf{x}}) = \frac{\partial U(\tilde{\mathbf{x}})}{\partial \tilde{\mathbf{x}}} \dot{\tilde{\mathbf{x}}} = \tilde{\mathbf{x}}^\top \boldsymbol{\eta}(t, \tilde{\mathbf{x}} + \boldsymbol{\chi}^\otimes, \mathbf{y}_{\text{ref}}) \leq 0$$

is nonpositive. Analogously to the proof of Lemma 9, one concludes in sequence the Lyapunov stability, asymptotic stability (LaSalle's invariance principle [9]), and exponential stability (Grönwall's inequality [10]) of the nominal system (44)'s equilibrium point $\tilde{\mathbf{x}}^* = \mathbf{0}$.

Since the equilibrium points of the nominal system (44) are exponentially stable and the corresponding Lyapunov function (45) satisfies

$$b_1 \|\tilde{\mathbf{x}}\|_2^2 \leq U(\tilde{\mathbf{x}}) \leq b_2 \|\tilde{\mathbf{x}}\|_2^2, \quad b_1 = b_2 = \frac{1}{2} K_x^{-1}, \quad (48a)$$

$$\frac{d}{dt} U(\tilde{\mathbf{x}}) \leq -b_3 \|\tilde{\mathbf{x}}\|_2^2, \quad b_3 = \frac{1}{2} (1 - M_{\text{sup}}^2) \quad (48b)$$

$$\left\| \frac{\partial U(\tilde{\mathbf{x}})}{\partial \tilde{\mathbf{x}}} \right\|_2 = K_x^{-1} \|\tilde{\mathbf{x}}^\top\|_2 \leq b_4 \|\tilde{\mathbf{x}}^\top\|_2, \quad b_4 = K_x^{-1}, \quad (48c)$$

$$\left\| \frac{\partial U(\tilde{\mathbf{x}})}{\partial [t \ \mathbf{y}_{\text{ref}}^\top \ \boldsymbol{\chi}^{\otimes \top}]^\top} \right\|_2 = 0 \leq b_5 \|\tilde{\mathbf{x}}^\top\|_2, \quad b_5 = 0, \quad (48d)$$

with constants b_1, b_2, b_3, b_4, b_5 , the stability theorem for *slowly varying systems* [11] (see also Theorem 5) is applicable to the perturbed system (43) with slowly varying perturbation $\boldsymbol{\chi}^\otimes$ (37) (cf. Remark 5). This results in

$$\|\tilde{\mathbf{x}}(t)\|_2 \leq \|\tilde{\mathbf{x}}(0)\|_2 \exp(-\kappa t) + \frac{b_4}{2b_1} \int_0^t \exp(-\kappa(t-\tau)) \|\dot{\boldsymbol{\chi}}^\otimes(\tau)\|_2 d\tau \quad (49a)$$

$$\leq \|\tilde{\mathbf{x}}(0)\|_2 \exp(-\kappa t) + \frac{b_4}{2b_1} \frac{D_{\boldsymbol{\chi}}}{\kappa} = \|\tilde{\mathbf{x}}(0)\|_2 \exp(-\kappa t) + \kappa^{-1} D_{\boldsymbol{\chi}}, \quad (49b)$$

where $\kappa \in \mathbb{R}_{>0}$ is defined in (41). Note that (49a) is identical to (40). Furthermore, the inequality (49b), together with (39), confirms Ansatz (46). \square

As expected, when $\boldsymbol{\chi}^\otimes = \text{const.}$ ($\Leftrightarrow \dot{\boldsymbol{\chi}}^\otimes = \mathbf{0}$), Lemma 12 degenerates to Lemma 10, matching the desired behavior in Problem 1.1. Furthermore, the upper bound (49b) of

$\|\bar{\mathbf{x}}(t)\|_2$ converges exponentially to $\kappa^{-1}D_\chi = K_x^{-1}(1 - M_{\text{sup}}^2)^{-1}2D_\chi$ as t increases. Since the constants M_{sup} and D_χ are related to the problem instance only, one concludes that the behavior in Problem 1.2 is addressed.

One may notice that Condition (39) does not seem to be trivial, in contrast to the other two conditions (37) and (38). Let us start considering the worst case where M_{sup} is very close to 1. It is still manageable to make $\kappa \gg \max\{1, D_\chi\}$ by choosing a sufficiently large $K_x > 0$. As a result, the right-hand side of (49) converges virtually instantaneously. Thus, one may express (49) as

$$\forall t \gg \kappa^{-1} \approx 0^+, \|\bar{\mathbf{x}}(t)\|_2 \lesssim \kappa^{-1}\|\chi^\circledast(t)\|_2 \leq \kappa^{-1}D_\chi \approx 0^+,$$

indicating a virtually immediate closeness of $\mathbf{x}(t)$ to $\chi^\circledast(t)$. Therefore, the inequality (39) is satisfied from a practical point of view. Furthermore, since $\mathbf{x}(t)$ is virtually immediately close to $\chi^\circledast(t)$, the supremum M_{sup} of convergence rate is small (see Lemma 3). A small M_{sup} leads to a larger κ , see (41). In summary, we conclude the following remark.

Remark 1 *A larger K_x practically increases the likelihood of satisfying (39) and a sufficiently large $K_x > 0$ practically makes (39) satisfied.*

Consequently, we have the following theorem.

Theorem 2 *Consider the time-variant system (1) with an initial condition $\mathbf{x}(0)$ for state and a reference $\mathbf{y}_{\text{ref}}(t)$ for output. Consider the time-variant optimization problem (2) with a differentiable trajectory $\chi^\circledast : \mathbb{R}_{>0} \rightarrow \mathbb{R}^{d_x}$ of local minimizer. Consider some constant $K_x \in \mathbb{R}_{>0}$. Suppose that Assumptions 1 hold. If (37), (38), and (39) are satisfied, then*

$$\mathbf{u} = \boldsymbol{\mu}(t, \mathbf{x}, \mathbf{y}_{\text{ref}}; K_x) = \mathbf{B}(\mathbf{x})^{-1}(-f_A(\mathbf{x}) + K_x \boldsymbol{\eta}(t, \mathbf{x}, \mathbf{y}_{\text{ref}})) \quad (50)$$

with $\boldsymbol{\eta}$ defined in (16)(9d)(9e) solves Problem 1. The resulting closed-loop trajectory $\mathbf{x}(t)$ follows $\chi^\circledast(t)$ in an exponentially convergent manner described by (40).

Proof. Equations (21), (22), and (27) constitute (50). Lemma (12) delineates the convergence behavior of the closed-loop system (1)(50). \square

Although Theorem 2 solves Problem 1, it requires the initial value $\mathbf{x}(0)$ of system's state to be sufficiently close to a local minimizer $\chi^\circledast(0)$ of (2) at the initial instant $t = 0$, cf. (38).

Remark 2 *In all lemmata and theorems above, the notation $\mathcal{N}(\chi^\circledast, \delta) = \{\mathbf{x} \in \mathbb{R}^{d_x} \mid \|\mathbf{x} - \chi^\circledast\|_2 < \delta\}$ shall be read as “the interior of a ball of radius δ and center χ^\circledast ” rather than “an open neighborhood of χ^\circledast ”. Hence, $\mathbf{x}(0) \in \mathcal{N}(\chi^\circledast, \delta)$ or, equivalently, $\|\mathbf{x}(0) - \chi^\circledast\|_2 < \delta$ shall be read as “ $\mathbf{x}(0)$ being sufficiently close to χ^\circledast ” rather than “ $\mathbf{x}(0)$ being very close to χ^\circledast ”.*

It needs to be emphasized that \mathbf{x}^* and δ are chosen as pairs in the proof of Lemma 9 to specify

- the local minimizer (denoted χ^\circledast) that is being concerned (although it can be any local minimizer), and

- the region in which the quotient-linear convergence of (15) is guaranteed (Theorem 1).

The chosen pairs of \mathbf{x}^* and δ display a sufficient condition for the exponential convergence of $\mathbf{x}(t)$ as stated in Lemmata 9, 10, and 12. This condition does not exclude other regions in \mathbb{R}^{d_x} that ensure this kind of convergence.

However, the above statement does not address whether there exist points that lie outside the basin of attraction for any equilibrium point of (28). For exploring this further, insights from researches on Newton fractals [12–15] become relevant, considering that (28) originates from a quasi-Newton method (15). State-of-the-art research in this field has primarily focused on one-dimensional complex polynomials [12–15]. These works have revealed that the basin boundaries exhibit a fractal structure, dividing the complex plane into three types of regions: i) regions where the Newton-Raphson iteration converges to a root, ii) regions where the iteration converges to a periodic cycle, and iii) regions where no convergence occurs. While a one-dimensional complex polynomial can be expressed as a two-dimensional real polynomial, generalizing these findings to multidimensional polynomials is not trivial. Nevertheless, we hypothesize that certain properties of fractal basin boundaries in the two-dimensional case may extend to more general multidimensional polynomials. Building on this hypothesis and the Stone-Weierstrass approximation theorem [16], which states that any continuous function of multiple variables can be approximated by a polynomial, we propose that analogous fractal structures and convergence behaviors may also be present in the case with multidimensional real-valued continuously differentiable functions as in (7a). Accordingly, we posit the following proposition:

Proposition 1 *The real domain $\mathbb{R}^{d_x} = \mathcal{X}_1 \cup \mathcal{X}_2 \cup \mathcal{X}_3$ is composed of three complementary domains \mathcal{X}_1 , \mathcal{X}_2 , and \mathcal{X}_3 such that*

1. *If $\chi[0] \in \mathcal{X}_1$, then $\chi[k]$ of the interior-point iteration (15) converges to one of the local minimizers of (2).*
2. *If $\chi[0] \in \mathcal{X}_2$, then $\chi[k]$ converges to a periodic cycle. The points that form these cycles (summarized in $\mathcal{X}'_2 \subseteq \mathcal{X}_2$), due to the discrete nature of the sequence $\chi[k]$, are isolated points in \mathbb{R}^{d_x} .*
3. *If $\chi[0] \in \mathcal{X}_3$, then $\chi[k]$ does not converge at all. The domain \mathcal{X}_3 (Julia set) is a closed set and is nowhere dense in \mathbb{R}^{d_x} .*

Proposition 1 accounts for the behavior of the discrete-time system (15). Even though being related to (15), the continuous-time system (28) is able to overcome the undesired Cases 2 and 3:

- Due to the continuous nature of (28), $\dot{\mathbf{x}}(t)$ always drives the point $\mathbf{x}(t)$ into the neighborhood of $\mathbf{x}(t)$. This means, if $\mathbf{x}(t) \in \mathcal{X}'_2$, it is able to leave \mathcal{X}'_2 . Remember that \mathcal{X}'_2 is composed of isolated points.
- Since $\mathbf{x}(t)$ converges to some hyperplane from *any* initial condition (see Lemma 6), Case 3 does not exist for (28).

These observations conclude the following theorem:

Theorem 3 *If Proposition 1 is true, then **any $\mathbf{x}(0) \in \mathbb{R}^{d_x}$ is sufficiently close** (as explained in Remark 2) to at least one local minimizer of (2) at $t = 0$, meeting the requirement for $\mathbf{x}(0)$ specified as (38) in Theorem 2.*

We leave rigorously proving Proposition 1 (and consequently, Theorem 3) for future work.

2.4 Optimal tracking controller

It is obvious that the optimal tracking control problem (3) exhibits a high similarity with the time-variant pseudoconvex optimization problem (2). The result $\boldsymbol{\phi}^{\circledast} : [0, t_f] \rightarrow \mathbb{R}^{d_x}$ (a local minimizer) of (3) can be used to constitute the control

$$\mathbf{u} = \mathbf{B}(\boldsymbol{\phi}^{\circledast})^{-1}(\dot{\boldsymbol{\phi}}^{\circledast} - \mathbf{f}_A(\boldsymbol{\phi}^{\circledast}))$$

for the time-variant system (1) such that its state $\mathbf{x}(t)$ behaves optimally, i.e., $\mathbf{x}(t) = \boldsymbol{\phi}^{\circledast}(t) \forall t \geq 0$.

Numerical methods may be applied to obtain an approximated result which is close to a local minimizer. In doing so, one converts the cost functional to a cost function in discrete time; that is

$$\int_0^{t_f} \sigma(t, \boldsymbol{\phi}(t)) dt \approx \sigma(0, \boldsymbol{\phi}(0))\delta t + \sum_{n=1}^N \sigma(n\delta t, \boldsymbol{\phi}(n\delta t))\delta t \quad (51)$$

using the rectangle rule, where $\delta t \in \{\delta \in \mathbb{R}_{>0} \mid t_f/\delta \in \mathbb{N}^+ \wedge t_f/\delta \gg 1\}$ is a small positive number. Since δt is a positive constant and $\boldsymbol{\phi}(0) = \mathbf{x}(0)$ (cf. (3)) is determined, the cost function (51) can be replaced by

$$\varsigma(\boldsymbol{\varphi}) := \sum_{n=1}^N \sigma(n\delta t, \boldsymbol{\phi}(n\delta t)).$$

in the context of minimization. Herein,

$$\boldsymbol{\varphi} := [\boldsymbol{\phi}(1\delta t)^\top \quad \boldsymbol{\phi}(2\delta t)^\top \quad \dots \quad \boldsymbol{\phi}(N\delta t)^\top]^\top \in \mathbb{R}^{d_x N}$$

is the discrete representation of $\boldsymbol{\phi} : \mathbb{R}_{>0} \rightarrow \mathbb{R}^{d_x}$. Ergo, the optimal tracking control problem (3) can be approximately written as the nonlinear optimization problem

$$\min_{\boldsymbol{\varphi}} \varsigma(\boldsymbol{\varphi}) \quad (52a)$$

subject to

$$\mathbf{0} = \boldsymbol{\mathcal{H}}(\boldsymbol{\varphi}) - \boldsymbol{\mathcal{Y}}_{\text{ref}} \in \mathbb{R}^{d_y N}, \quad \boldsymbol{\mathcal{H}}(\boldsymbol{\varphi}) := \begin{bmatrix} \mathbf{h}(1\delta t, \boldsymbol{\phi}(1\delta t)) \\ \mathbf{h}(2\delta t, \boldsymbol{\phi}(2\delta t)) \\ \vdots \\ \mathbf{h}(N\delta t, \boldsymbol{\phi}(N\delta t)) \end{bmatrix}, \quad \boldsymbol{\mathcal{Y}}_{\text{ref}} := \begin{bmatrix} \mathbf{y}_{\text{ref}}(1\delta t) \\ \mathbf{y}_{\text{ref}}(2\delta t) \\ \vdots \\ \mathbf{y}_{\text{ref}}(N\delta t) \end{bmatrix}, \quad (52b)$$

$$\mathbf{0} \geq \boldsymbol{\mathcal{G}}(\boldsymbol{\varphi}) := \begin{bmatrix} \mathbf{g}(1\delta t, \boldsymbol{\phi}(1\delta t)) \\ \mathbf{g}(2\delta t, \boldsymbol{\phi}(2\delta t)) \\ \vdots \\ \mathbf{g}(N\delta t, \boldsymbol{\phi}(N\delta t)) \end{bmatrix} \in \mathbb{R}^{d_c N}. \quad (52c)$$

Since δt can be chosen arbitrarily close to zero, the problems (3) and (52) are isomorphic to each other.

It is reasonable to believe that the trajectory $\chi^\otimes : \mathbb{R}_{\geq 0} \rightarrow \mathbb{R}^{d_x}$ with $\chi^\otimes(t)$ being a local minimizer of (2) at time instant t is a local minimizer ϕ^\otimes of the optimal control problem (3), i.e., $\chi^\otimes(t) = \phi^\otimes(t) \forall t \in (0, t_f]$. Since (3) is not always analytically solvable, we analyze its discrete-time approximation (52) and present its equivalency to (2).

Lemma 13 *Let $\mathcal{E}^\otimes(t) \subset \mathbb{R}^{d_x}$ be the set of all local minimizers of the optimization problem (2) at instant t . For any local minimizer*

$$\varphi^\otimes = [\phi^\otimes(1\delta t)^\top \ \phi^\otimes(2\delta t)^\top \ \cdots \ \phi^\otimes(N\delta t)^\top]^\top$$

of the optimization problem (52) and any $n \in \mathbb{N}^+ \cap [1, N]$, there exists $\chi^\otimes(n\delta t) \in \mathcal{E}^\otimes(n\delta t)$ such that $\chi^\otimes(n\delta t) = \phi^\otimes(n\delta t)$.

Proof. For later use, we derive the partial derivatives of ς , \mathfrak{h} , and \mathfrak{g} as follows.

$$\mathfrak{q}(\varphi) := \left[\frac{\partial \varsigma(\varphi)}{\partial \varphi} \right]^\top = [\mathbf{q}(1\delta t, \phi(1\delta t))^\top \ \mathbf{q}(2\delta t, \phi(2\delta t))^\top \ \cdots \ \mathbf{q}(N\delta t, \phi(N\delta t))^\top]^\top,$$

$$\mathfrak{Q}(\varphi) := \frac{\partial \mathfrak{q}(\varphi)}{\partial \varphi} = \begin{bmatrix} \mathbf{Q}(1\delta t, \phi(1\delta t)) & \mathbf{0} & \cdots & \mathbf{0} \\ \mathbf{0} & \mathbf{Q}(2\delta t, \phi(2\delta t)) & \ddots & \mathbf{0} \\ \vdots & \mathbf{0} & \ddots & \mathbf{0} \\ \mathbf{0} & \mathbf{0} & \cdots & \mathbf{Q}(N\delta t, \phi(N\delta t)) \end{bmatrix},$$

$$\mathfrak{H}(\varphi) := \frac{\partial \mathfrak{h}(\varphi)}{\partial \varphi} = \begin{bmatrix} \mathbf{H}(1\delta t, \phi(1\delta t)) & \mathbf{0} & \cdots & \mathbf{0} \\ \mathbf{0} & \mathbf{H}(2\delta t, \phi(2\delta t)) & \ddots & \mathbf{0} \\ \vdots & \mathbf{0} & \ddots & \mathbf{0} \\ \mathbf{0} & \mathbf{0} & \cdots & \mathbf{H}(N\delta t, \phi(N\delta t)) \end{bmatrix}, \quad (53)$$

$$\mathfrak{G} := \frac{\partial \mathfrak{g}(\varphi)}{\partial \varphi} = \begin{bmatrix} \mathbf{G}(1\delta t) & \mathbf{0} & \cdots & \mathbf{0} \\ \mathbf{0} & \mathbf{G}(2\delta t) & \ddots & \mathbf{0} \\ \vdots & \mathbf{0} & \ddots & \mathbf{0} \\ \mathbf{0} & \mathbf{0} & \cdots & \mathbf{G}(N\delta t) \end{bmatrix},$$

where $\mathbf{q}(t, \mathbf{x})$, $\mathbf{H}(t, \mathbf{x})$, and $\mathbf{Q}(t, \mathbf{x})$ are given in (7c), (7d), and (8d), respectively.

Let the optimization problem (52) be solved by the interior-point iteration (15); it means that

$$\begin{aligned}\boldsymbol{\varphi}^{[k]} &= [\boldsymbol{\phi}^{[k]}(1\delta t)^\top \boldsymbol{\phi}^{[k]}(2\delta t)^\top \cdots \boldsymbol{\phi}^{[k]}(N\delta t)^\top]^\top, \\ \boldsymbol{\varphi}^{[k+1]} &= \boldsymbol{\varphi}^{[k]} + \mathcal{H}(\boldsymbol{\varphi}^{[k]})_{\mathcal{R}(\boldsymbol{\varphi}^{[k]})}^\# (\boldsymbol{y}_{\text{ref}} - \boldsymbol{h}(\boldsymbol{\varphi}^{[k]})) \\ &\quad - \left(\mathbf{I} - \mathcal{H}(\boldsymbol{\varphi}^{[k]})_{\mathcal{R}(\boldsymbol{\varphi}^{[k]})}^\# \mathcal{H}(\boldsymbol{\varphi}^{[k]}) \right) \mathcal{R}(\boldsymbol{\varphi}^{[k]})^{-1} \boldsymbol{r}(\boldsymbol{\varphi}^{[k]})\end{aligned}\quad (54)$$

converges to a local minimizer $\boldsymbol{\varphi}^\circledast$ as $k \in \mathbb{N}$ increases (Theorem 1). Herein, $\boldsymbol{r}(\boldsymbol{\varphi}) := [\partial \varrho(\boldsymbol{\varphi}) / \partial \boldsymbol{\varphi}]^\top$ and $\mathcal{R}(\boldsymbol{\varphi}) := \partial \boldsymbol{r}(\boldsymbol{\varphi}) / \partial \boldsymbol{\varphi}$ are the gradient and the Hessian, respectively, of the augmented cost function

$$\varrho(\boldsymbol{\varphi}) = \varsigma(\boldsymbol{\varphi}) + \frac{1}{2} \boldsymbol{\beta}(\boldsymbol{g}(\boldsymbol{\varphi}))^\top \boldsymbol{\beta}(\boldsymbol{g}(\boldsymbol{\varphi})),$$

cf. Definition 2. Easily, one can deduct

$$\begin{aligned}\boldsymbol{r}(\boldsymbol{\varphi}) &= \boldsymbol{g}(\boldsymbol{\varphi}) + \mathcal{G}^\top \boldsymbol{\xi}(\boldsymbol{g}(\boldsymbol{\varphi})), \quad \boldsymbol{\xi}(s) := \frac{\partial \boldsymbol{\beta}(s)^\top}{\partial s} \boldsymbol{\beta}(s) = \left[\frac{\partial \beta(s_i)}{\partial s_i} \beta(s_i) \right], \\ \mathcal{R}(\boldsymbol{\varphi}) &= \mathcal{Q}(\boldsymbol{\varphi}) + \mathcal{G}^\top \boldsymbol{\Xi}(\boldsymbol{g}(\boldsymbol{\varphi})) \mathcal{G}, \quad \boldsymbol{\Xi}(s) := \frac{\partial \boldsymbol{\xi}(s)}{\partial s}.\end{aligned}$$

Herein, $\boldsymbol{\xi} : \mathbb{R}^{d_s} \rightarrow \mathbb{R}^{d_s}$ is an element-wise function, and $\boldsymbol{\Xi} : \mathbb{R}^{d_s} \rightarrow \mathbb{R}^{d_s \times d_s}$ returns a diagonal and positive semidefinite matrix. This leads to

$$\boldsymbol{\xi}(\boldsymbol{g}(\boldsymbol{\varphi})) = \begin{bmatrix} \boldsymbol{\xi}(\boldsymbol{g}(1\delta t, \boldsymbol{\phi}(1\delta t))) \\ \boldsymbol{\xi}(\boldsymbol{g}(2\delta t, \boldsymbol{\phi}(2\delta t))) \\ \vdots \\ \boldsymbol{\xi}(\boldsymbol{g}(N\delta t, \boldsymbol{\phi}(N\delta t))) \end{bmatrix},$$

$$\boldsymbol{\Xi}(\boldsymbol{g}(\boldsymbol{\varphi})) = \begin{bmatrix} \boldsymbol{\Xi}(\boldsymbol{g}(1\delta t, \boldsymbol{\phi}(1\delta t))) & \mathbf{0} & \cdots & \mathbf{0} \\ \mathbf{0} & \boldsymbol{\Xi}(\boldsymbol{g}(2\delta t, \boldsymbol{\phi}(2\delta t))) & \ddots & \mathbf{0} \\ \vdots & \mathbf{0} & \ddots & \mathbf{0} \\ \mathbf{0} & \mathbf{0} & \cdots & \boldsymbol{\Xi}(\boldsymbol{g}(N\delta t, \boldsymbol{\phi}(N\delta t))) \end{bmatrix}.$$

Consequently, one obtains

$$\boldsymbol{r}(\boldsymbol{\varphi}) = \begin{bmatrix} \boldsymbol{r}(1\delta t, \boldsymbol{\phi}(1\delta t)) \\ \boldsymbol{r}(2\delta t, \boldsymbol{\phi}(2\delta t)) \\ \vdots \\ \boldsymbol{r}(N\delta t, \boldsymbol{\phi}(N\delta t)) \end{bmatrix},$$

$$\mathcal{R}(\boldsymbol{\varphi}) = \begin{bmatrix} \boldsymbol{R}(1\delta t, \boldsymbol{\phi}(1\delta t)) & \mathbf{0} & \cdots & \mathbf{0} \\ \mathbf{0} & \boldsymbol{R}(2\delta t, \boldsymbol{\phi}(2\delta t)) & \ddots & \mathbf{0} \\ \vdots & \mathbf{0} & \ddots & \mathbf{0} \\ \mathbf{0} & \mathbf{0} & \cdots & \boldsymbol{R}(N\delta t, \boldsymbol{\phi}(N\delta t)) \end{bmatrix}, \quad (55)$$

and that $\mathcal{R}(\boldsymbol{\varphi})$ is a block diagonal matrix where each block matrix $\boldsymbol{R}(t, \boldsymbol{x})$ is SPD. Herein, $\boldsymbol{r}(t, \boldsymbol{x})$ and $\boldsymbol{R}(t, \boldsymbol{x})$ are given in (7b) and (8c), respectively.

Since the weighted right pseudoinverse $\mathcal{H}(\boldsymbol{\varphi})_{\mathcal{R}(\boldsymbol{\varphi})}^{\#}$ is the key component of (54), we explore firstly its properties. By inserting (53) and (55) into $\mathcal{H}(\boldsymbol{\varphi})_{\mathcal{R}(\boldsymbol{\varphi})}^{\#}$ that is defined in (10), one obtains

$$\begin{aligned} \mathcal{H}(\boldsymbol{\varphi})_{\mathcal{R}(\boldsymbol{\varphi})}^{\#} &= \mathcal{R}(\boldsymbol{\varphi})^{-1} \mathcal{H}(\boldsymbol{\varphi})^{\top} \left(\mathcal{H}(\boldsymbol{\varphi}) \mathcal{R}(\boldsymbol{\varphi})^{-1} \mathcal{H}(\boldsymbol{\varphi})^{\top} \right)^{-1} \\ &= \begin{bmatrix} \boldsymbol{R}_{(1)} & \mathbf{0} & \cdots & \mathbf{0} \\ \mathbf{0} & \boldsymbol{R}_{(2)} & \ddots & \mathbf{0} \\ \vdots & \mathbf{0} & \ddots & \mathbf{0} \\ \mathbf{0} & \mathbf{0} & \cdots & \boldsymbol{R}_{(N)} \end{bmatrix}^{-1} \begin{bmatrix} \boldsymbol{H}_{(1)} & \mathbf{0} & \cdots & \mathbf{0} \\ \mathbf{0} & \boldsymbol{H}_{(2)} & \ddots & \mathbf{0} \\ \vdots & \mathbf{0} & \ddots & \mathbf{0} \\ \mathbf{0} & \mathbf{0} & \cdots & \boldsymbol{H}_{(N)} \end{bmatrix}^{\top} \left(\begin{bmatrix} \boldsymbol{H}_{(1)} & \mathbf{0} & \cdots & \mathbf{0} \\ \mathbf{0} & \boldsymbol{H}_{(2)} & \ddots & \mathbf{0} \\ \vdots & \mathbf{0} & \ddots & \mathbf{0} \\ \mathbf{0} & \mathbf{0} & \cdots & \boldsymbol{H}_{(N)} \end{bmatrix} \begin{bmatrix} \boldsymbol{R}_{(1)} & \mathbf{0} & \cdots & \mathbf{0} \\ \mathbf{0} & \boldsymbol{R}_{(2)} & \ddots & \mathbf{0} \\ \vdots & \mathbf{0} & \ddots & \mathbf{0} \\ \mathbf{0} & \mathbf{0} & \cdots & \boldsymbol{R}_{(N)} \end{bmatrix}^{-1} \begin{bmatrix} \boldsymbol{H}_{(1)} & \mathbf{0} & \cdots & \mathbf{0} \\ \mathbf{0} & \boldsymbol{H}_{(2)} & \ddots & \mathbf{0} \\ \vdots & \mathbf{0} & \ddots & \mathbf{0} \\ \mathbf{0} & \mathbf{0} & \cdots & \boldsymbol{H}_{(N)} \end{bmatrix}^{\top} \right)^{-1} \\ &= \begin{bmatrix} \boldsymbol{R}_{(1)}^{-1} \boldsymbol{H}_{(1)}^{\top} (\boldsymbol{H}_{(1)} \boldsymbol{R}_{(1)}^{-1} \boldsymbol{H}_{(1)}^{\top})^{-1} & \mathbf{0} & \cdots & \mathbf{0} \\ \mathbf{0} & \boldsymbol{R}_{(2)}^{-1} \boldsymbol{H}_{(2)}^{\top} (\boldsymbol{H}_{(2)} \boldsymbol{R}_{(2)}^{-1} \boldsymbol{H}_{(2)}^{\top})^{-1} & \ddots & \mathbf{0} \\ \vdots & \mathbf{0} & \ddots & \mathbf{0} \\ \mathbf{0} & \mathbf{0} & \cdots & \boldsymbol{R}_{(N)}^{-1} \boldsymbol{H}_{(N)}^{\top} (\boldsymbol{H}_{(N)} \boldsymbol{R}_{(N)}^{-1} \boldsymbol{H}_{(N)}^{\top})^{-1} \end{bmatrix} = \begin{bmatrix} [\boldsymbol{H}_{(1)}]_{\boldsymbol{R}_{(1)}}^{\#} & \mathbf{0} & \cdots & \mathbf{0} \\ \mathbf{0} & [\boldsymbol{H}_{(2)}]_{\boldsymbol{R}_{(2)}}^{\#} & \ddots & \mathbf{0} \\ \vdots & \mathbf{0} & \ddots & \mathbf{0} \\ \mathbf{0} & \mathbf{0} & \cdots & [\boldsymbol{H}_{(N)}]_{\boldsymbol{R}_{(N)}}^{\#} \end{bmatrix}, \end{aligned}$$

where $\boldsymbol{H}_{(n)} := \boldsymbol{H}(n\delta t, \boldsymbol{\phi}(n\delta t))$ and $\boldsymbol{R}_{(n)} := \boldsymbol{R}(n\delta t, \boldsymbol{\phi}(n\delta t))$. It shows evidently that the pseudoinverse of $\mathcal{H}(\boldsymbol{\varphi})$ for the entire time interval is equivalent to the pseudoinverse of $\boldsymbol{H}(t, \boldsymbol{\phi}(t))$ at each time instant and there is no interference among time instants. In fact, this observation is valid for the entire equation (54) (deduction is omitted). As a result, one concludes that for all $n \in \mathbb{N}^+ \cap [1, N]$

$$\begin{aligned} \boldsymbol{\phi}^{[k+1]}(n\delta t) &= \boldsymbol{\phi}^{[k]}(n\delta t) + [\boldsymbol{H}_{(n)}]_{\boldsymbol{R}_{(n)}}^{\#} \left(\boldsymbol{y}_{\text{ref}}(n\delta t) - \boldsymbol{h}(n\delta t, \boldsymbol{\phi}^{[k]}(n\delta t)) \right) \\ &\quad - \left(\boldsymbol{I} - [\boldsymbol{H}_{(n)}]_{\boldsymbol{R}_{(n)}}^{\#} \boldsymbol{H}_{(n)} \right) [\boldsymbol{R}_{(n)}]^{-1} \boldsymbol{r}(n\delta t, \boldsymbol{\phi}^{[k]}(n\delta t)) \\ &= \boldsymbol{\phi}^{[k]}(n\delta t) + \boldsymbol{\eta}(n\delta t, \boldsymbol{\phi}^{[k]}(n\delta t), \boldsymbol{y}_{\text{ref}}(n\delta t)) \end{aligned}$$

converges to $\phi^\circledast(n\delta t)$ as $k \in \mathbb{N}$ increases. This behavior is the same as that of $\chi^{[k]}(t)$, see (17). Therefore, one concludes that $\forall n \in \mathbb{N}^+ \cap [1, N]$, if $\phi^{[0]}(n\delta t) = \chi^{[0]}(n\delta t)$, then $\phi^\circledast(n\delta t) = \chi^\circledast(n\delta t)$. \square

Lemma 13 shows the equivalency between ϕ^\circledast and χ^\circledast in discrete time, and, consequently, the numerical equivalency between (2) and (3). Since δt can be chosen arbitrarily close to zero, we conclude $\phi^\circledast(t) = \chi^\circledast(t) \forall t \in (0, t_f]$. Therefore, Lemma 12, Remark 1, and Theorem 2 can be analogously applied here. Formally, we formulate the following theorem and remark.

Theorem 4 *Consider the time-variant system (1) with an initial condition $\mathbf{x}(0)$ for state and a reference trajectory \mathbf{y}_{ref} for output. Consider the controller (50) with $K_x = \text{const.} > 0$. Consider an arbitrary local minimizer*

$$\varphi^\circledast = [\phi^\circledast(1\delta t)^\top \phi^\circledast(2\delta t)^\top \dots \phi^\circledast(N\delta t)^\top]^\top$$

of (52). Suppose that

$$\phi^\circledast(0) = \mathbf{x}(0), \quad (56)$$

$$\|\dot{\phi}^\circledast(t)\|_2 \leq D_\phi \quad \forall t \geq 0. \quad (57)$$

There exists $\delta : \mathbb{R}^{d_x} \rightarrow \mathbb{R}_{>0}$ and $M : \mathbb{R}^{d_x} \rightarrow (0, M_{\text{sup}}]$ with $M_{\text{sup}} < 1$ such that if

$$\kappa^{-1} D_\phi < \delta(\phi^\circledast(t)) \quad \forall t > 0 \quad (58)$$

then

$$\|\mathbf{x}(t) - \phi^\circledast(t)\|_2 \leq \int_0^t \exp(-\kappa(t-\tau)) \|\dot{\phi}^\circledast(\tau)\|_2 d\tau, \quad (59)$$

where

$$\kappa = \frac{1}{2}(1 - M_{\text{sup}}^2)K_x.$$

Proof. It can be concluded immediately from Lemma 12, Theorem 2, and Lemma 13. It must be noted that (39) and (40) degenerate to (58) and (59), respectively, due to (56). \square

Remember that (56) is an equality constraint in (3), and it can be easily guaranteed.

Remark 3 *A larger K_x practically increases the likelihood of satisfying (58) and a sufficiently large $K_x > 0$ practically makes (58) satisfied.*

Since Theorem 4 addresses Problem 2 completely, we conclude that $\boldsymbol{\mu}$ in (50) is an OTC (Definition 1).

3 Computational complexity

In this section, we delve into a comprehensive analysis and comparison of computational complexity of OTC alongside the well-established and popular state-of-the-art methods interior-point algorithm (IPA) [1, 2, 5] and sequential quadratic programming (SQP) [1, 5, 8]. We analyze only the asymptotic upper bound of complexity denoted by the Bachmann-Landau big \mathcal{O} notation [17]. Also, we adopt $\mathcal{T}(\omega)$ and $\mathcal{S}(\omega)$ to denote the time and space complexity, respectively, of performing operation or procedure ω .

3.1 Optimal tracking controller

Time complexity

The time complexity of OTC (50) can be derived by counting the number of arithmetic operations. This results in

$$\mathcal{T}(\text{OTC}) = \mathcal{T}(\boldsymbol{\mu}) = \mathcal{T}(\mathbf{B}) + \mathcal{O}(d_x^3) + \mathcal{T}(\mathbf{f}_A) + \mathcal{T}(\boldsymbol{\eta}). \quad (60)$$

From the derivation of $\boldsymbol{\eta}$ in Section 2, we deduce the time complexity $\mathcal{T}(\boldsymbol{\eta})$ of $\boldsymbol{\eta}$ as follows:

$$\begin{aligned} \mathcal{T}(\boldsymbol{\eta}) &\stackrel{(9a)}{=} \mathcal{T}(\boldsymbol{\Lambda}(\cdot, \cdot, \mathbf{0})) + \mathcal{T}(\boldsymbol{\Lambda}) + \mathcal{O}((d_x + d_y)^3) \\ &\stackrel{(7)(8)}{=} \mathcal{T}(\mathbf{R}) + \mathcal{T}(\mathbf{H}) + \mathcal{T}(\mathbf{r}) + \mathcal{T}(\mathbf{h}) + \mathcal{O}((d_x + d_y)^3) \\ &= \mathcal{T}(\mathbf{Q}) + \mathcal{T}(\boldsymbol{\Xi}) + \mathcal{O}(d_c^2 d_x) + \mathcal{O}(d_c d_x^2) + \mathcal{T}(\mathbf{H}) \\ &\quad + \mathcal{T}(\mathbf{q}) + \mathcal{T}(\boldsymbol{\xi}) + \mathcal{O}(d_x d_c^2) + \mathcal{T}(\mathbf{h}) + \mathcal{O}((d_x + d_y)^3). \end{aligned} \quad (61)$$

By inserting (61) into (60), one obtains

$$\begin{aligned} \mathcal{T}(\text{OTC}) &= \mathcal{O}((d_x + d_y)^3) + \mathcal{O}(d_c^2 d_x) + \mathcal{O}(d_c d_x^2) + \mathcal{O}(d_x^3) \\ &\quad + \mathcal{T}(\mathbf{Q}) + \mathcal{T}(\boldsymbol{\Xi}) + \mathcal{T}(\mathbf{H}) + \mathcal{T}(\mathbf{q}) + \mathcal{T}(\boldsymbol{\xi}) + \mathcal{T}(\mathbf{h}) + \mathcal{T}(\mathbf{B}) + \mathcal{T}(\mathbf{f}_A). \end{aligned} \quad (62)$$

Space complexity

The required memory space is dominated by the matrices $\mathbf{R}(t, \mathbf{x}) \in \mathbb{R}^{d_x \times d_x}$, $\mathbf{H}(t, \mathbf{x}) \in \mathbb{R}^{d_y \times d_x}$, and $\boldsymbol{\Xi}(s) \in \mathbb{R}^{d_c \times d_c}$. This means

$$\mathcal{S}(\text{OTC}) = \mathcal{O}(d_x^2) + \mathcal{O}(d_y d_x) + \mathcal{O}(d_c^2). \quad (63)$$

3.2 Interior-point algorithm

Although the state-of-the-art IPA [1, 5] differs from the one we constructed in Section 2.1, it is still a sequence of Newton-Raphson iterations. In each iteration, a system of linear equation with a $(d_x + d_y + 2d_c)$ -by- $(d_x + d_y + 2d_c)$ symmetric coefficient matrix \mathbf{A} is established and solved. After sufficiently many iterations, the resulting

χ^\circledast must be converted to \mathbf{u} in order to drive (1). The simplest choice would be

$$\mathbf{u} = \mathbf{B}(\mathbf{x})^{-1}(-f_A(\mathbf{x}) + K_\chi(\chi^\circledast - \mathbf{x})), \quad K_\chi > 0. \quad (64)$$

Time complexity

By assuming the symmetric coefficient matrix \mathbf{A} to be also positive definite, one concludes $\mathcal{O}((d_x + d_y + 2d_c)^3)$ arithmetic operations, plus those required to evaluate σ , \mathbf{h} , logarithmic barrier function, and their derivatives, per iteration. Under some conservative assumptions (such as convex problem, $\chi^{[0]}$ is sufficiently close to χ^\circledast , among others), the IPA requires $k^\circledast = \mathcal{O}(\sqrt{d_c} \log(d_c \|\chi^{[0]} - \chi^\circledast(t)\|_2 / \varepsilon))$ iterations to achieve $\|\chi^{[k^\circledast]} - \chi^\circledast(t)\|_2 \leq \varepsilon$ [2, 4]. While the target precision ε can be set constant, the local minimizer $\chi^\circledast(t)$ is time-variant due to the time-variant problem (2). As a conclusion, the IPA's time complexity is

$$\begin{aligned} \mathcal{T}(\text{IPA})(t) = & \overbrace{\mathcal{O}(\sqrt{d_c} \log(d_c \ell(t)))}^{\text{number of iterations}} \times \overbrace{\left(\mathcal{O}((d_x + d_y + 2d_c)^3) + \mathcal{T}(\mathbf{Q}) + \mathcal{T}(\mathbf{H}) + \mathcal{T}(\mathbf{q}) + \mathcal{T}(\mathbf{h}) \right)}^{\text{number of operations within an iteration}} \\ & + \mathcal{O}(d_x^3) + \mathcal{T}(\mathbf{B}) + \mathcal{T}(f_A), \end{aligned} \quad (65)$$

where $\ell(t) := \|\chi^{[0]}(t) - \chi^\circledast(t)\|_2 / \varepsilon$, and $\mathcal{T}(\text{IPA})(t)$ inherits the time-variant property from $\ell(t)$. In general, one cannot choose the initial guess to be immediately close to $\chi^\circledast(t)$ without introducing further algorithmic procedures. Therefore, $\ell(t) \gg 1$ is a large number.

Space complexity

The required memory space is dominated by the coefficient matrix in each iteration. This means

$$\mathcal{S}(\text{IPA}) = \mathcal{O}((d_x + d_y + 2d_c)^2). \quad (66)$$

3.3 Sequential quadratic programming

As an iterative method, SQP [1, 5, 8] approximates a general nonlinear optimization problem with a sequence of quadratic programming (QP) subproblems and solves these QP subproblems at each iteration. In each iteration, the state-of-the-art SQP implementation [5] deploys an active-set method, which undertakes three steps:

- Step 1: Establish $d_y + d_a$ *active constraints* from all d_y equality constraints and the $d_a \in [0, d_c]$ inequality constraints on whose boundaries the current χ is. This turns the QP subproblem with equality and inequality constraints to an equality-constrained QP problem.
- Step 2: Solve the equality-constrained QP problem analytically using the method of Lagrange multipliers. This involves solving a system of linear equations with a $(d_x + d_y + d_a)$ -by- $(d_x + d_y + d_a)$ symmetric coefficient matrix. The resulting χ and the associated Lagrange multiplier ζ , relatively to those in the previous iteration, provides a search direction.

- Step 3: Given the search direction, a line-search procedure iteratively determines the step length that provides a sufficient decrease in a merit function. The merit function is constituted from the cost function and all constraints of the general nonlinear optimization problem.

After sufficiently many iterations, the resulting χ^{\otimes} must be converted to \mathbf{u} via, e.g., (64).

Time complexity

Hence, we conclude the time complexity of SQP

$$\begin{aligned} \mathcal{T}(\text{SQP}) = & \sum_{k=1}^{N_{\text{SQP}}} \left(\overbrace{\underbrace{\mathcal{O}(d_c d_x)}_{=\mathcal{O}(\mathbf{g})} + \mathcal{T}(\mathbf{Q}) + \mathcal{T}(\mathbf{H}) + \mathcal{T}(\mathbf{q}) + \mathcal{T}(\mathbf{h})}_{\text{Step 1}}} + \overbrace{\mathcal{O}((d_x + d_y + d_a[k])^3)}_{\text{Step 2}} \right. \\ & \left. + N_{\text{LS}}[k] \times \overbrace{(\mathcal{O}(d_c d_x) + \mathcal{T}(\sigma) + \mathcal{T}(\mathbf{h}))}_{\text{Step 3}} \right) \\ & + \mathcal{T}(\mathbf{B}) + \mathcal{O}(d_x^3) + \mathcal{T}(\mathbf{f}_A), \end{aligned}$$

where $d_y + d_a[k] \in [d_y, d_y + d_c]$ is the number of active constraints at the k -th iteration, $N_{\text{LS}}[k] \in \mathbb{N}$ the number of line search at the k -th iteration, and $N_{\text{SQP}} \in \mathbb{N}^+$ the number of the major SQP iterations. Since the active constraints (both size and content) vary over iterations, it is difficult to determine a formula for the upper bound of N_{SQP} [18, 19]. While several works [19, 20] focus on improving the update strategy of active constraints, we analyze in this work the SQP's iteration complexity under the following considerations:

1. SQP is a quasi-Newton method whose convergence behavior is described by Lemma 2 (mathematically proven [1, 8]).
2. If the initial guess satisfies all constraints, then SQP requires fewer iterations than IPA (empirical knowledge [1]).

Therefore, we conclude $N_{\text{LS}}[k] = 0 \forall k \in \mathbb{N}^+$ and $N_{\text{SQP}} = \mathcal{O}(\sqrt{d_c} \log(d_c \ell(t)))$ (cf. (65)), respectively, as the best-case upper-bound estimate. In summary,

$$\begin{aligned} \mathcal{T}(\text{SQP})(t) = & \overbrace{\mathcal{O}(\sqrt{d_c} \log(d_c \ell(t)))}_{\text{number of iterations}} \times \overbrace{(\mathcal{O}((d_x + d_y + d_c)^3) + \mathcal{T}(\mathbf{Q}) + \mathcal{T}(\mathbf{H}) + \mathcal{T}(\mathbf{q}) + \mathcal{T}(\mathbf{h}))}_{\text{number of operations within an iteration}} \\ & + \mathcal{O}(d_x^3) + \mathcal{T}(\mathbf{B}) + \mathcal{T}(\mathbf{f}_A), \end{aligned} \tag{67}$$

if the initial guess is sufficiently close to a local minimizer and satisfies all inequality and equality constraints. With this formula, the SQP's time complexity $\mathcal{T}(\text{SQP})(t)$ is time-variant, inheriting from $\ell(t)$.

Space complexity

The required memory space is dominated by the coefficient matrix in Step 2. This means

$$\mathcal{S}(\text{SQP}) = \mathcal{O}((d_x + d_y + d_c)^2). \quad (68)$$

3.4 Discussion

The comparison (62) vs. (65) vs. (67) makes it evident that OTC exhibits lower time complexity than IPA and SQP, while the comparison (63) vs. (66) vs. (68) suggests that OTC's space complexity is not higher than those of IPA and SQP. Particularly, in contrast to $\mathcal{T}(\text{IPA})(t)$ and $\mathcal{T}(\text{SQP})(t)$, which fluctuate over time, the time complexity $\mathcal{T}(\text{OTC})$ is steady and constant. This time-invariant performance is of substantial importance in addressing the time-variant control Problem 1 for the dynamical system (1) in real time.

It may become practically more usable if (62)–(68) are written in a more compact form. In fact, $d_y \ll d_x$ and $d_c \propto d_x$ is a valid assumption in most practical situations. Besides, it is reasonable to assume that $\mathcal{T}(\mathbf{Q}) + \mathcal{T}(\mathbf{Z}) + \mathcal{T}(\mathbf{H}) + \mathcal{T}(\mathbf{q}) + \mathcal{T}(\mathbf{\xi}) + \mathcal{T}(\mathbf{h}) + \mathcal{T}(\mathbf{B}) + \mathcal{T}(\mathbf{f}_A)$ grows not faster than $\mathcal{O}(d_x^3)$. These two assumptions allow us to simplify (62)–(68) without losing practical meanings. As a result,

$$\begin{aligned} \mathcal{T}(\text{OTC}) &= \mathcal{O}(d_x^3), & \mathcal{S}(\text{OTC}) &= \mathcal{O}(d_x^2), \\ \mathcal{T}(\text{IPA})(t) &= \mathcal{O}(\sqrt{d_x} \log(d_x \ell(t))) \times \mathcal{O}(d_x^3), & \mathcal{S}(\text{IPA}) &= \mathcal{O}(d_x^2), \\ \mathcal{T}(\text{SQP})(t) &= \mathcal{O}(\sqrt{d_x} \log(d_x \ell(t))) \times \mathcal{O}(d_x^3), & \mathcal{S}(\text{SQP}) &= \mathcal{O}(d_x^2). \end{aligned}$$

4 Implementation remark

In implementing OTC (50), we use the barrier function example β (5) in this work. The two parameters p_1 and p_2 of β need to be infinitely and sufficiently large, respectively, according to Lemma 1. In this section, we present a way to design p_1 and p_2 that satisfy the requirement of Lemma 1.

The derivations (7)–(9) show that β is not explicitly required, rather implicitly through functions ξ and Ξ , which are related to the derivatives of β , cf. (7c) and (8d). By analytically deriving ξ and Ξ , one is able to let $p_1 \rightarrow +\infty$; this results in

$$\lim_{p_1 \rightarrow +\infty} \xi(s) = \begin{cases} p_2^2 s & \text{if } s > 0, \\ 0 & \text{if } s \leq 0, \end{cases} \quad (69a)$$

$$\lim_{p_1 \rightarrow +\infty} \Xi(s) = \begin{cases} p_2^2 & \text{if } s > 0, \\ \frac{1}{4} (\ln(2) + 1) p_2^2 & \text{if } s = 0, \\ 0 & \text{if } s < 0, \end{cases} \quad (69b)$$

see Figure S2 for graphs.

When \mathbf{x} is in the interior of $\{\boldsymbol{\alpha} \mid \mathbf{g}(t, \boldsymbol{\alpha}) \leq \mathbf{0}\}$, the quantities $\xi(\mathbf{g}(t, \mathbf{x}))$ and $\Xi(\mathbf{g}(t, \mathbf{x}))$ become zero, regardless of p_2 's value. Otherwise, p_2 must be chosen sufficiently large such that the vector $\mathbf{R}(t, \mathbf{x})^{-1} \mathbf{r}(t, \mathbf{x})$ —which is a term related to ξ and Ξ in OTC (50), cf. (16), (9e), (8c), and (7b)—is dominated by the component directing to the interior, i.e.,

$$\begin{aligned} (\bar{\mathbf{G}}(t)^\top \bar{\mathbf{G}}(t))^{-1} \bar{\mathbf{G}}(t)^\top \bar{\mathbf{g}}(t, \mathbf{x}) &\approx \mathbf{R}(t, \mathbf{x})^{-1} \mathbf{r}(t, \mathbf{x}) & (70) \\ &\stackrel{(8c)(7b)}{=} (\mathbf{Q}(t, \mathbf{x}) + \mathbf{G}(t)^\top \Xi(\mathbf{g}(t, \mathbf{x})) \mathbf{G}(t))^{-1} (\mathbf{q}(t, \mathbf{x}) + \mathbf{G}(t)^\top \xi(\mathbf{g}(t, \mathbf{x}))) \\ &\stackrel{(69)}{=} (\mathbf{Q}(t, \mathbf{x}) + p_2^2 \bar{\mathbf{G}}(t)^\top \bar{\mathbf{G}}(t))^{-1} (\mathbf{q}(t, \mathbf{x}) + p_2^2 \bar{\mathbf{G}}(t)^\top \bar{\mathbf{g}}(t, \mathbf{x})). \end{aligned}$$

Herein, $\bar{\mathbf{g}}(t, \mathbf{x}) = \bar{\mathbf{G}}(t) \mathbf{x} + \bar{\mathbf{c}}(t)$ is the vector of positive elements in $\mathbf{g}(t, \mathbf{x})$, and the left-hand side of (70) corresponds to a Newton-Raphson step in finding the root of $\mathbf{0} = \bar{\mathbf{g}}(t, \mathbf{x})$ (cf. Section 7.1). This dominance can be ensured by

$$\|\mathbf{R}(t, \mathbf{x})\| \gg \|\mathbf{Q}(t, \mathbf{x})\| \Leftrightarrow K_{R/Q} := \frac{\|\mathbf{R}(t, \mathbf{x})\|}{\|\mathbf{Q}(t, \mathbf{x})\|} \gg 1.$$

Here, $\|\cdot\|$ denotes an arbitrary matrix norm. Using the triangle inequality

$$\|\mathbf{R}(t, \mathbf{x})\| = \|\mathbf{Q}(t, \mathbf{x}) + p_2^2 \bar{\mathbf{G}}(t)^\top \bar{\mathbf{G}}(t)\| \leq \|\mathbf{Q}(t, \mathbf{x})\| + p_2^2 \|\bar{\mathbf{G}}(t)^\top \bar{\mathbf{G}}(t)\|$$

leads to

$$K_{R/Q} \leq 1 + \frac{p_2^2 \|\bar{\mathbf{G}}(t)^\top \bar{\mathbf{G}}(t)\|}{\|\mathbf{Q}(t, \mathbf{x})\|},$$

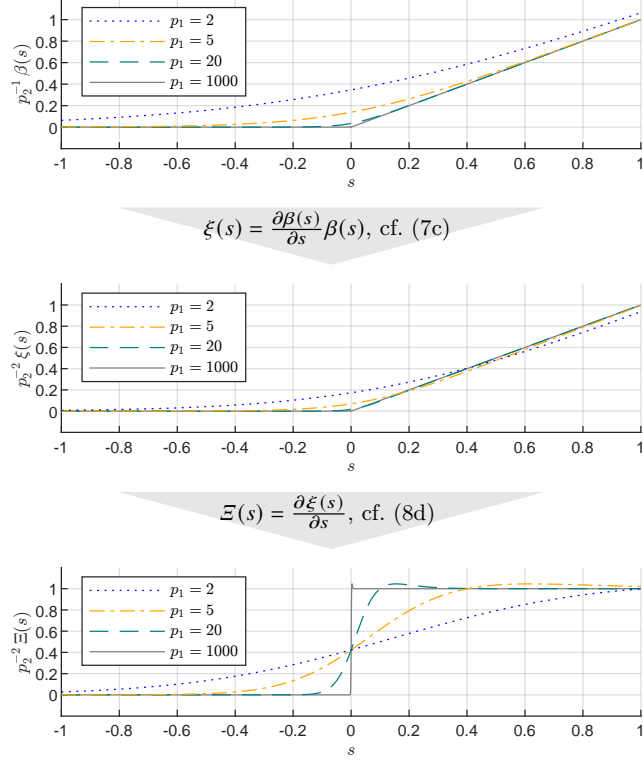


Fig. S2 Barrier function β and its derivative-related functions ξ and Ξ with various values for parameter p_1 .

which is equivalently

$$p_2^2 \geq \frac{(K_{R/Q} - 1) \|\mathbf{Q}(t, \mathbf{x})\|}{\|\bar{\mathbf{G}}(t)^\top \bar{\mathbf{G}}(t)\|}. \quad (71)$$

Any p_2 that satisfies (71) with a sufficiently large design parameter $K_{R/Q} \gg 1$ (typically, $K_{R/Q} > 1000$) can be considered sufficiently large in the concerned numerical context. Moreover, for a minimum computational overhead, we choose the maximum norm (maximum absolute row sum) for $\|\cdot\|$ and the equal sign in (71) for finding p_2 .

As already indicated in the deduction above, we construct

$$\mathbf{R}(t, \mathbf{x}) = \begin{cases} \mathbf{Q}(t, \mathbf{x}) & \text{if } \mathbf{g}(t, \mathbf{x}) \leq \mathbf{0}, \\ \mathbf{Q}(t, \mathbf{x}) + p_2^2 \bar{\mathbf{G}}(t)^\top \bar{\mathbf{G}}(t) & \text{otherwise,} \end{cases}$$

$$\mathbf{r}(t, \mathbf{x}) = \begin{cases} \mathbf{q}(t, \mathbf{x}) & \text{if } \mathbf{g}(t, \mathbf{x}) \leq \mathbf{0}, \\ \mathbf{q}(t, \mathbf{x}) + p_2^2 \bar{\mathbf{G}}(t)^\top \bar{\mathbf{g}}(t, \mathbf{x}) & \text{otherwise} \end{cases}$$

for $\boldsymbol{\eta}$ in OTC (50), cf (16), (9d), and (9e), depending on the violation of inequality constraint.

For a large p_2 , it is likely that the SPD matrix $\mathbf{R}(t, \mathbf{x})$ becomes ill-conditioned. This may cause non-negligible numerical errors in computing its inverse. To overcome this, we apply the following numerical procedure:

- If $\mathbf{R}(t, \mathbf{x})$ is diagonal, we construct a diagonal matrix whose diagonal elements are reciprocal of the corresponding elements of $\mathbf{R}(t, \mathbf{x})$.
- Otherwise, we apply the Cholesky decomposition on $\mathbf{R}(t, \mathbf{x})$ followed by forward and back substitutions.

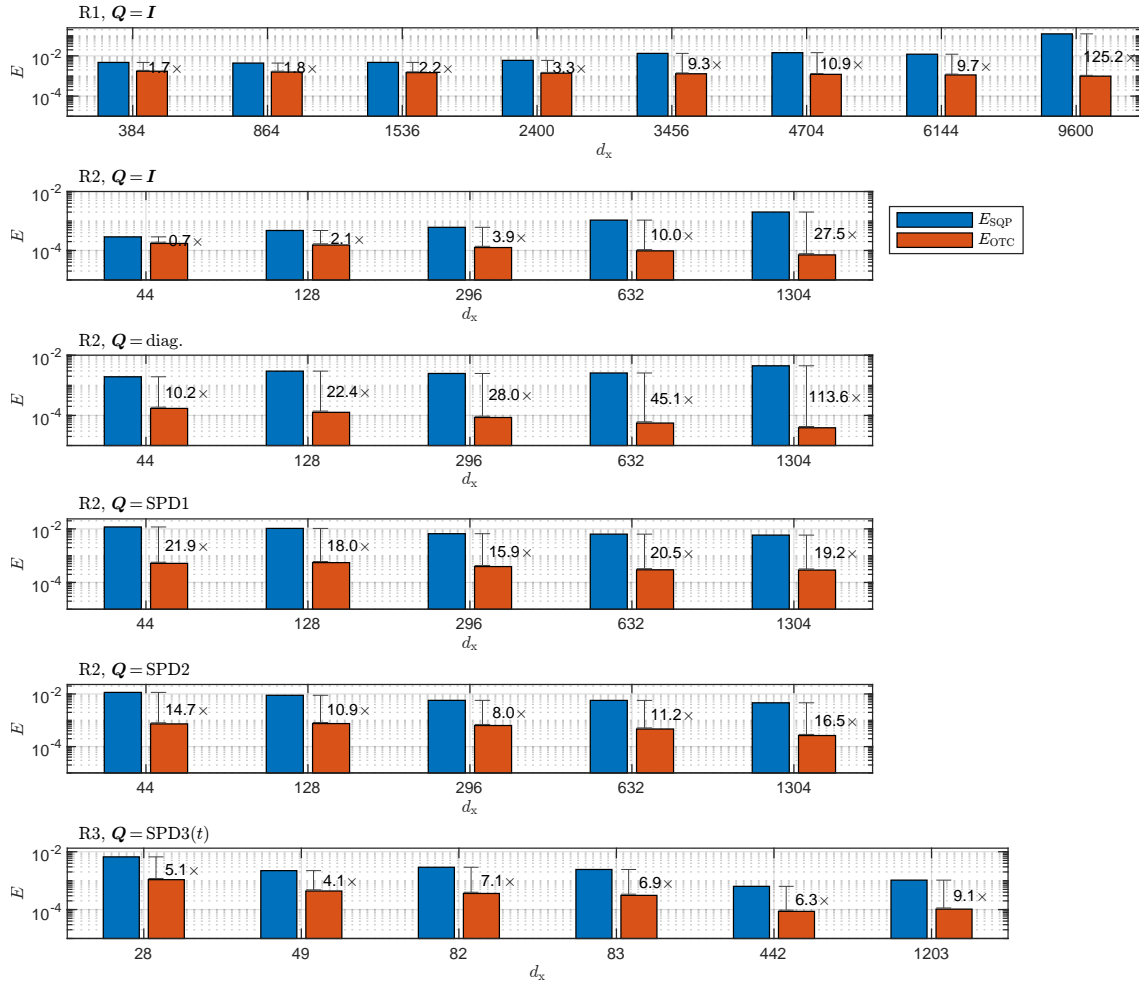


Fig. S3 Values of absolute accuracy metrics E_{OTC} and E_{SQP} , cf. (72), for all Examples R1–R3 of real-world problems. Each plot represents a numerical scenario characterized by the system’s dimension d_x and the cost function’s Hessian matrix Q (identity matrices I , diagonal matrices, and three different types of symmetric and positive definite matrices).

6 State-constrained systems

In this section, we consider the system

$$\dot{\boldsymbol{x}} = \boldsymbol{f}_A(\boldsymbol{x}) + \boldsymbol{B}(\boldsymbol{x})\boldsymbol{u}, \quad \boldsymbol{x}(t) \in \mathcal{X}(t) := \{ \boldsymbol{x} \in \mathbb{R}^{d_x} \mid \boldsymbol{h}(t, \boldsymbol{x}) = \mathbf{0} \wedge \boldsymbol{g}(t, \boldsymbol{x}) \leq \mathbf{0} \} \quad (73)$$

whose state \boldsymbol{x} is subject to both equality and inequality constraints. Here, the functions \boldsymbol{f}_A , \boldsymbol{B} , \boldsymbol{h} , and \boldsymbol{g} are the same as in the system and problem class (1)–(3), i.e., system (73) is identical to (1)–(3), except that there is no cost function σ involved.

Even though σ is not present, the augmented cost function ρ (4) can still be constructed solely from $\boldsymbol{g}(t, \boldsymbol{x})$, allowing the derivation of OTC in Section 2 and the design of the barrier function in Section 4 to be applied on system (73). This results in the controller

$$\boldsymbol{u} = \boldsymbol{\omega}(t, \boldsymbol{x}, \boldsymbol{v}) := \boldsymbol{B}(\boldsymbol{x})^{-1} \left(-\boldsymbol{f}_A(\boldsymbol{x}) + K_x \boldsymbol{\omega}_A(t, \boldsymbol{x}) + \boldsymbol{\Omega}_B(t, \boldsymbol{x})\boldsymbol{v} \right), \quad K_x > 0 \quad (74a)$$

with

$$\boldsymbol{\omega}_A(t, \boldsymbol{x}) := \begin{cases} -\boldsymbol{H}(t, \boldsymbol{x}) \#_I \boldsymbol{h}(t, \boldsymbol{x}) & \text{if } \boldsymbol{g}(t, \boldsymbol{x}) \leq \mathbf{0}, \\ -\boldsymbol{H}(t, \boldsymbol{x}) \#_I \boldsymbol{h}(t, \boldsymbol{x}) - (\boldsymbol{I} - \boldsymbol{H}(t, \boldsymbol{x}) \#_I \boldsymbol{H}(t, \boldsymbol{x})) (\overline{\boldsymbol{G}}(t)^\top \overline{\boldsymbol{G}}(t))^{-1} \overline{\boldsymbol{G}}(t)^\top \overline{\boldsymbol{g}}(t, \boldsymbol{x}) & \text{otherwise,} \end{cases} \quad (74b)$$

$$\boldsymbol{\Omega}_B(t, \boldsymbol{x}) := \begin{cases} \boldsymbol{I} - \boldsymbol{H}(t, \boldsymbol{x}) \#_I \boldsymbol{H}(t, \boldsymbol{x}) & \text{if } \boldsymbol{g}(t, \boldsymbol{x}) \leq \mathbf{0}, \\ \boldsymbol{I} - \begin{bmatrix} \overline{\boldsymbol{G}}(t) \\ \boldsymbol{H}(t, \boldsymbol{x}) \end{bmatrix} \#_I \begin{bmatrix} \overline{\boldsymbol{G}}(t) \\ \boldsymbol{H}(t, \boldsymbol{x}) \end{bmatrix} & \text{otherwise,} \end{cases} \quad (74c)$$

and a new input $\boldsymbol{v} \in \mathbb{R}^{d_x}$. Herein, $\overline{\boldsymbol{g}}(t, \boldsymbol{x}) = \overline{\boldsymbol{G}}(t)\boldsymbol{x} + \overline{\boldsymbol{c}}(t)$ is the vector of positive elements in $\boldsymbol{g}(t, \boldsymbol{x})$, i.e., the components of inequality constraints that are active at t and \boldsymbol{x} .

Since $\boldsymbol{\omega}_A$ is a variant of $\boldsymbol{\eta}$ (16) in absence of σ and when $\boldsymbol{y}_{\text{ref}} = \mathbf{0}$, Theorem 2 is applicable here; this means, $\boldsymbol{x}(t)$ of the closed-loop system (73)(74) converges exponentially to $\mathcal{X}(t)$ as $t \geq 0$ increases. Furthermore, the matrix $\boldsymbol{\Omega}_B(t, \boldsymbol{x})$ projects \boldsymbol{v} into a local null space of $\boldsymbol{h}(t, \cdot)$ (equality constraint) and $\overline{\boldsymbol{g}}(t, \cdot)$ (active inequality constraint); this means, \boldsymbol{v} can be freely chosen without violating the state constraints. Therefore, the control \boldsymbol{u} provided by (74) is admissible.

With the aid of the admissible transformation $\boldsymbol{\omega}$ in (74), the state-constrained feedback control problem, i.e., finding \boldsymbol{u} for (73), is reduced to an unconstrained one, i.e., finding \boldsymbol{v} for

$$\dot{\boldsymbol{x}} = K_x \boldsymbol{\omega}_A(t, \boldsymbol{x}) + \boldsymbol{\Omega}_B(t, \boldsymbol{x})\boldsymbol{v}. \quad (75)$$

This unconstrained problem can be solved by standard control methods [11] such as feedback linearization, sliding mode control, and, when applicable, linear-quadratic regulator (LQR) [21]. This provides a way for generalizing a wide spectrum of control methods to accommodate state constraints. As an example, we demonstrate in the following section the generalization of LQR to a *state-constrained LQR*.

6.1 State-constrained linear-quadratic regulator

Let us consider the following state-constrained linear-quadratic (LQ) problem

$$\min_{\mathbf{x}, \mathbf{u}} \int_0^\infty \mathbf{x}(t)^\top \mathbf{Q}_{xx} \mathbf{x}(t) + \mathbf{u}(t)^\top \mathbf{Q}_{uu} \mathbf{u}(t) dt \quad (76a)$$

subject to

$$\dot{\mathbf{x}} = \mathbf{A}\mathbf{x} + \mathbf{B}\mathbf{u}, \quad (76b)$$

$$\mathbf{0} = \mathbf{H}\mathbf{x}. \quad (76c)$$

In order to approach (76), we apply the admissible transformation

$$\mathbf{u} = \boldsymbol{\omega}(\mathbf{x}, \mathbf{v}) = \mathbf{B}^{-1} \left(-\mathbf{A}\mathbf{x} - K_x \mathbf{H}_I^\# \mathbf{H}\mathbf{x} + (\mathbf{I} - \mathbf{H}_I^\# \mathbf{H})\mathbf{v} \right), \quad (77)$$

which is a special case of (74) with $\mathbf{g}(t, \mathbf{x}) = \mathbf{O}\mathbf{x} - 1 \leq \mathbf{0} \forall \mathbf{x}$. The transformation (77) reduces (76) to the unconstrained LQ problem

$$\min_{\mathbf{x}, \mathbf{v}} \int_0^\infty \mathbf{x}(t)^\top (\mathbf{Q}_{xx} + \boldsymbol{\Omega}_A^\top \mathbf{Q}_{uu} \boldsymbol{\Omega}_A) \mathbf{x}(t) + \mathbf{v}(t)^\top \boldsymbol{\Omega}_B^\top \mathbf{Q}_{uu} \boldsymbol{\Omega}_B \mathbf{v}(t) + 2\mathbf{x}(t)^\top \boldsymbol{\Omega}_A^\top \mathbf{Q}_{uu} \boldsymbol{\Omega}_B \mathbf{v}(t) dt \quad (78a)$$

subject to

$$\dot{\mathbf{x}} = \boldsymbol{\Omega}_A \mathbf{x} + \boldsymbol{\Omega}_B \mathbf{v}, \quad \boldsymbol{\Omega}_A := -K_x \mathbf{H}_I^\# \mathbf{H}, \quad \boldsymbol{\Omega}_B := \mathbf{I} - \mathbf{H}_I^\# \mathbf{H}, \quad (78b)$$

which can be solved by the LQR [21]. We denote the solution as

$$\mathbf{v} = \mathbf{v}_{\text{LQR}}(\mathbf{x}). \quad (79)$$

Inserting (79) into (77) yields the *state-constrained linear-quadratic regulator* (SCLQR)

$$\mathbf{u} = \mathbf{B}^{-1} \left(-\mathbf{A}\mathbf{x} - K_x \mathbf{H}_I^\# \mathbf{H}\mathbf{x} + (\mathbf{I} - \mathbf{H}_I^\# \mathbf{H})\mathbf{v}_{\text{LQR}}(\mathbf{x}) \right). \quad (80)$$

A numerical example demonstrating this SCLQR's effectiveness will be shown later in this section.

It must be noted that incorporating linear inequality constraint in (76) results in an unconstrained optimal control problem with a *non-quadratic* cost functional and a *nonlinear* system. Addressing this class of problem requires advanced optimal control methods, which are beyond the scope of this work.

6.2 Outlook into optimal trajectory planner

Accompanying with (73) there is usually an output function

$$\mathbf{z} = \mathbf{f}_C(t, \mathbf{x}). \quad (81)$$

One may want to find an optimal trajectory regarding some cost functional, e.g., (76a), such that the output \mathbf{z} eventually reaches a predefined goal \mathbf{z}_g . If the trajectory generated by a state-constrained optimal controller

$$\mathbf{u} = \boldsymbol{\omega}(t, \mathbf{x}, \mathbf{v}) := \mathbf{B}(\mathbf{x})^{-1} \left(-f_A(\mathbf{x}) + K_x \boldsymbol{\omega}_A(t, \mathbf{x}) + \boldsymbol{\Omega}_B(t, \mathbf{x}) \mathbf{v}^\otimes(t, \mathbf{x}) \right), \quad (82)$$

such as (80), somehow passes through \mathbf{z}_g , i.e.,

$$\left\{ \tau \geq 0 \left| \begin{array}{l} \mathbf{z}_g = f_C(\tau, \mathbf{x}(\tau)) \\ \dot{\mathbf{x}}(t) = K_x \boldsymbol{\omega}_A(t, \mathbf{x}(t)) + \boldsymbol{\Omega}_B(t, \mathbf{x}(t)) \mathbf{v}^\otimes(t, \mathbf{x}(t)) \\ \mathbf{x}(0) \in \mathcal{X}(0) \end{array} \right. \right\} \neq \emptyset,$$

then (82) is the optimal trajectory planner. This insight points to a new methodological direction for solving optimal trajectory planning problems using closed-form feedback controllers. For instance, the controller (82) can be applied to each agent in a multi-agent system setting, enabling the entire swarm to chart a whole state space by labeling each point with the reachability of \mathbf{z}_g and the associated cost starting from that point. The resulting *map* of the labeled state space can serve as valuable prior knowledge for the higher-level optimal controller targeting \mathbf{z}_g . A numerical example illustrating this idea of multi-agent cartography is shown in the following subsection.

6.3 Numerical example and result

In order to illustrate the ideas mentioned above, we construct an example for (76):

$$\begin{aligned} \mathbf{x} &= \begin{bmatrix} x_1 \\ x_2 \\ x_3 \end{bmatrix}, \quad \mathbf{u} = \begin{bmatrix} u_1 \\ u_2 \\ u_3 \end{bmatrix}, \\ \mathbf{Q}_{xx} &= \begin{bmatrix} 1.04 & -0.01695 & 0.2303 \\ -0.01695 & 0.7284 & 0.2473 \\ 0.2303 & 0.2473 & 1.898 \end{bmatrix}, \quad \mathbf{Q}_{uu} = \begin{bmatrix} 7.331 & 0.1877 & 2.067 \\ 0.1877 & 2.328 & -0.6628 \\ 2.067 & -0.6628 & 3.956 \end{bmatrix} \times 10^{-5}, \\ \mathbf{A} &= \begin{bmatrix} 0.1086 & -0.2032 & -0.02073 \\ 0.1763 & 0.6136 & 0.5626 \\ -0.5076 & -0.3963 & -0.1000 \end{bmatrix}, \quad \mathbf{B} = \begin{bmatrix} 0.6665 & 0.9614 & -0.8088 \\ 0.3533 & 0.1329 & -0.875 \\ -0.8267 & -0.5846 & -0.9484 \end{bmatrix}, \\ \mathbf{H} &= [-0.3317 \ 0.1136 \ 0.6919], \\ f_C(t, \mathbf{x}) &= \left(x_1 + \frac{46}{25} \right)^2 - (x_2 - 2)^2 - \left(3x_3 - \frac{12}{25} \right) \left(x_3 - \frac{4}{25} \right) + 4, \quad \mathbf{z}_g = 0. \end{aligned}$$

The matrix \mathbf{H} defines \mathcal{X} to be a two-dimensional plane in the three-dimensional space. This 2-D plane can be parametrically represented as

$$\mathbf{x} = \boldsymbol{\psi}(\boldsymbol{\gamma}) = \begin{bmatrix} \gamma_1 \\ \gamma_2 \\ 0.4795 \gamma_1 - 0.1642 \gamma_2 \end{bmatrix}$$

with parametric coordinates $\boldsymbol{\gamma} = [\gamma_1 \ \gamma_2]^\top$. We use this coordinate transformation to project the constraint into a 2-D space, providing a more informative and readable illustration in Figure S4(a).

Figure S4 shows the resulting trajectories of system (73)'s state $\mathbf{x}(t)$ starting from two distinct initial conditions $\mathbf{x}(0)$ and driven by a control \mathbf{u} that is

- determined numerically using iterative algorithm for constrained optimization [5].
- provided by the SCLQR (80) with $K_x = 500$.

Merely a slight difference between these two trajectories \mathbf{x}_{num} and $\mathbf{x}_{\text{SCLQR}}$ is noticeable, see Figure S4. In fact, the difference

$$\|\Delta\mathbf{x}(t)\|_2 := \|\mathbf{x}_{\text{num}}(t) - \mathbf{x}_{\text{SCLQR}}(t)\|_2$$

is on the order of magnitude of 10^{-3} , see Figure S4(b). Also, the values of running cost

$$c_{\square}(t) := \int_0^t (\mathbf{x}_{\square}(\tau)^\top \mathbf{Q}_{\text{xx}} \mathbf{x}_{\square}(\tau) + \mathbf{u}_{\square}(\tau)^\top \mathbf{Q}_{\text{uu}} \mathbf{u}_{\square}(\tau)) \, d\tau$$

are almost the same, with a difference

$$\Delta c(t) := c_{\text{num}}(t) - c_{\text{SCLQR}}(t)$$

on the order of magnitude of 10^{-4} , see Figure S4(b). These very small differences $\|\Delta\mathbf{x}(t)\|_2$ and $\Delta c(t)$ are presumably numerical in nature, probably originating from

- discrete-time integral (numerical solver and SCLQR),
- the convex but not strongly convex cost functional (78a) due to rank-deficient \mathbf{Q}_{B} (SCLQR),
- finite horizon $t \in [0, 0.5]$ (numerical solver) instead of infinite horizon $t \in [0, +\infty)$ (SCLQR), and
- premature termination of iteration due to numerical resolution (numerical solver).

Note, this example can be viewed as the simplest multi-agent system with two agents only. The trajectory of agent ① passes through the curve that defines all solutions in the state space that correspond to the goal z_g , see Figure S4(a).

These numerical results showcase the effectiveness of the proposed SCLQR that combines OTC and LQR, suggesting OTC's capability in generalizing standard control methods to incorporate state constraints. Also, they demonstrate the potential of OTC for simultaneous optimal trajectory planning and tracking control, which will be further investigated in the future.

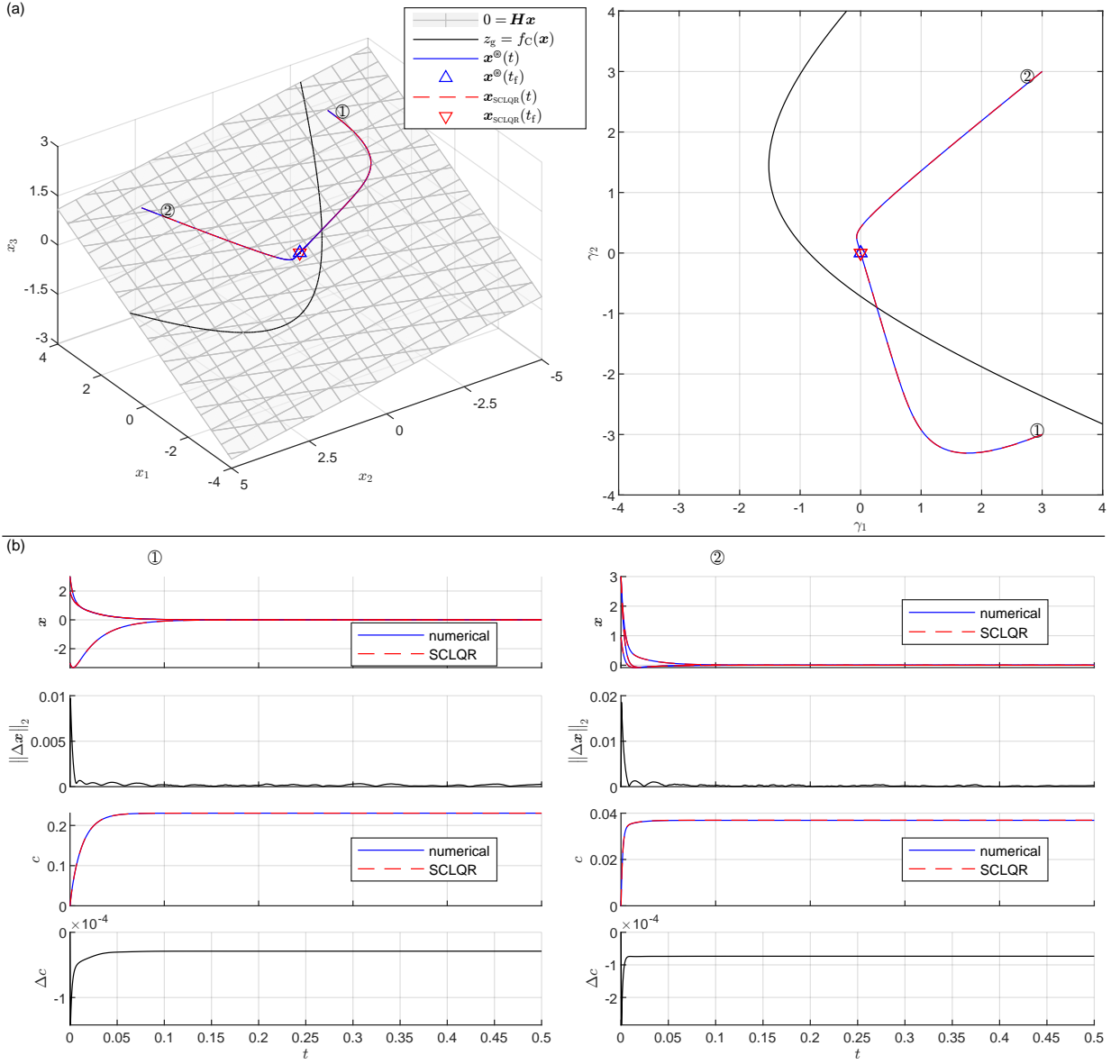


Fig. S4 Exemplary three-dimensional state-constrained linear-quadratic problem (76) solved numerically and by SCLQR (80). The difference between the resulting state trajectories, colored with blue and red, respectively, is negligible, being tested with two initial conditions $\mathbf{x}(0)$. (a) State trajectories in the 3-D coordinate system (left) and in the 2-D parametric coordinate system (right). (b) Time evolution of relevant quantities. Refer to texts for detailed description.

7 Background material

7.1 Newton-Raphson method

The Newton-Raphson method is a root-finding algorithm which produces successively better approximations to a root of a system of nonlinear equations

$$\mathbf{0} = \mathbf{r}(\boldsymbol{\chi}) \quad (83)$$

with continuously differentiable $\mathbf{r} : \mathbb{R}^m \rightarrow \mathbb{R}^n$. Given a suitable initial guess $\boldsymbol{\chi}^{[0]}$, the iterative formula

$$\boldsymbol{\chi}^{[k+1]} = \boldsymbol{\chi}^{[k]} - \mathbf{R}(\boldsymbol{\chi}^{[k]})^\# \mathbf{r}(\boldsymbol{\chi}^{[k]}) \quad (84)$$

improves the guess at each iteration [6]. Herein, $\boldsymbol{\chi}^{[k]}$ denotes the estimate of a root at the k -th iteration, $\mathbf{R}(\boldsymbol{\chi}) = \partial \mathbf{r}(\boldsymbol{\chi}) / \partial \boldsymbol{\chi}$ the Jacobian of \mathbf{r} , and $\mathbf{A}^\#$ a suitable pseudoinverse of the matrix \mathbf{A} . Should $m = n$ and $\mathbf{R}(\boldsymbol{\chi})$ be invertible for all $\boldsymbol{\chi} \in \mathbb{R}^m$, the pseudoinverse $\mathbf{R}(\boldsymbol{\chi}^{[k]})^\#$ becomes the inverse $\mathbf{R}(\boldsymbol{\chi}^{[k]})^{-1}$. The update

$$\boldsymbol{\chi}^{[k+1]} - \boldsymbol{\chi}^{[k]} = -\mathbf{R}(\boldsymbol{\chi}^{[k]})^\# \mathbf{r}(\boldsymbol{\chi}^{[k]})$$

is known as a *Newton-Raphson step*. The convergence behavior of (84) is described in Lemma 2.

Application in optimization

Optimization aims at finding critical points—which are local minima, local maxima, or saddle points (minimax points)—of a twice continuously differentiable scalar function $\rho : \mathbb{R}^m \rightarrow \mathbb{R}$ [1]. This is equivalent to finding the zeros of ρ 's gradient $\mathbf{r}(\boldsymbol{\chi}) := [\partial \rho(\boldsymbol{\chi}) / \partial \boldsymbol{\chi}]^\top$, i.e., finding the roots of (83).

7.2 Stability of slowly varying systems

Theorem 5 (Stability theorem for slowly varying systems [11]) *Consider the system*

$$\dot{\boldsymbol{\theta}} = \mathbf{f}(\boldsymbol{\theta}, \mathbf{v}) \quad (85)$$

with state $\boldsymbol{\theta} \in \mathbb{R}^{d_\theta}$, input $\mathbf{v} \in \mathcal{V} \subset \mathbb{R}^{d_v}$, and locally Lipschitz continuous $\mathbf{f} : \mathbb{R}^{d_\theta} \times \mathcal{V} \rightarrow \mathbb{R}^{d_\theta}$. Suppose

$$\boldsymbol{\psi} \in \{\boldsymbol{\psi} : \mathbb{R}^{d_v} \rightarrow \mathbb{R}^{d_\theta} \mid \mathbf{0} = \mathbf{f}(\boldsymbol{\psi}(\mathbf{v}), \mathbf{v}) \ \forall \mathbf{v} \in \mathcal{V}\} \quad (86)$$

exists uniquely and is differentiable. Let $\boldsymbol{\Psi}(\mathbf{v}) := \partial \boldsymbol{\psi}(\mathbf{v}) / \partial \mathbf{v}$. Suppose $\|\boldsymbol{\Psi}(\mathbf{v})\|_2 \leq D_\Psi$ for all $\mathbf{v} \in \mathbb{R}^{d_v}$. Suppose $\mathbf{v}(t)$ is continuously differentiable and $\|\dot{\mathbf{v}}(t)\|_2 \leq D_v$ for all $t \geq 0$. Suppose there exists for

$$\tilde{\boldsymbol{\theta}}(t) := \boldsymbol{\theta}(t) - \boldsymbol{\psi}(\mathbf{v}(t)), \quad (87a)$$

$$\dot{\tilde{\boldsymbol{\theta}}} = \tilde{\mathbf{f}}(\tilde{\boldsymbol{\theta}}, \mathbf{v}) := \mathbf{f}(\tilde{\boldsymbol{\theta}} + \boldsymbol{\psi}(\mathbf{v}), \mathbf{v}) \quad (87b)$$

a Lyapunov function $U(\tilde{\boldsymbol{\theta}}, \mathbf{v})$ which satisfies

$$b_1 \|\tilde{\boldsymbol{\theta}}\|_2^2 \leq U(\tilde{\boldsymbol{\theta}}, \mathbf{v}) \leq b_2 \|\tilde{\boldsymbol{\theta}}\|_2^2, \quad (88a)$$

$$\frac{\partial U(\tilde{\boldsymbol{\theta}}, \mathbf{v})}{\partial \tilde{\boldsymbol{\theta}}} \tilde{\mathbf{f}}(\tilde{\boldsymbol{\theta}}, \mathbf{v}) \leq -b_3 \|\tilde{\boldsymbol{\theta}}\|_2^2, \quad (88b)$$

$$\left\| \frac{\partial U(\tilde{\boldsymbol{\theta}}, \mathbf{v})}{\partial \tilde{\boldsymbol{\theta}}} \right\|_2 \leq b_4 \|\tilde{\boldsymbol{\theta}}\|_2, \quad (88c)$$

$$\left\| \frac{\partial U(\tilde{\boldsymbol{\theta}}, \mathbf{v})}{\partial \mathbf{v}} \right\|_2 \leq b_5 \|\tilde{\boldsymbol{\theta}}\|_2^2 \quad (88d)$$

for all $\tilde{\boldsymbol{\theta}} \in \mathcal{N}(\mathbf{0}, \delta)$ and $\mathbf{v} \in \mathcal{V}$, where $b_1 > 0$, $b_2 > 0$, $b_3 > 0$, $b_4 > 0$, $b_5 \geq 0$ are constants independent of \mathbf{v} . Note that (87) is equivalent to (85).

If δ is such that

$$D_v < \frac{b_1 b_3}{b_2} \frac{\delta}{b_5 \delta + b_4 D_\Psi}, \quad (89)$$

then with initial condition

$$\boldsymbol{\theta}(0) \in \mathcal{N}(\boldsymbol{\Psi}(\mathbf{v}(0)), \delta \sqrt{b_1/b_2}), \quad (90)$$

the state $\boldsymbol{\theta}(t)$ of (85) satisfies

$$\|\tilde{\boldsymbol{\theta}}(t)\|_2 \leq \sqrt{\frac{b_2}{b_1}} \|\tilde{\boldsymbol{\theta}}(0)\|_2 \exp(-\kappa t) + \frac{b_4 D_\Psi}{2b_1} \int_0^t \exp(-\kappa(t-\tau)) \|\dot{\mathbf{v}}(\tau)\|_2 d\tau \quad (91a)$$

$$\leq \sqrt{\frac{b_2}{b_1}} \|\tilde{\boldsymbol{\theta}}(0)\|_2 \exp(-\kappa t) + \frac{b_4 D_\Psi}{2b_1} \int_0^t \exp(-\kappa(t-\tau)) D_v d\tau \quad (91b)$$

$$\leq \sqrt{\frac{b_2}{b_1}} \|\tilde{\boldsymbol{\theta}}(0)\|_2 \exp(-\kappa t) + \frac{b_4 D_\Psi D_v}{2b_1 \kappa}, \quad (91c)$$

where

$$\kappa = \frac{b_3 - b_5 D_v}{2b_1}. \quad (92)$$

Proof. See Theorem 9.3 in [11]. \square

Remark 4 [11] *Inequalities (88a) and (88b) state the usual requirements that U be positive definite and has a negative definite derivative along the trajectories of system (87). On top of that, they show that $\boldsymbol{\theta}^* = \mathbf{0}$ is exponentially stable.*

Remark 5 *The following facts must be noted when applying Theorem 5 to prove Lemma 12:*

1. *As reasoned in the proof of Lemma 3, the function $\boldsymbol{\eta}$ -defined in (16)(9d)(9e)- is locally Lipschitz continuous. Note that $\boldsymbol{\eta}$ in Lemma 12 corresponds to \mathbf{f} in Theorem 5.*
2. *Analogously to Definition 5, one may define $\boldsymbol{\theta}^*(t) := \boldsymbol{\Psi}(\mathbf{v}(t))$ as an equilibrium point of system (85) at instant t . This analogy makes (37) in Lemma 12 be an instance of*

$$\|\dot{\boldsymbol{\theta}}^*\|_2 = \|\boldsymbol{\Psi}(\mathbf{v})\dot{\mathbf{v}}\|_2 \leq \|\boldsymbol{\Psi}(\mathbf{v})\|_2 \|\dot{\mathbf{v}}\|_2 \leq D_\Psi D_v,$$

- i.e.*, D_χ in Lemma 12 corresponds to $D_\Psi D_\nu$ in Theorem 5.
3. Given b_i in (48) of Lemma 12, inequality (89) in Theorem 5 becomes

$$D_\nu D_\Psi < \frac{1}{2}(1 - M_{\text{sup}}^2)K_x \delta = \kappa \delta,$$

- which is covered by (39) in Lemma 12.*
4. Given b_1 and b_2 in (48) of Lemma 12, the condition (90) in Theorem 5 becomes (38) in Lemma 12.
5. Given b_i in (48) of Lemma 12, the constant κ (92) in Theorem 5 becomes (41) in Lemma 12.

References

- [1] Nocedal, J., Wright, S.J.: Numerical Optimization. Springer, New York, NY, USA (2006)
- [2] Boyd, S., Vandenberghe, L.: Convex Optimization. Cambridge University Press
- [3] Li, S.J., Xu, S.: Sufficient conditions of isolated minimizers for constrained programming problems **31**(6), 715–727 <https://doi.org/10.1080/01630563.2010.490970>
- [4] Potra, S.J. F. A.; Wright: Interior-point methods. J. Comput. Appl. Math. **124**, 281–302 (2000)
- [5] Optimization Toolbox™ User’s Guide, R2020b edn. The MathWorks, Inc. (2020)
- [6] Kelley, C.T.: Iterative Methods for Linear and Nonlinear Equations. Society for Industrial and Applied Mathematics. <https://doi.org/10.1137/1.9781611970944>
- [7] Marinov, R.: Convergence of the method of chords for solving generalized equations. Rendiconti Del Circolo Matematico Di Palermo **58**, 11–27 (2009) <https://doi.org/10.1007/s12215-009-0002-6>
- [8] Fletcher, R.: Practical Methods of Optimization, 2nd edn. John Wiley & Sons, Chichester, West Sussex, England (1987)
- [9] LaSalle, J.: Some extensions of Liapunov’s second method. IRE Transactions on Circuit Theory **7**(4), 520–527 (1960) <https://doi.org/10.1109/TCT.1960.1086720>
- [10] Gronwall, T.H.: Note on the derivatives with respect to a parameter of the solutions of a system of differential equations. Annals of Mathematics **20**(4), 292–296 (1919)
- [11] Khalil, H.K.: Nonlinear Systems, 3rd edn. Prentice-Hall, Inc., Upper Saddle River, NJ, USA (2002)
- [12] Curry, J.H., Garnett, L., Sullivan, D.: On the iteration of a rational function: computer experiments with Newton’s method. Communications in Mathematical Physics **91**(2), 267–277 (1983)
- [13] Beardon, A.F.: Iteration of Rational Functions: Complex Analytic Dynamical Systems. Graduate Texts in Mathematics. Springer, New York, NY, USA (1991)
- [14] Epureanu, B.I., Greenside, H.S.: Fractal basins of attraction associated with a damped Newton’s method **40**(1), 102–109 <https://doi.org/10.1137/S0036144596310033>
- [15] Devaney, R.L.: Chapter 4 - Complex Exponential Dynamics. Handbook of

Dynamical Systems, vol. 3, pp. 125–223. Elsevier Science. [https://doi.org/10.1016/S1874-575X\(10\)00312-7](https://doi.org/10.1016/S1874-575X(10)00312-7)

- [16] Stone, M.H.: The generalized weierstrass approximation theorem. *Mathematics Magazine* **21**(4), 167–184 (1948). Accessed 2024-10-22
- [17] Cormen, T.H., Leiserson, C.E., Rivest, R.L., Stein, C.: *Introduction to Algorithms*, 3rd edn. The MIT Press, Cambridge, Massachusetts (2009)
- [18] Cimini, G., Bemporad, A.: Exact complexity certification of active-set methods for quadratic programming. *IEEE Transactions on Automatic Control* **62**(12), 6094–6109 (2017) <https://doi.org/10.1109/TAC.2017.2696742>
- [19] Arnström, D., Axehill, D.: A unifying complexity certification framework for active-set methods for convex quadratic programming. *IEEE Transactions on Automatic Control* **67**(6), 2758–2770 (2022) <https://doi.org/10.1109/TAC.2021.3090749>
- [20] Cimini, G., Bemporad, A.: Complexity and convergence certification of a block principal pivoting method for box-constrained quadratic programs. *Automatica* **100**, 29–37 (2019) <https://doi.org/10.1016/j.automatica.2018.10.050>
- [21] Mehrmann, V.: *The autonomous linear quadratic control problem: Theory and numerical solution*. (1991)